



THE UNIVERSITY OF
SYDNEY

COPYRIGHT AND USE OF THIS THESIS

This thesis must be used in accordance with the provisions of the Copyright Act 1968.

Reproduction of material protected by copyright may be an infringement of copyright and copyright owners may be entitled to take legal action against persons who infringe their copyright.

Section 51 (2) of the Copyright Act permits an authorized officer of a university library or archives to provide a copy (by communication or otherwise) of an unpublished thesis kept in the library or archives, to a person who satisfies the authorized officer that he or she requires the reproduction for the purposes of research or study.

The Copyright Act grants the creator of a work a number of moral rights, specifically the right of attribution, the right against false attribution and the right of integrity.

You may infringe the author's moral rights if you:

- fail to acknowledge the author of this thesis if you quote sections from the work
- attribute this thesis to another author
- subject this thesis to derogatory treatment which may prejudice the author's reputation

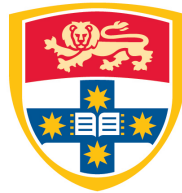
For further information contact the University's Copyright Service.

sydney.edu.au/copyright

DESIGN OF NETWORK CODING SCHEMES AND RF ENERGY TRANSFER IN WIRELESS COMMUNICATION NETWORKS

Yuanye Ma

A THESIS SUBMITTED IN FULFILMENT OF THE REQUIREMENTS FOR THE DEGREE
OF
DOCTOR OF PHILOSOPHY



THE UNIVERSITY OF
SYDNEY

SCHOOL OF ELECTRICAL AND INFORMATION ENGINEERING
FACULTY OF ENGINEERING AND INFORMATION TECHNOLOGIES
THE UNIVERSITY OF SYDNEY

APRIL 2016

© Copyright by **Yuanye Ma**, 2016

*To my beloved parents,
Xiangying Ma and Chaolan Duan.*

Acknowledgements

I would like to express my sincere appreciation to those who so generously contributed to this thesis and supported me along this amazing journey.

Profound gratitude should first be given to my supervisor Professor Branka Vucetic, for her guidance and tremendous academic support. Her constructive and valuable comments have significantly improved the level of my research. She has generously provided financial support to me for attending international conferences. She is a source of encouragement.

My sincere gratitude is reserved for my co-supervisor Dr. Zihuai Lin for his innumerable and valuable comments, discussions and encouragement. His deep insights helped me in various aspects, including but not limited to the research. I am deeply indebted for his understanding, help and financial support during the past years. His attitudes towards research and life will continuously affect me in the future.

I wish to express my sincere thanks to my co-authors, Prof. Yonghui Li, Dr. He (Henry) Chen, Prof. Guoqiang Mao, Prof. Jinhong Yuan, Prof. Degan Zhang, Dr. Jun Li and Dr. Tao Huang, for their passionate discussions, brilliant comments and suggestions. Thanks Dr. Peng Wang for his instructive suggestions.

A special thank you goes to Henry for his continuous help and inexhaustible inspiration along the way.

I would like to thank all my colleagues in the University of Sydney for making the working environment friendly and making the postgraduate study interesting.

I am indebted to all my friends for making the life in Australia full of surprise. I love you all.

I am grateful to the financial support of China Scholarship Council (CSC), Norman I Price Supplementary Scholarship and the University of Sydney's PRSS.

I would like to thank Mr. Nathanael Pree for his careful proofreading of my thesis.

Last but not least, I would like to express my deepest gratitude to my grandparents, relatives and my parents for their unwavering support, understanding, encouragement and unreserved love.

Sydney, Australia
August, 2015

Yuanye Ma

Statement of Originality

The work presented in this thesis is the result of original research carried out by myself, in collaboration with my supervisors, while enrolled in the School of Electrical and Information Engineering at the University of Sydney as a candidate for the Doctor of Philosophy.

These studies were conducted under the supervision of Prof. Branka Vucetic and Dr. Zihuai Lin. It has not been submitted for any other degree or award in any other university or educational institution.

Yuanye Ma
School of Electrical and Information Engineering
The University of Sydney
August 2015

Abstract

This thesis focuses on the design of network coding schemes and radio frequency (RF) energy transfer in wireless communication networks. Novel network coding designs are considered in the first part and then RF energy transfer/harvesting based schemes are investigated in the second part. During the past few years, network coding has attracted significant attention because of its capability to transmit maximum possible information in a network from multiple sources to multiple destinations via a relay. Normally, the destinations are only able to decode the information with sufficient prior knowledge. To enable the destinations to decode the information in the cases with less/no prior knowledge, a novel idea on multiple interpretations by using nested codes is adopted in this thesis.

To begin with, I construct a pattern of nested codes with multiple interpretations using binary convolutional codes in a multi-source multi-destination wireless relay network. Additionally, an opportunistic scheduling technique is employed at the relay to maximise the system capacity. The detailed coding process of the proposed scheme is presented. The upper bounds on bit error probability of the schemes with and without opportunistic scheduling are derived. Good codes for the proposed system are then investigated and simulations are carried out to validate the theoretical analysis.

To improve the spectrum efficiency of network coding schemes, the design of nested codes could be considered in a high-dimensional coding field. Lattice codes, which are defined in Euclidean space, have been widely adopted to enable simultaneous transmissions from multiple sources to multiple relays with multi-user interference. In this context, I reconstruct nested codes with convolutional codes and lattice codes in multi-way relay channels. In particular, a class of novel nested convolutional lattice codes (NCLC) is proposed over a finite field, which can achieve multiple interpretations for each source in two time slots. A theoretical upper bound on word error rate for the NCLC is derived and, on that basis, code design criteria are developed.

Simulation results show that the derived upper bound is asymptotically tight with the increase of normalised signal-to-effective-noise ratio.

Although the spectrum efficiency is improved with the proposed NCLC, the decoding complexity increases exponentially as the lattice dimension grows. Since low-density generator matrix (LDGM) codes can be regarded as a special type of low-density parity-check (LDPC) codes with a linear encoding complexity, constructing lattices based on LDGM codes can guarantee a manageable encoding/decoding complexity with a desired error performance. Based on the above discussions, in this thesis, a network coded non-binary LDGM code structure is proposed for a multi-access relay system, where multiple sources transmit lattice signals to a destination with the help of a relay. A corresponding low complexity decoder is also designed and simulation results show that the proposed code outperforms a designed reference scheme.

Another focus of this thesis is on the design of RF-enabled wireless energy transfer (WET) schemes. Much attention has been attracted by RF-enabled WET technology because of its capability enabling wireless devices to harvest energy from wireless signals for their intended applications. In practice, wireless energy transmitters, referred to as power beacons (PBs), could be deployed to provide dedicated wireless charging services. Accordingly, system designers can configure a PB-assisted wireless-powered communication network (PB-WPCN), which consists of a set of hybrid access point (AP)-source pairs and a PB. In this thesis, both cooperative and non-cooperative scenarios are considered, based on whether the PB is cooperative with the APs or not. For the cooperative scenario, a social welfare maximisation problem is formulated to maximise the weighted sum-throughput of all AP-source pairs, which is subsequently solved by a water-filling based distributed algorithm. In the non-cooperative scenario, I formulate an auction game and propose an auction based distributed algorithm by considering the PB as the auctioneer and the APs as the bidders. Finally, numerical results are performed to validate the convergence of both proposed algorithms and demonstrate the effects of various system parameters.

In addition to delivering wireless energy, RF signals are also used to carry information in wireless communications. A simultaneous wireless information and power transfer (SWIPT) could thus be considered to realise the dual utilisation of RF signals at the same time. In this thesis, I develop a new distributed power control scheme for a power splitting-based interference channel (IFC) with SWIPT. The considered IFC consists of multiple source-destination pairs. Each pair adjusts its transmit power and power splitting ratio to meet both signal-to-interference-plus-noise ratio (SINR) and

energy harvesting (EH) constraints at its corresponding destination. To characterise rational behaviours of source-destination pairs, a non-cooperative game is formulated for the considered system. A sufficient condition is derived for the existence and uniqueness of the Nash equilibrium (NE) of the formulated game. The best response strategy of each player is also presented and then the NE can be achieved iteratively. Numerical results show that the performance of the proposed game-theoretic approach closely matches that of an optimal strategy under various SINR and EH constraints.

Table of Contents

Acknowledgements	iii
Statement of Originality	v
Abstract	vi
Table of Contents	ix
List of Tables	xii
List of Figures	xiii
List of Acronyms	xv
Glossary of Notations	xvii
List of Publications	xviii
1 Introduction	1
1.1 History and Motivation	1
1.2 Research Problems and Contributions	7
2 Background	13
2.1 Nested Codes	14
2.1.1 Encoding	14
2.1.2 Hard-Decision Decoding	15
2.1.3 Soft-Decision Decoding	15
2.2 The Soft-Output Viterbi Algorithm (SOVA)	16
2.3 Lattices	20
2.3.1 Lattice Network Coding	21
2.4 RF Energy Transfer	22

2.5	Wireless-Powered Communication	24
3	Multiple Interpretations for Multi-Source Multi-Destination Wireless Relay Network Coded Systems	25
3.1	System Model	26
3.2	Coding with Nested Codes and the OS	27
3.2.1	Encoding with Nested Codes	28
3.2.2	The Opportunistic Scheduling (OS)	28
3.2.3	Decoding with Nested Codes	30
3.3	Analytical Bounds on the Bit Error Probability	31
3.4	Code Search	34
3.5	Simulation Results	35
4	Novel Nested Convolutional Lattice Codes for Multi-Way Relaying Systems over Fading Channels	40
4.1	System Model and Preliminaries	41
4.2	Nested Convolutional Lattice Codes (NCLC)	43
4.3	Performance Analysis	48
4.4	Simulation Results	52
5	Network Coded Non-Binary LDGM Codes Based on Lattices for a Multi-Access Relay System	54
5.1	System Model	55
5.2	Nested LDGM Codes Based on Lattices	57
5.3	Achievable Computation Rate (ACR)	60
5.4	Code Optimisation	61
5.5	Reference Scheme	63
5.6	Simulation Results	63
6	Distributed and Optimal Resource Allocation for Power Beacon-Assisted Wireless-Powered Communications	68
6.1	System Model	69
6.2	Cooperative Scenario	74
6.2.1	Problem Formulation	74
6.2.2	Optimal Solution and Distributed Algorithm	76
6.3	Non-Cooperative Scenario	84
6.3.1	Utility Functions	85
6.3.2	Auction Game	85
6.3.3	Analysis of the Formulated Game	89

6.4	Numerical Results	90
7	Distributed Power Control in Interference Channel with SWIPT: A Game-Theoretic Approach	98
7.1	System Model and Game Formulation	99
7.1.1	System Model	99
7.1.2	Game Formulation	100
7.2	Existence and Uniqueness of the NE	102
7.2.1	The Best Response Strategy	102
7.2.2	A Sufficient Condition	104
7.3	Numerical Results	105
8	Conclusions	109
A	Proofs for Chapter 4. Novel Nested Convolutional Lattice Codes for Multi-Way Relaying Systems over Fading Channels	112
A.1	Proof of Theorem 4.1	112
B	Proofs for Chapter 5. Network Coded Non-Binary LDGM Codes Based on Lattices for a Multi-Access Relay System	114
B.1	Proof of Theorem 5.1	114
B.2	Proof of Proposition 5.2	115
B.3	Proof of Proposition 5.3	115
C	Proofs for Chapter 6. Distributed and Optimal Resource Allocation for Power Beacon-Assisted Wireless-Powered Communications	117
C.1	Proof of Proposition 6.2	117
C.2	Proof of Lemma 6.3 and Proposition 6.4	119
C.3	Proof of Proposition 6.6	120
C.4	Proof of Proposition 6.7	122
D	Proofs for Chapter 7. Distributed Power Control in Interference Channel with SWIPT: A Game-Theoretic Approach	124
D.1	Proof of Proposition 7.1	124
D.2	Proof of Proposition 7.3	125
	Bibliography	127

List of Tables

3.1	Good nested codes	35
3.2	The performance analysis of the selected 4/6 code.	36
6.1	System parameters	91

List of Figures

2.1	An illustration of the reliability vector update procedure for SOVA, where a $(1, 3, 1)$ convolutional code is employed with the memory order $m = 1$ and the constraint length $v = 2$	18
2.2	A typical RF energy receiver.	22
2.3	A conceptual network model of wireless-powered communication. . . .	23
3.1	An example of the considered network coded system model.	26
3.2	The coding process of the proposed network coded system.	27
3.3	The bit error probability of the received network coded packet before the convolutional decoder at a destination under different OS selections.	37
3.4	The performance of nested codes with different side information when the OS level $k = 1$ and the RCPC code rate is $1/3$	38
4.1	The system model of a MWRC.	41
4.2	Processes of the NCLC at the relay node and the source node s_j	44
4.3	The Monte-Carlo simulation result and the analytical upper bound. . .	53
5.1	A multi-access relay network model with multiple sources, one relay and one destination.	56
5.2	The ACR performance of the proposed system with an optimal \mathbf{a} and different choices of b , compared with that of the reference scheme. . .	64
5.3	The average detection error performance with different values of b . . .	65
5.4	The average symbol error performance of the proposed codes.	66
6.1	System model for the proposed PB-WPCN.	69
6.2	An illustration of the time diagram for i th AP-source pair in a transmission block \mathcal{T}	71

6.3	Graphical interpretations for the functions (6.2.7), (6.2.10) and (6.2.12) in the proposed cooperative scenario.	80
6.4	The convergence properties of both the proposed algorithms when $N = 3$	92
6.5	The optimal allocated energy and optimal DL WET time for each AP-source pair versus E_b^{tot} for both cooperative and non-cooperative scenarios.	93
6.6	The average allocated energy and average DL WET time for each AP-source pair versus E_b^{tot} for both cooperative and non-cooperative scenarios.	95
6.7	The average social welfare (i.e., the weighted sum throughput) of both the proposed cooperative and non-cooperative scenarios versus E_b^{tot} in the case of different number of participating AP-source pairs.	96
7.1	The convergence of best-response dynamics in the formulated non-cooperative game with four source-destination pairs starting from two different sets of initial points, which are distinguished by solid lines and dash lines.	106
7.2	Averaged total transmit power versus the EH constraint with different SINR constraints in a two-pair network.	107

List of Acronyms

AF	amplify-and-forward
AP	access point
ACR	achievable computation rate
AWGN	additive white Gaussian noise
BPSK	binary phase-shift keying
CSI	channel state information
DC	direct current
DF	decode-and-forward
DL	downlink
EH	energy harvesting
FFT	fast fourier transform
ID	information decoding
IFC	interference channel
LDGM	low-density generator matrix
LDPC	low-density parity-check
L-EMS	lattice-based extended min-sum
MIMO	multiple-input multiple-output
MISO	multiple-input single-output
ML	maximum likelihood
MMSE	minimum mean square error
MRT	maximum ratio transmission
MWRC	multi-way relay channel

NCLC	nested convolutional lattice codes
NE	Nash equilibrium
OS	opportunistic scheduling
PB	power beacon
PB-WPCN	power beacon-assisted wireless-powered communication network
PNC	physical-layer network coding
RCPC	rate-compatible punctured convolutional
RF	radio frequency
SDMA	space division multiple access
SDP	semidefinite programming
SENR	signal-to-effective-noise ratio
SENR_{norm}	normalised signal-to-effective-noise ratio
SINR	signal-to-interference-plus-noise ratio
SNR	signal-to-noise ratio
SOCP	second-order cone programming
SOVA	soft-output Viterbi algorithm
SWIPT	simultaneous wireless information and power transfer
TDMA	time division multiple access
UL	uplink
WER	word error rate
WET	wireless energy transfer
WPCN	wireless-powered communication network
WSN	wireless sensor network
XOR	exclusive or

Glossary of Notations

$(\mathbf{X})^T$	the transpose of \mathbf{X}
$(\mathbf{X})^H$	the Hermitian transpose of \mathbf{X}
$ X $	the absolute value of X
$\ \mathbf{X}\ $	the Euclidean norm of vector \mathbf{X}
$\mathbb{E}[X]$	the expectation of X
$\Pr(X)$	the probability of the event X
\mathbb{R}	the real number field
\mathbb{C}	the complex number field
\mathbb{Z}	the integer field
\mathbb{F}_q	the finite field of size q
η	the RF-to-DC energy conversion efficiency

List of Publications

The following is a list of publications in refereed journals and conference proceedings produced during my Ph.D. candidature. In some cases, the journal papers contain materials overlapping with the conference publications.

Journal Papers

- [J1] Y. Ma, H. Chen, Z. Lin, Y. Li, and B. Vucetic, “Distributed and optimal resource allocation for power beacon-assisted wireless-powered communications,” *IEEE Transactions on Communications*, to be published. [Online]. Available: <http://arxiv.org/abs/1508.01617>.
- [J2] Y. Ma, H. Chen, Z. Lin, Y. Li, and B. Vucetic, “Distributed power control in interference channel with SWIPT: A game-theoretic approach,” *IEEE Transactions on Vehicular Technology*, resubmitted after major revisions, Jul. 2015.
- [J3] Y. Ma, Z. Lin, B. Vucetic, G. Mao, L. Ma, and J. Li, “Design and reliability analysis of network coding schemes in lossy wireless networks for all-to-all broadcast,” submitted to *IEEE Transactions on Vehicular Technology*, 2015.
- [J4] H. Chen, Y. Li, Y. Jiang, Y. Ma, and B. Vucetic, “Distributed power splitting for SWIPT in relay interference channels using game theory,” *IEEE Transactions on Wireless Communications*, vol. 14, no. 1, pp. 410-420, Jan. 2015.
- [J5] H. Chen, Y. Li, Z. Han, Y. Ma, and B. Vucetic, “Energy trading in power beacon-assisted wireless-powered communication networks: A Stackelberg game approach,” submitted to *IEEE Transactions on Signal Processing*, 2015.
- [J6] D. Zhang, X. Song, X. Wang, and Y. Ma, “Extended AODV routing method based on distributed minimum transmission (DMT) for WSN,” *AEU-International Journal of Electronics and Communications*, vol. 69, no. 1, pp. 371-381, Jan. 2015.

Conference Papers

- [C1] Y. Ma, H. Chen, Z. Lin, B. Vucetic, and X. Li, “Spectrum sharing in RF-powered cognitive radio networks using game theory,” in *Proceedings of IEEE International Symposium on Personal, Indoor and Mobile Radio Communications (PIMRC)*, Hong Kong, China, Sep. 2015, pp. 1142–1146.
- [C2] Y. Ma, Z. Lin, J. Li, G. Mao, and B. Vucetic, “Network coded non-binary LDGM codes based on lattices for a multi-access relay system,” in *Proceedings of IEEE International Symposium on Personal, Indoor and Mobile Radio Communications (PIMRC)*, Hong Kong, China, Sep. 2015, pp. 189–193.
- [C3] Y. Ma, H. Chen, Z. Lin, Y. Li, and B. Vucetic, “Distributed resource allocation for power beacon-assisted wireless-powered communications,” in *Proceedings of IEEE International Conference on Communications (ICC)*, London, U.K., Jun. 2015, pp. 3849–3854.
- [C4] H. Chen, Y. Jiang, Y. Li, Y. Ma, and B. Vucetic, “A game-theoretical model for wireless information and power transfer in relay interference channels,” in *Proceedings of IEEE International Symposium on Information Theory (ISIT)*, Honolulu, USA, Jul. 2014, pp. 1161–1165.
- [C5] Y. Ma, T. Huang, J. Li, J. Yuan, Z. Lin, and B. Vucetic, “Novel nested convolutional lattice codes for multi-way relaying systems over fading channels,” in *Proceedings of IEEE Wireless Communications and Networking Conference (WCNC)*, Shanghai, China, Apr. 2013, pp. 2671–2676.
- [C6] Y. Ma, Z. Lin, H. Chen, and B. Vucetic, “Multiple interpretations for multi-source multi-destination wireless relay network coded systems,” in *Proceedings of IEEE International Symposium on Personal, Indoor and Mobile Radio Communications (PIMRC)*, Sydney, Australia, Sep. 2012, pp. 2253–2258.

Chapter 1

Introduction

This chapter first introduces the history and motivation of my research. The major research problems and the main contributions of this thesis are then summarised.

1.1 History and Motivation

Future communications are envisioned to support high data rates and a large coverage. Network coding [1–3] has attracted much attention as a coding approach to enhance high data rates. One significant feature of network coding is its capability to transmit maximum possible information in a network from multiple sources to multiple destinations via relays [4]. This benefit of network coding has also been widely discussed in the open literature [2, 5, 6] via the demonstration of a butterfly network, where the capacity for such a network coding scheme could be improved by combining data packets at relay nodes.

To further enhance the capacity of network coding schemes, Yomo and Popovski proposed an opportunistic scheduling (OS) approach in [7]. It is an opportunistic selective mechanism by dynamically changing the set of destinations to maximise the average capacity. However, in this scheme, it is assumed that the destinations have

sufficient prior knowledge, i.e., previous knowledge of some packets, which is somewhat unrealistic in practice. In [8], a novel idea on multiple interpretations by using nested codes is proposed, which enables the destinations to decode the information in the cases with less/no prior knowledge. Codes with multiple interpretation capability are the codes that can be decoded at different rates by different destinations. The basic idea of [8] is that different packets encoded with linearly independent generators are combined at a relay and then forwarded to different destinations. Because the generators are mutually independent, the destinations can decode their desired information from the combined packets with less/no prior knowledge. In Chapter 3 of this thesis, a convolutional code structure is proposed by considering both the OS approach and nested codes, which achieves a desired code performance even with no prior knowledge at destinations.

To improve the spectrum efficiency in network coding schemes, extensive work has been done based on lattice codes [9–12]. The pattern of lattice codes enables simultaneous transmissions from multiple sources to a relay with multi-user interference, which results in a high spectrum efficiency. A strategy of compute-and-forward is proposed in [9] obtaining significantly higher rates by exploiting interference between users. Rather than treating the interference as noise, the relays decode the linear functions of transmitted messages into integer combinations of codewords, where lattice codes are employed due to their algebraic structure. In [11], a general algebraic framework, called lattice network coding, is developed based on the physical-layer network coding (PNC) [12] schemes. The lattice network coding scheme reinterprets the compute-and-forward strategy in a generalised construction, which results in a form of linear network coding over modules. It is worth noting that different from the

topic of (digital) network coding, where data packets are mixed using a finite field representation in the “digital domain”, the PNC (lattices) based schemes consider the combination of signals in the wireless medium. In this thesis, nested codes are reconstructed based on lattices in order to achieve a high spectrum efficiency. In Chapter 4, a multi-way relay channel (MWRC) [13–15] is considered, where all users, without direct links among them, exchange their information via a single relay. A class of nested convolutional lattice codes (NCLC) over a finite field is then proposed for the MWRC model, which achieves multiple interpretations for each user in two time slots.

Although the spectrum efficiency is improved with the proposed NCLC, the decoding complexity increases exponentially with the increasing of lattice dimensions. Since low-density generator matrix (LDGM) codes are special types of low-density parity-check (LDPC) codes [16] with a linear encoding complexity, constructing lattices based on LDGM codes can guarantee a manageable encoding/decoding complexity with a desired error performance. In Chapter 5, a network coded non-binary LDGM code structure is proposed for a multi-access relay system, where multiple sources transmit lattice signals to a destination with the help of a relay. By designing a lattice-based decoder for the proposed code structure, the decoding complexity is significantly reduced.

Another focus of this thesis is the design of radio frequency (RF)-enabled wireless energy transfer (WET) schemes. Recently, the WET technologies have drawn wide attention with their capability of energy supply [17]. Conventionally, the very limited energy of wireless devices powered by batteries largely constrains their communication performance in many practical cases, such as wireless sensor networks (WSNs)

[18]. Also, the battery replacement for wireless devices is not convenient or feasible in many applications. These challenging issues have boosted the development of WET technologies, which enable wireless devices to harvest energy from wireless signals for their intended applications. As one category of existing WET techniques, the RF-enabled WET [19] considered in this thesis provides the feasibility of a long-range energy transfer (up to tens of meters [20]) compared to other technologies, such as inductive coupling [21] and magnetic resonance coupling [22]. RF-enabled WET has not been widely used in practice, largely due to high propagation losses of RF signals. However, due to the latest breakthroughs in wireless communications, for example, small cells [23], transmission using large-scale antenna arrays (i.e., massive MIMO) [24], millimeter-wave communications [25] and sharp beamforming, the transmission distances could be dramatically reduced and much higher WET efficiencies are feasible [20]. Furthermore, the energy consumption of communication devices will be continuously reduced by the advances in low-power electronics [26]. Thus, it is believed that the RF-enabled WET has great potential to be widely implemented in the next-generation wireless communication systems. By applying the RF-enabled WET techniques, a fully wireless-powered communication network (WPCN) can be established with no need for battery replacement [27]. In a WPCN, wireless devices are only powered by WET in the downlink (DL) and transmit their information using the harvested energy in the uplink (UL) [28].

There have been several published papers that focused on the design of WPCNs for different setups [26, 28–31]. In [28], a “harvest-then-transmit” protocol was proposed for a multi-user WPCN, where users first harvest energy from RF signals broadcast by a single antenna hybrid access point (AP) in the DL and then transmit information

to the AP in the UL via time division multiple access (TDMA). Moreover, the DL WET time from the AP and UL information transmission time of individual users were jointly optimised to maximise the system sum-throughput. [29] extended [28] to a multi-antenna WPCN scenario, where a multi-antenna AP enables simultaneous UL transmissions via space division multiple access (SDMA). In [30] and [31], the authors considered full-duplex WPCNs, where a full-duplex AP is adopted to provide the simultaneous DL WET and UL information transmission. In all aforementioned papers, only the AP is considered as the energy source of the whole network. In [26], the authors proposed the idea of deploying dedicated power nodes, named power beacons (PBs), to enable WET in the DL. By resorting to the stochastic geometry theory, the densities and transmit power of PBs are investigated under data links' outage constraint. With this PB-based WET, a new network setup thus could be considered, namely "PB-assisted WPCN (PB-WPCN)", in which each user can harvest wireless energy not only from the AP but also from the deployed PB. For this new model, a natural question that arises is how to optimally allocate the resources of PB-WPCNs, including the PBs' energy, and the time for DL WET as well as the UL information transmission. To the best of my knowledge, this is still an open question, which motivated Chapter 6 of this thesis.

The recent emerging WET techniques enable wireless devices to harvest energy from ambient/dedicated RF signals. It is well known that RF signals are also used to carry information in wireless communications. As a result, simultaneous wireless information and power transfer (SWIPT) [32, 33] has recently been proposed to realise the dual utilisation of RF signals for joint information and energy transfer at the same time. Such dual utilisation of RF signals in SWIPT leads to different system designs

in various setups and applications. For example, in an interference channel (IFC) with SWIPT, the cross-link interference is still harmful to the information decoding (ID) at the receiver side, but it becomes beneficial when we focus on the energy harvesting (EH) aspect.

There have been several papers in the open literature that focus on the design of SWIPT in IFCs [34–38]. Specifically, authors in [34] considered SWIPT in a multiple-input single-output (MISO) IFC, where the weighted sum-rate was maximised subject to individual EH constraints and transmit power constraints. In [35], all possible transmission strategies with different combinations of ID and energy harvesting at the receiver side were investigated and compared in a two-user multiple-input multiple-output (MIMO) IFC, which was subsequently extended to the general K -user case in [36]. Authors in [37] investigated a joint beamforming and power splitting problem in a MISO IFC, where the total transmit power of all transmitters was minimised under both rate and EH constraints, by employing a semidefinite programming (SDP) method. A second-order cone programming (SOCP) relaxation-based approach was developed in [38] as an alternative solution to resolve the same total power minimisation problem in a decentralised manner. In all aforementioned papers that designed SWIPT schemes in IFCs, it is assumed that all source-destination pairs cooperate to achieve the optimal network-wide performance (e.g., maximising the sum-rate/minimising the total transmit power of all pairs). However, in many practical scenarios, source-destination pairs may focus on maximising their own performance instead of the overall one (see [39] and references therein). To the best of my knowledge, there has been no work that designs SWIPT for the IFC with

self-interested source-destination pairs reported in the open literature. This gap motivated Chapter 7 of this thesis.

1.2 Research Problems and Contributions

The main topics of the thesis are the design of network coding schemes and RF energy transfer in wireless communication networks. The novel network coding designs are presented in Chapters 3, 4 and 5, followed by the RF energy transfer/harvesting based schemes investigated in Chapters 6 and 7. I first investigate the network coding design based on nested codes and the OS technique in Chapter 3, then employ lattices in the designed nested codes to further improve the spectrum efficiency in Chapter 4. To reduce the high decoding complexity caused by the adopted convolutional codes in Chapter 3 and 4, a pattern of lattice based LDGM codes is proposed in Chapter 5. In Chapter 6, the RF energy transfer based schemes are considered in a new network setup named “PB-assisted WPCN”. I then make a further research in SWIPT protocol in Chapter 7. In the sequel of this section, I elaborate the thesis research problems and the corresponding contributions.

The *first* research problem in this thesis is the joint design of nested codes and the OS technique to achieve a desired code performance with less/no prior knowledge at destinations. It is commonly assumed in conventional systems that the destinations have sufficient prior knowledge, i.e., adequate previous knowledge of some packets, which motivated this idea to consider the cases with less/no prior knowledge. The considered network consists of multiple sources, multiple destinations and a single relay, where the relay collects all messages from multiple sources and forwards a combination of selected messages to the destinations. To enable the destinations to

extract their desired messages with less/no prior knowledge, sources are assumed to encode their messages with low-rate linearly independent generators. All the generators actually compose the nested codes. As the nested codes can be decoded at different rates, i.e., the rates of the packets resulting from cancellations with the prior knowledge owned by different destinations, we say such codes have multiple interpretations. Besides, to maximise the capacity of the considered network, the OS technique is adopted at the relay. The main contributions regarding this research problem include:

- A structure of convolutional codes based on nested codes and the OS is proposed in a multi-source multi-destination wireless relay network. Multiple interpretations at different destinations are thus achieved in the cases with less/no prior knowledge. System capacity is maximised by employing the OS at the relay.
- Upper bounds on bit error probability of the proposed schemes with and without the OS are respectively derived.
- A code search is conducted based on designed criteria. The theoretical analysis is validated through simulations and it is shown that upper bounds become tight with the increase of signal-to-noise ratio (SNR).

The *second* research problem is the construction of nested codes based on lattices to achieve multiple interpretations with a high spectrum efficiency in a MWRC with fading. A common application scenario of the MWRC is the satellite communication, where all earth stations exchange their information via a satellite. The existing scenarios usually consider that all users (earth stations) transmit their information to a relay (satellite) via orthogonal channels. To improve the spectrum efficiency, I

would like to consider the transmissions from all users to the relay via a multi-user interference channel by exploiting the benefits of lattice codes. The transmissions for the considered MWRC model are divided in two time slots, i.e., all users simultaneously transmit their own information to a relay with multi-user interference in the first time slot, and the relay combines all the information and broadcasts a network coded packet to all the users in the second time slot. At the end of the second time slot, each user is able to extract all the other users' information from the network coded packet due to the employment of nested codes. The main contributions along this research problem include:

- I propose a class of novel nested convolutional lattice codes (NCLC) over a finite field in a MWRC with fading, which enables each user to obtain all the other users' information in two time slots.
- A theoretical upper bound on word error rate (WER) is derived for the NCLC.
- According to the derived theoretical upper bound, code design criteria are developed to optimise the NCLC. Simulation results show that the derived upper bound is asymptotically tight with the increase of the normalised signal-to-effective-noise ratio ($\text{SENR}_{\text{norm}}$, see Eq. (4.3.8) in Chapter 4).

The *third* research problem is the design of network coded LDGM codes based on lattices to achieve a high spectral efficiency with a low encoding/decoding complexity. In other words, I focus on the reduction of the decoding complexity while maintaining a desired error performance, as the proposed NCLC in the previous work has a high decoding complexity, which increases exponentially with the increasing of lattice dimensions. I consider a multi-access relay system with multiple sources, one

relay and one destination, where sources encode their messages with LDGM codes and transmit lattice signals simultaneously to the common destination via the relay. The LDGM codes are employed at sources due to their linear encoding complexities. The main contributions regarding to this research problem are summarised as follows:

- I develop a network coded non-binary LDGM code scheme by considering lattice-signal transmissions at both the sources and the relay.
- An achievable computation rate (ACR) of the proposed system is derived and the corresponding key parameters in the proposed code scheme are optimised to maximise the ACR.
- A low complexity decoder is designed for the proposed code. Simulation results show that (1) the optimal setting of the parameters is consistent with that obtained from the analysis; (2) the proposed code performs 2dB better than the reference scheme at an average symbol error rate of 10^{-4} .

The *fourth* research problem is the optimal resource allocation of a PB-WPCN, which is constituted of one multi-antenna PB and multiple single-antenna AP-source pairs. Different from the existing WPCNs, which consider that sources only harvest energy from APs, the PB-WPCN introduces the PB to assist the APs by providing a wireless charging service. The introducing of the PB could be beneficial as a whole based on the following considerations: (1) The PB could be dedicated designed for WET only and thus can achieve a higher WET efficiency by exploiting the benefits of energy beamforming enabled by multiple antennas [40, 41]. (2) The deployment of the PB could be more flexible since it has much looser backhaul requirements. (3) By using both the AP and PB to perform WET simultaneously, the transmit

diversity could be achieved and thus could make the RF energy harvesting at the user side more robust. Besides, note that the energy allocation of the PB and time allocation of each AP-source pair are tangled together. This makes the distributed and optimal resource allocation for the considered PB-WPCN not trivial at all. For the PB-WPCN, in particular, I consider both cooperative and non-cooperative scenarios based on whether the PB is cooperative with the APs or not. The main contributions regarding this research problem are summarised as follows:

- For the cooperative scenario, a social welfare maximisation problem is formulated and a water-filling based algorithm is proposed to optimally solve the problem in a distributed manner.
- For non-cooperative scenario, an auction game is formulated by considering the PB as the auctioneer and the APs as the bidders. An auction based distributed algorithm is proposed to analyse the formulated game and its convergence is subsequently proved.

The *fifth* research problem is to develop a game-theoretic framework for the distributed power control in a power-splitting based IFC with SWIPT. The considered IFC consists of multiple source-destination pairs. Different from the existing works, which assume that all source-destination pairs cooperate to achieve the optimal network-wide performance, I consider that all pairs are self-interested and focus on maximising their own performance instead of the overall one, which would be more practical (see [36] and references therein). The main contributions regarding this research problem are summarised as follows:

- A non-cooperative game is formulated for the considered IFC-SWIPT system,

where each source-destination pair is modeled as a strategic player who aims to minimise the source transmit power while satisfying both signal-to-interference-plus-noise ratio (SINR) and EH constraints at the destination.

- A sufficient condition is derived to guarantee the existence and uniqueness for the Nash equilibrium (NE) of the formulated game.
- The best response strategy for each pair is derived and then the NE is achieved in a distributed manner. Numerical results validate the theoretical analysis and show that the proposed game-theoretic approach can achieve a near-optimal network-wide performance.

Chapter 2

Background

In this chapter, a brief review of some general concepts is provided, in the context of network coding design and radio frequency (RF) energy transfer, respectively. In particular, I first describe the encoding and decoding procedures of nested codes, the soft-output Viterbi algorithm (SOVA) as well as lattices. Brief introductions to RF energy transfer and wireless-powered communication are then presented.

2.1 Nested Codes

Nested codes with multiple interpretations are first proposed in [8]. Codes with multiple interpretation capability are the codes that can be decoded at different rates at different destinations. The different rates are the results of cancellations with the prior knowledge owned by different destinations. In the following, the principles of encoding, hard-decision decoding and soft-decision decoding for the nested codes will be presented respectively.

2.1.1 Encoding

Let boldface lowercase and uppercase letters denote vectors and matrices, respectively. We denote by \mathbf{i}_j and \mathbf{G}_j the message and generator matrix corresponding to the j th node, $\forall j \in \{1, 2, \dots, N\}$. The encoding process can be regarded as the exclusive or (XOR) of all codewords, i.e.,

$$\mathbf{c} = \mathbf{i}_1 \mathbf{G}_1 \oplus \mathbf{i}_2 \mathbf{G}_2 \oplus \dots \oplus \mathbf{i}_N \mathbf{G}_N = [\mathbf{i}_1, \mathbf{i}_2, \dots, \mathbf{i}_N] \begin{bmatrix} \mathbf{G}_1 \\ \mathbf{G}_2 \\ \vdots \\ \mathbf{G}_N \end{bmatrix}, \quad (2.1.1)$$

where $\mathbf{G}_1, \mathbf{G}_2, \dots, \mathbf{G}_N$ are assumed to be linearly independent and \oplus denotes the XOR operation. The representations of the XORed codewords on the right-hand side in (2.1.1) suggest how the codewords should be processed at the receiver. If the receiver knows some of the messages, then those messages can be cancelled by XORing their codewords first. Otherwise, the receiver can directly decode all the messages associated with the “stacked” generator matrix on the right-hand side of (2.1.1).

2.1.2 Hard-Decision Decoding

In hard-decision decoding, we have the input of a decoder as $\hat{\mathbf{r}} = \mathbf{c} \oplus \mathbf{e}$, where \mathbf{e} denotes the binary error pattern. At the j th receiver, $\hat{\mathbf{r}}$ can be interpreted as

$$\hat{\mathbf{r}} = \bigoplus_{\ell \notin \mathcal{K}_j} \mathbf{i}_\ell \mathbf{G}_\ell \oplus \bigoplus_{\ell' \in \mathcal{K}_j} \mathbf{i}_{\ell'} \mathbf{G}_{\ell'} \oplus \mathbf{e}, \quad (2.1.2)$$

where \mathcal{K}_j denotes the indices of the messages known a priori to the receiver j . Because the part $\bigoplus_{\ell' \in \mathcal{K}_j} \mathbf{i}_{\ell'} \mathbf{G}_{\ell'}$ in (2.1.2) is known to the receiver j , it can be cancelled by XORing to obtain

$$\hat{\mathbf{r}}_j = \hat{\mathbf{r}} \oplus \bigoplus_{\ell' \in \mathcal{K}_j} \mathbf{i}_{\ell'} \mathbf{G}_{\ell'} = \bigoplus_{\ell \notin \mathcal{K}_j} \mathbf{i}_\ell \mathbf{G}_\ell \oplus \mathbf{e}. \quad (2.1.3)$$

The right-hand side of (2.1.3) represents the nested code with the “stacking” generator matrices corresponding to all messages that are not known to receiver j . To extract the desired messages \mathbf{i}_ℓ , $\forall \ell \notin \mathcal{K}_j$, from $\hat{\mathbf{r}}_j$ in (2.1.3), a decoding algorithm corresponding to the “stacking” generator needs to be employed. If the generators are constructed by convolutional codes, the Viterbi algorithm [42] can be employed to extract the desired messages.

2.1.3 Soft-Decision Decoding

In soft-decision decoding, the input of a decoder is a log-likelihood ratio or L-value of the i th bit in the codeword \mathbf{c} , denoted by $L_{\mathbf{c}(i)}$. Mathematically, we have

$$L_{\mathbf{c}(i)} = \ln \frac{\Pr(\mathbf{c}(i) = 0)}{\Pr(\mathbf{c}(i) = 1)}, \quad (2.1.4)$$

where $\Pr(X)$ denotes the probability of the event X . As the j th receiver may process some prior knowledge, the codeword \mathbf{c} can be decomposed as

$$\mathbf{c} = \underbrace{\bigoplus_{\ell \notin \mathcal{K}_j} \mathbf{i}_\ell \mathbf{G}_\ell}_{\mathbf{c}_u} \oplus \underbrace{\bigoplus_{\ell' \in \mathcal{K}_j} \mathbf{i}_{\ell'} \mathbf{G}_{\ell'}}_{\mathbf{c}_c}, \quad (2.1.5)$$

where \mathbf{c}_u represents the collection of unknown information and \mathbf{c}_c is the collection of the prior known information at the receiver j . It is apparent that the prior known information \mathbf{c}_c should be cancelled. With the cancellation of the prior knowledge \mathbf{c}_c , at the j th receiver, we can compute the L-value of the i th bit of the desired information \mathbf{c}_u by

$$L_{\mathbf{c}_u(i)} \triangleq \ln \frac{\Pr(\mathbf{c}_u(i) = 0)}{\Pr(\mathbf{c}_u(i) = 1)} = \begin{cases} L_{\mathbf{c}(i)} = \ln \frac{\Pr(\mathbf{c}_u \oplus \mathbf{c}_c(i)=0)}{\Pr(\mathbf{c}_u \oplus \mathbf{c}_c(i)=1)}, & \text{if } \mathbf{c}_c = 0, \\ -L_{\mathbf{c}(i)} = \ln \frac{\Pr(\mathbf{c}_u \oplus \mathbf{c}_c(i)=1)}{\Pr(\mathbf{c}_u \oplus \mathbf{c}_c(i)=0)}, & \text{if } \mathbf{c}_c = 1. \end{cases} \quad (2.1.6)$$

Note that there is no information lost via the above cancellation operation, because it only changes the sign of the L-value. Then we have the calculated L-value $L_{\mathbf{c}_u}$, which is the estimated soft information of unknown packets to receiver j . To extract the unknown messages with the L-value $L_{\mathbf{c}_u}$, the soft-output Viterbi algorithm (SOVA) [42], which will be briefly reviewed in the next section, can be employed if the generators \mathbf{G}_ℓ are constructed based on convolutional codes.

Note that this review on nested codes is mainly adopted from [8].

2.2 The Soft-Output Viterbi Algorithm (SOVA)

Consider a rate- k/n convolutional code. The encoder of the convolutional code has k inputs, n outputs and k input shift registers for storing information bits. Let m_i be the length of the i th input register, i.e., the i th input register has m_i memory

elements, for $i = 1, 2, \dots, k$. The total memory of this encoder can be expressed by

$$M = \sum_{i=1}^k m_i. \quad (2.2.1)$$

The information bits stored in this memory define the state of the encoder. The parameter

$$m = \max_{1 \leq i \leq k} \{m_i\}, \quad (2.2.2)$$

is called the memory order and $v = m + 1$ is called the constraint length of the code. A rate- k/n convolutional code of memory order m is commonly called an (n, k, m) convolutional code.

The SOVA is almost identical to the Viterbi algorithm, except that a reliability indicator is appended to the hard-decision output for each information bit. The combination of the reliability indicator and the hard-decision output is called a soft output. For ease of illustration, I take a rate-1/ n convolutional code as an example. Let u , c and r denote an information bit, a codeword symbol, and a received symbol, respectively. Let \mathbf{u} , \mathbf{c} and \mathbf{r} denote the information sequence, the codeword sequence, and the received sequence, respectively. The L-value of a received symbol r at the output of a channel with binary inputs $c = \pm 1$ can be expressed by

$$L_r = \ln \frac{\Pr(r|c = +1)}{\Pr(r|c = -1)}, \quad (2.2.3)$$

and the L-value of an information bit u is defined as

$$L_u = \ln \frac{\Pr(u = +1)}{\Pr(u = -1)}. \quad (2.2.4)$$

Let S_i denote the i th state, $i = 0, 1, \dots, 2^v - 1$. Let \mathbf{c}_t and \mathbf{c}'_t denote the maximum likelihood (ML) path and an incorrect path starting from time 0 till time t , respectively. Assume that a comparison is being made at the state S_i between the ML path \mathbf{c}_t and an incorrect path \mathbf{c}'_t at time t . The probability that the ML path is correctly

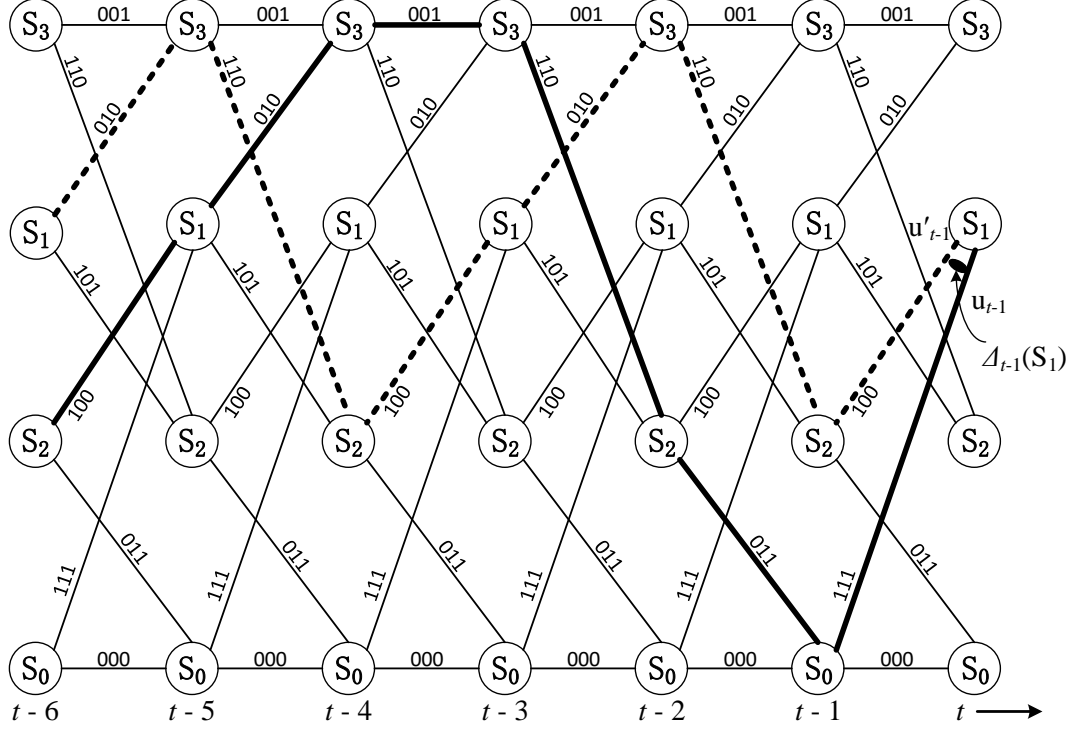


Figure 2.1: An illustration of the reliability vector update procedure for SOVA, where a (1, 3, 1) convolutional code is employed with the memory order $m = 1$ and the constraint length $v = 2$.

selected at time t , denoted by $P(C)$, is given by

$$P(C) = \frac{\Pr(\mathbf{c}_t|\mathbf{r})}{\Pr(\mathbf{c}_t|\mathbf{r}) + \Pr(\mathbf{c}'_t|\mathbf{r})}. \quad (2.2.5)$$

The L-value, or reliability, of this path decision is defined by

$$\Delta_{t-1}(S_i) = \ln \frac{P(C)}{1 - P(C)}. \quad (2.2.6)$$

Now we show how the reliability of a path decision is associated with the hard-decision outputs of a Viterbi decoder. First, consider the path decisions made at $\tau = m + 1$. The path decision at the state S_i has the reliability $\Delta_m(S_i)$ given by (2.2.6). The bits positions in which the two information sequences, that is, \mathbf{u}_m

corresponding to the codeword \mathbf{c}_m and \mathbf{u}'_m corresponding to the codeword \mathbf{c}'_m , differ are the error positions. At time $\tau = m + 1$, a reliability vector can be formed for the state S_i as

$$\mathbf{L}_{m+1}(S_i) = [L_0(S_i), L_1(S_i), \dots, L_m(S_i)], \quad (2.2.7)$$

where

$$L_\tau(S_i) = \begin{cases} \Delta_m(S_i), & \text{if } u_\tau \neq u'_\tau \\ \infty, & \text{if } u_\tau = u'_\tau \end{cases}, \quad \tau = 0, 1, \dots, m. \quad (2.2.8)$$

At time $\tau = m + 2$, the path decisions result in reliability $\Delta_{m+1}(S_i)$, and the reliability vector is given by

$$\mathbf{L}_{m+2}(S_i) = [L_0(S_i), L_1(S_i), \dots, L_{m+1}(S_i)]. \quad (2.2.9)$$

The reliability vector is updated by first determining $L_{m+1}(S_i)$ as in (2.2.8). For the remaining entries, the minimum of $\Delta_{m+1}(S_i)$ and the previous entry in the reliability vector will be taken. This updated procedure is repeated after each path decision. At time $\tau = t$, for the state S_i , the reliability vector is updated to

$$\mathbf{L}_t(S_i) = [L_0(S_i), L_1(S_i), \dots, L_{t-1}(S_i)], \quad (2.2.10)$$

where

$$L_\tau(S_i) = \begin{cases} \min [\Delta_{t-1}(S_i), L_\tau(S_i)], & \text{if } u_\tau \neq u'_\tau \\ L_\tau(S_i), & \text{if } u_\tau = u'_\tau \end{cases}, \quad \tau = 0, 1, \dots, t-1. \quad (2.2.11)$$

For ease of understanding, Fig. 2.1 is obtained from [42] to graphically illustrate the reliability vector update procedure of the SOVA. A $(1, 3, 1)$ convolutional code is employed with the memory order $m = 1$ and the constraint length $v = 2$. The “up” branch leaving each state represents an input 1, and the “down” branch represents an input 0.

Note that this review on SOVA is mainly adopted from [42, 43].

2.3 Lattices

Lattices are patterns of points with a periodic structure arranged in Euclidean space. Mathematically, we consider an infinite, discrete set of vectors (points) $\boldsymbol{\lambda}$ in Euclidean space \mathbb{R}^N [44], i.e.,

$$\Lambda = \{\boldsymbol{\lambda}\} \subset \mathbb{R}^N, \text{ with } \boldsymbol{\lambda} = \begin{bmatrix} l_1 \\ l_2 \\ \vdots \\ l_N \end{bmatrix}, \quad (2.3.1)$$

where Λ denotes an N -dimensional lattice. Due to the underlying Euclidean space, a lattice is endowed with attributes such as distances, volumes or shapes.

For the algebraic properties, a lattice is an abelian group under ordinary vector addition in \mathbb{R}^N . For Λ being a lattice, we have the following requirements:

$$\begin{aligned} \text{Closure:} \quad & \boldsymbol{\lambda}_i + \boldsymbol{\lambda}_j \in \Lambda, \forall \boldsymbol{\lambda}_i, \boldsymbol{\lambda}_j \in \Lambda \\ \text{Associativity:} \quad & (\boldsymbol{\lambda}_i + \boldsymbol{\lambda}_j) + \boldsymbol{\lambda}_k = \boldsymbol{\lambda}_i + (\boldsymbol{\lambda}_j + \boldsymbol{\lambda}_k) \\ \text{Identity:} \quad & \exists \mathbf{0} \in \Lambda \text{ with } \boldsymbol{\lambda}_i + \mathbf{0} = \mathbf{0} + \boldsymbol{\lambda}_i = \boldsymbol{\lambda}_i, \forall \boldsymbol{\lambda}_i \in \Lambda \\ \text{Inverse:} \quad & \exists -\boldsymbol{\lambda}_i \in \Lambda, \text{ with } \boldsymbol{\lambda}_i + (-\boldsymbol{\lambda}_i) = \mathbf{0}, \forall \boldsymbol{\lambda}_i \in \Lambda \\ \text{Commutativity:} \quad & \boldsymbol{\lambda}_i + \boldsymbol{\lambda}_j = \boldsymbol{\lambda}_j + \boldsymbol{\lambda}_i, \forall \boldsymbol{\lambda}_i, \boldsymbol{\lambda}_j \in \Lambda \end{aligned}$$

There exists a set of N linearly independent vectors \mathbf{x}_i . Because of the group structure, all lattice points $\boldsymbol{\lambda} \in \Lambda$ can be expressed as linear combinations of integer multiples and these basis vectors \mathbf{x}_i , i.e.,

$$\boldsymbol{\lambda} = \sum_{i=1}^N k_i \mathbf{x}_i, \quad k_i \in \mathbb{Z}. \quad (2.3.2)$$

The basis vectors have to be linearly independent and to span the N -space. Note that the choice of the basis vectors is not unique. It is common to combine the basis vectors \mathbf{g}_i as columns into a generator matrix, i.e.,

$$\mathbf{G}_\Lambda = [\mathbf{g}_1, \mathbf{g}_2, \dots, \mathbf{g}_N]. \quad (2.3.3)$$

With \mathbf{G}_Λ , the lattices can be specified as

$$\Lambda = \left\{ \mathbf{G}_\Lambda \begin{bmatrix} k_1 \\ \vdots \\ k_N \end{bmatrix} \middle| k_i \in \mathbb{Z}, i = 1, \dots, N \right\}. \quad (2.3.4)$$

Note, the generator matrix is not unique; any linear transformation of the basis vectors, which preserves the full rank of \mathbf{G}_Λ , can be used as well. In addition, for the combined scaling and translation operation, we write briefly,

$$a\Lambda + \mathbf{b} \triangleq (a\boldsymbol{\lambda} + \mathbf{b} | \boldsymbol{\lambda} \in \Lambda), \text{ with } a \in \mathbb{R}, \mathbf{b} \in \mathbb{R}^N. \quad (2.3.5)$$

Note that this review on lattices is mainly adopted from [44].

2.3.1 Lattice Network Coding

In addition, we briefly review some basic concepts of lattice network coding [11].

A coarse lattice Λ' is a subset of a fine lattice Λ , i.e., $\Lambda' \subset \Lambda$. The set of all the cosets of Λ' in Λ , denoted by Λ/Λ' , forms a partition of Λ .

For lattice codes, the message space \mathcal{W} is $\mathcal{W} = \Lambda/\Lambda'$.

The message rate for each user is defined as $R \triangleq \frac{1}{n} \log_2 |\mathcal{W}|$, where n is the code length and $|\mathcal{W}|$ is the cardinality of \mathcal{W} .

Let \mathbb{C} denote the complex number field. A map $\mathcal{Q}_\Lambda : \mathbb{C}^N \rightarrow \Lambda$ is defined as a nearest-lattice-point quantiser, which sends a point $\mathbf{x} \in \mathbb{C}^N$ to the nearest lattice point in Euclidean distance, i.e.,

$$\mathcal{Q}_\Lambda(\mathbf{x}) \triangleq \arg \min_{\boldsymbol{\lambda} \in \Lambda} \|\mathbf{x} - \boldsymbol{\lambda}\|. \quad (2.3.6)$$

Let $[\mathbf{s}] \bmod \Lambda$ denote the quantisation error of $\mathbf{x} \in \mathbb{C}^N$ with respect to the lattice Λ , and we have

$$[\mathbf{x}] \bmod \Lambda = \mathbf{x} - \mathcal{Q}_\Lambda(\mathbf{s}). \quad (2.3.7)$$

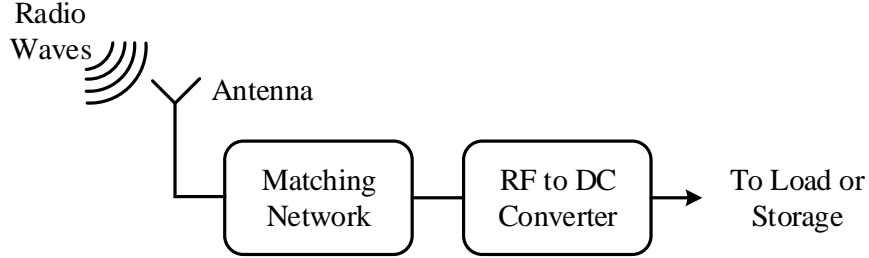


Figure 2.2: A typical RF energy receiver.

Let \mathcal{V} denote the fundamental Voronoi region of a lattice, which is the set of all points in \mathbb{C}^N that are closest to the zero vector,

$$\mathcal{V} = \{\mathbf{s} : \mathcal{Q}_\Lambda(\mathbf{s}) = 0\}. \quad (2.3.8)$$

2.4 RF Energy Transfer

RF energy transfer is a process of delivering energy by wireless from an energy transmitter to energy harvesting devices [45]. The features of RF energy transfer, namely lower-power and long-distance energy transfer, make it suitable for powering a large number of terminals spread over a relatively wide area. For the energy harvesting device, an energy scavenging module, in terms of an RF energy receiver, should be specifically designed to collaborate with RF energy transfer. Fig. 2.2 illustrates a typical RF energy receiver, which consists of a receiver antenna (or antenna array), a matching network, and an RF-to-direct current (DC) converter/rectifier [46]. The antenna can be designed to work on either single frequency or multiple frequency bands. The matching network is a resonator circuit operating at the designed frequency band to maximise the power transfer from the antenna to the RF-to-DC converter. The

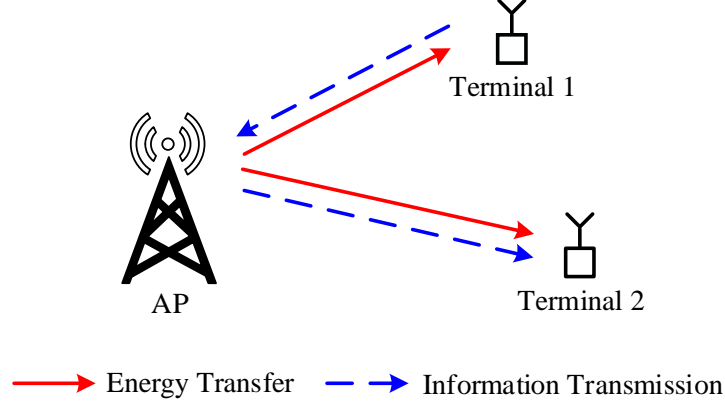


Figure 2.3: A conceptual network model of wireless-powered communication.

converter converts RF signals into DC voltage that can be used to either power the load directly or charge an energy storage. The conversion efficiency of the RF energy receiver depends on the accuracy of the impedance matching between the antenna and the converter, and the power efficiency of the converter that rectifies the received RF signals to DC voltage.

For the RF energy transfer, the amount of harvested energy, denoted by E_H , can be calculated based on the Friis equation [47] as

$$E_H = P_T \times G_T \times P_L \times G_R \times \eta \times \tau, \quad (2.4.1)$$

where P_T denotes the transmit power, G_T denotes the transmit antenna gain, P_L is the path loss, G_R is the receiver antenna gain, η is the RF-to-DC energy conversion efficiency and τ is the energy transfer duration.

2.5 Wireless-Powered Communication

Enabled by the RF energy transfer, a new research paradigm, named wireless-powered communication, can be established with no need for battery replacement. In wireless-powered communication networks, wireless terminals can harvest energy from RF signals radiated by dedicated energy transmitter(s) and use the harvested energy for information processing or transmission [27].

A conceptual network model of wireless-powered communication is presented in Fig. 2.3 with an AP and two terminals. There are two basic operation modes illustrated in Fig. 2.3. The first mode is that the AP transmits energy to Terminal 1 in the DL, and then Terminal 1 transmits information to the AP during the UL using the energy harvested in the DL. The second mode is the simultaneous information and energy transfer from the AP to Terminal 2. This dual utilisation of RF signals is referred to as SWIPT.

For more background information regarding RF energy transfer, please refer to Chapters 6 and 7.

Chapter 3

Multiple Interpretations for Multi-Source Multi-Destination Wireless Relay Network Coded Systems

In this chapter, a multi-source multi-destination wireless relay network coded system is investigated. To achieve multiple interpretations at different receivers, nested codes are constructed based on convolutional codes in the proposed system. Besides, an opportunistic scheduling (OS) technique is adopted at the relay to maximise the system capacity. The proposed system model combines the merits of both nested codes and the OS. First, I present the detailed coding process of the proposed scheme. Then, the upper bounds on the bit error probability of the schemes with and without the OS are derived. Finally, good codes are investigated for the considered system and simulations are carried out to validate the theoretical analysis.

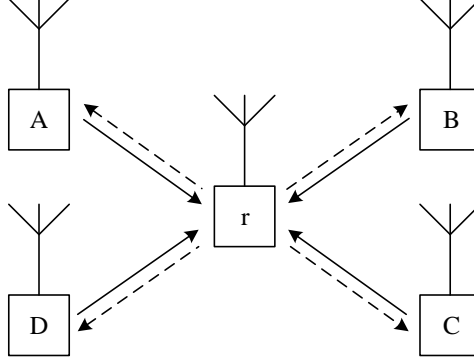


Figure 3.1: An example of the considered network coded system model.

3.1 System Model

Consider a network coding group, which consists of one relay and multiple sources and destinations. A source can also be a destination of other sources. It is assumed that all sources transmit to their respective destinations via the single relay and there are no direct links between the sources and their destinations. Besides, all sources/destinations in the network coding group are assumed to be within the communication range of the relay. Note that one source may have multiple destinations and let \mathfrak{D}_s denote the set of destinations of the source s , $\forall s \in \mathfrak{S}$, where \mathfrak{S} denotes the set of sources. Let $\mathfrak{D} \triangleq \bigcup_{s \in \mathfrak{S}} \mathfrak{D}_s$ denote the set of destinations.

It is assumed that all sources transmit different packets via orthogonal channels to the relay, and the relay broadcasts a combination of selected packets to a set of selected destinations based on an opportunistic scheduling (OS) technique [7]. This process will be made clear in the next section. It is also assumed that all the links, between sources and the relay and between the relay and destinations, experience independent quasi-static Rayleigh fading, i.e., the channel coefficients remain constant

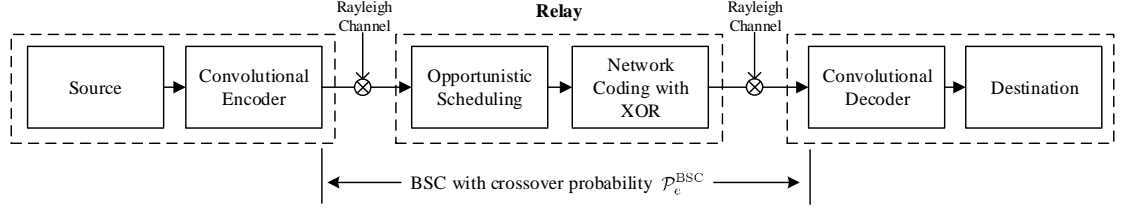


Figure 3.2: The coding process of the proposed network coded system.

over the length of one packet, but change independently from packet to packet [48]. Perfect channel state information (CSI) is assumed to be available at the relay side. Let boldface lowercase and uppercase letters denote vectors and matrices. Let \mathbf{i}_s and \mathbf{G}_s , $\forall s \in \mathfrak{S}$, denote the information sequence and the generator matrix of the source s , respectively. An example of the considered scenario is illustrated in Fig. 3.1, in which four sources transmit different packets to their destinations through the relay r . $\mathfrak{S} = \{A, B, C, D\}$. The sets of the destinations corresponding to the sources A , B , C , and D are denoted by \mathfrak{D}_A , \mathfrak{D}_B , \mathfrak{D}_C and \mathfrak{D}_D , respectively. \mathfrak{D}_s , $\forall s \in \{A, B, C, D\}$, can be an arbitrarily non-empty subset of $\{A, B, C, D\} \setminus s$.

3.2 Coding with Nested Codes and the OS

The coding process of the proposed network coded system is shown in Fig. 3.2. It can be observed that the entire process could be divided into three main parts: encoding with nested codes at sources, implementing the OS and network coding at the relay, and decoding with nested codes at destinations. In the following, we elaborate the three parts respectively.

3.2.1 Encoding with Nested Codes

Nested codes, which have been reviewed in Chapter 2, are employed in the considered network coding system. It is required that sources encode their respective information with different linear independent generators. In this chapter, it is assumed that an information sequence \mathbf{i} is encoded with a binary convolutional generator matrix \mathbf{G} . A coded packet sent by a source is \mathbf{iG} . A binary phase-shift keying (BPSK) modulation is assumed at each source side. Note that the modulator and demodulator corresponding to the BPSK are ignored in Fig. 3.2.

The relay can observe all the coded packets sent by sources. For simplicity, it is assumed that the relay makes hard decision on the coded packets received from sources. As an example, if the relay forwards a mixed packet of all the received packets to the destinations, recalling the coding structure of nested codes, we have

$$\mathbf{c}_{nested} = \mathbf{i}_1 \mathbf{G}_1 \oplus \mathbf{i}_2 \mathbf{G}_2 \oplus \cdots \oplus \mathbf{i}_{|\mathfrak{S}|} \mathbf{G}_{|\mathfrak{S}|} = [\mathbf{i}_1, \mathbf{i}_2, \cdots, \mathbf{i}_{|\mathfrak{S}|}] \begin{bmatrix} \mathbf{G}_1 \\ \mathbf{G}_2 \\ \vdots \\ \mathbf{G}_{|\mathfrak{S}|} \end{bmatrix}, \quad (3.2.1)$$

where \mathbf{c}_{nested} is the combination of all the coded packets from sources, \oplus denotes the XOR operation and $|\mathfrak{S}|$ denotes the cardinality of the set of sources. Note that $\mathbf{G}_1, \mathbf{G}_2, \cdots, \mathbf{G}_{|\mathfrak{S}|}$ are assumed to be mutually linearly independent.

3.2.2 The Opportunistic Scheduling (OS)

The instantaneous SNR of the link between the source s and the relay r at the time instant μ is given by [7]

$$\gamma_{sr}(\mu) = \frac{P |h_{sr}(\mu)|^2}{\sigma_{sr}^2}, \quad (3.2.2)$$

where P is the transmit power from each source, $h_{sr}(\mu)$ is the channel coefficient of the link between s and r at the time instant μ , and σ_{sr}^2 denotes the variance of the additive white Gaussian noise (AWGN).

The OS is an opportunistic selective mechanism by dynamically changing the set of destinations at the relay to maximise the system capacity. The relay can order the instantaneous SNRs of the links between the relay and the destinations into an ascending sequence, where the higher SNR is always placed after the smaller one. Let γ_k denote the k th instantaneous SNR in the sequence. The parameter k is named the *scheduling level* [49]. According to the OS, only the destinations whose instantaneous SNRs are equal to or higher than γ_k , will be selected. Then, the packets to be sent to the selected destinations will be selected by the relay. Let $N_d \triangleq |\mathfrak{D}|$ denote the cardinality of the set of destination nodes \mathfrak{D} . For the scheduling level k , the number of the selected destinations, denoted by N_k , should be $N_k = N_d - k + 1$. In this case, the instantaneous capacity per unit bandwidth can be expressed as

$$C_{inst}^k = N_k \log_2(1 + \gamma_k). \quad (3.2.3)$$

At the relay, the selected packets according to the OS are linearly combined by the XOR operation. Let $\mathfrak{S}_r, \mathfrak{S}_r \subseteq \mathfrak{S}$, denote the set of sources whose packets are selected to be forwarded. We can obtain a network coded packet with the OS at the relay as

$$\mathbf{c}_{nested}^{OS} = \bigoplus_{s \in \mathfrak{S}_r} \mathbf{i}_s \mathbf{G}_s = [\mathbf{i}_1, \mathbf{i}_2, \dots, \mathbf{i}_{|\mathfrak{S}_r|}] \begin{bmatrix} \mathbf{G}_1 \\ \mathbf{G}_2 \\ \vdots \\ \mathbf{G}_{|\mathfrak{S}_r|} \end{bmatrix}. \quad (3.2.4)$$

To adapt the maximised capacity by the OS, a class of rate-compatible punctured convolutional (RCPC) codes [50, 51] can be employed at the relay. The RCPC codes

are utilised to change the code rate of the network coded packet. If the maximum capacity exceeds a predetermined threshold, the RCPC codes with the highest puncturing rate can be employed. Otherwise, a lower puncturing rate should be considered. In this work, a convolutional code $(1, 3, 2)$ with the optimum distance spectrum is used as the parent code. The corresponding puncturing matrices of rates $1/3$, $2/5$, $2/4$ and $2/3$ are respectively chosen as [50]

$$\begin{aligned} \mathbf{P}_{1/3} &= \begin{bmatrix} 1 & 1 \\ 1 & 1 \\ 1 & 1 \end{bmatrix}, \quad \mathbf{P}_{2/5} = \begin{bmatrix} 1 & 1 \\ 1 & 1 \\ 1 & 0 \end{bmatrix}, \\ \mathbf{P}_{2/4} &= \begin{bmatrix} 1 & 1 \\ 1 & 1 \\ 0 & 0 \end{bmatrix}, \quad \mathbf{P}_{2/3} = \begin{bmatrix} 1 & 0 \\ 1 & 1 \\ 0 & 0 \end{bmatrix}. \end{aligned} \quad (3.2.5)$$

For ease of illustration, the effect of RCPC codes is ignored in the proposed network coding scheme by choosing the puncture rate to be the same as the parent code $1/3$.

3.2.3 Decoding with Nested Codes

At a destination, after the demodulator, a log-likelihood ratio or L-value of the i th bit in \mathbf{c}_{nested}^{OS} , denoted by $L_{\mathbf{c}_{nested}^{OS}(i)}$, can be obtained. Mathematically, we have

$$L_{\mathbf{c}_{nested}^{OS}(i)} = \ln \frac{\Pr(\mathbf{c}_{nested}^{OS}(i) = 0)}{\Pr(\mathbf{c}_{nested}^{OS}(i) = 1)}. \quad (3.2.6)$$

Because the destinations may possess some packets received at previous transmissions from the relay, i.e., prior knowledge, the codeword \mathbf{c}_{nested}^{OS} can be decomposed as

$$\mathbf{c}_{nested}^{OS} = \underbrace{\bigoplus_{l \notin \mathcal{K}_d} \mathbf{i}_l \mathbf{G}_l}_{\mathbf{c}_u} \oplus \underbrace{\bigoplus_{l' \in \mathcal{K}_d} \mathbf{i}_{l'} \mathbf{G}_{l'}}_{\mathbf{c}_c}, \quad (3.2.7)$$

where \mathcal{K}_d denotes the indices of the information prior known to the destination d , \mathbf{c}_u represents the collection of unknown information and \mathbf{c}_c is the collection of the

prior known information. By cancelling the prior knowledge \mathbf{c}_c , we can compute the L-value of the i th bit of \mathbf{c}_u by

$$L_{\mathbf{c}_u(i)} \triangleq \ln \frac{\Pr(\mathbf{c}_u(i) = 0)}{\Pr(\mathbf{c}_u(i) = 1)} = \begin{cases} L_{\mathbf{c}_{nested}^{OS}(i)} = \ln \frac{\Pr(\mathbf{c}_u \oplus \mathbf{c}_c(i)=0)}{\Pr(\mathbf{c}_u \oplus \mathbf{c}_c(i)=1)}, & \text{if } \mathbf{c}_c = 0, \\ -L_{\mathbf{c}_{nested}^{OS}(i)} = \ln \frac{\Pr(\mathbf{c}_u \oplus \mathbf{c}_c(i)=1)}{\Pr(\mathbf{c}_u \oplus \mathbf{c}_c(i)=0)}, & \text{if } \mathbf{c}_c = 1. \end{cases} \quad (3.2.8)$$

Note that there is no information loss via the above cancellation operation, because it only changes the sign of the L-value. The $L_{\mathbf{c}_u}$ is the estimated soft information of unknown packets to the destination d . A SOVA (see Chapter 2) then can be employed to extract the desired information with the L-value $L_{\mathbf{c}_u}$.

Note that in the case that the destination d has no prior knowledge, it still can decode all the information out based on $L_{\mathbf{c}_{nested}^{OS}}$, i.e., the L-value of the codeword \mathbf{c}_{nested}^{OS} , and the “stacked” generator matrix in the right-hand side of (3.2.4).

3.3 Analytical Bounds on the Bit Error Probability

In this section, an upper bound on the bit error probability for the proposed scheme is derived. To obtain a closed-form expression of the upper bound, as shown in Fig. 3.2, we regard the part between the output of the convolutional encoder and the input of the convolutional decoder, as a binary symmetric channel (BSC), which has a crossover probability $\mathcal{P}_e^{\text{BSC}}$.

We first derive the expression of the crossover probability $\mathcal{P}_e^{\text{BSC}}$. This probability will be used for the derivation of the bit error probability for the link from a source s to a destination d , and this will become evident later. Let $\mathcal{P}_c^{\text{XOR}}$ denote the correct bit transmission probability for the network coded packet at the relay. Let $\mathcal{P}_c^{r \rightarrow d}$

denote the correct bit transmission probability for the link from the relay r to the destination d before the convolutional decoder. Then, the crossover probability $\mathcal{P}_e^{\text{BSC}}$ can be expressed as

$$\mathcal{P}_e^{\text{BSC}} \leq 1 - \mathcal{P}_c^{\text{XOR}} \mathcal{P}_c^{r \rightarrow d}. \quad (3.3.1)$$

Due to the OS at the relay, only the packets from the sources in the set \mathfrak{S}_r will be selected and network coded. Since the probability that different packets suffer from bit errors at the same positions is very small, especially at high SNR, the correct bit transmission probability for the network coded packet can be approximated as

$$\mathcal{P}_c^{\text{XOR}} \approx \prod_{s \in \mathfrak{S}_r} \mathcal{P}_c^{s \rightarrow r}, \quad (3.3.2)$$

where $\mathcal{P}_c^{s \rightarrow r}$ is the correct bit transmission probability for the link from s to r . For an uncoded BPSK modulation over a Rayleigh fading channel, the correct bit transmission probability of $\mathcal{P}_c^{s \rightarrow r}$ can be expressed as [52]

$$\begin{aligned} \mathcal{P}_c^{s \rightarrow r} &= 1 - \mathcal{P}_e^{s \rightarrow r} \\ &\geq 1 - \frac{1}{2} \left(1 - \sqrt{\frac{\bar{\gamma}_{sr} R_1}{1 + \bar{\gamma}_{sr} R_1}} \right) \\ &= \frac{1}{2} \left(1 + \sqrt{\frac{\bar{\gamma}_{sr} R_1}{1 + \bar{\gamma}_{sr} R_1}} \right), \end{aligned} \quad (3.3.3)$$

where $\mathcal{P}_e^{s \rightarrow r}$ is the bit error probability for the link from s to r . $\bar{\gamma}_{sr}$ is the average SNR for the link from s to r . R_1 is the code rate of the convolutional encoder at the source s .

Let $\mathcal{P}_e^{r \rightarrow d}$ denote the bit error probability for the link from r to d . Then, the correct bit transmission probability $\mathcal{P}_c^{r \rightarrow d}$ can be expressed as

$$\mathcal{P}_c^{r \rightarrow d} = 1 - \mathcal{P}_e^{r \rightarrow d}. \quad (3.3.4)$$

With the consideration of RCPC codes over the link from r to d , $\mathcal{P}_e^{r \rightarrow d}$ can be upper

bounded by [53–55],

$$\mathcal{P}_e^{r \rightarrow d} \leq \frac{1}{p} \sum_{\varphi=d'_{free}}^{\infty} c_{\varphi} P_{\varphi}, \quad (3.3.5)$$

where p is the puncturing period, d'_{free} is the free distance of the RCPC codes, c_{φ} is the total number of bit errors for different incorrect track paths at distance φ , and P_{φ} is the pairwise error probability. For the BPSK modulation over a quasi-static Rayleigh fading channel with perfect channel estimation and soft decision decoding at the receiver, P_{φ} can be written by

$$P_{\varphi} = q^{\varphi} \sum_{\delta=0}^{\varphi-1} \binom{\varphi-1+\delta}{\delta} (1-q)^{\delta}, \quad (3.3.6)$$

with

$$q = \frac{1}{2} \left(1 - \sqrt{\frac{\bar{\gamma}_{rd} R_2}{1 + \bar{\gamma}_{rd} R_2}} \right), \quad (3.3.7)$$

where $\bar{\gamma}_{rd}$ is the average SNR for the link from r to d and R_2 is the code rate of the employed RCPC code. Inserting (3.3.5) into (3.3.4), we can obtain a lower bound on $\mathcal{P}_e^{r \rightarrow d}$. Inserting this lower bound and (3.3.2) into (3.3.1), we then obtain an upper bound on the crossover probability of $\mathcal{P}_e^{\text{BSC}}$.

Subsequently, by treating the channel between the source s and the destination d as a BSC channel with the crossover probability $\mathcal{P}_e^{\text{BSC}}$, referring to [56], we can have an upper bound on the bit error probability for the convolutional coded link from the source s to the destination d , i.e., from the input of the convolutional encoder to the output of the convolutional decoder, as

$$\mathcal{P}_e^{s \rightarrow d} < \frac{1}{m} \sum_{\varphi=d'_{free}}^{\infty} a_{\varphi} \left(4 \mathcal{P}_e^{\text{BSC}} (1 - \mathcal{P}_e^{\text{BSC}}) \right)^{\frac{\varphi}{2}}, \quad (3.3.8)$$

where m is the number of message bits fed to the convolutional encoder at the source s , d'_{free} is the free distance of the convolutional code, and a_{φ} is the number of paths at a distance φ from the all-zero path. It is worth noting that since the process of the

cancellation at the destination only discards the known information from the received network coded packet, it will not change the degree of error and the packet's length. Therefore, the crossover probability for BSC is still $\mathcal{P}_e^{\text{BSC}}$ after the cancellation process at destinations.

Finally, a closed-form expression of the upper bound for the bit error probability of the proposed scheme with the OS can be written by

$$\begin{aligned}
 \mathcal{P}_e^{s \rightarrow d} &< \frac{1}{m} \sum_{\varphi=d'_{free}}^{\infty} a_{\varphi} 2^{\varphi} \left(1 - \frac{1}{p} \sum_{\varphi=d'_{free}}^{\infty} c_{\varphi} q^{\varphi} \sum_{\delta=0}^{\varphi-1} \binom{\varphi-1+\delta}{\delta} (1-q)^{\delta} \right)^{\frac{\varphi}{2}} \\
 &\times \left(\prod_{s \in \mathfrak{S}_r} \frac{1}{2} \left(1 + \sqrt{\frac{\bar{\gamma}_{sr} R_1}{1 + \bar{\gamma}_{sr} R_1}} \right) \right)^{\frac{\varphi}{2}} \\
 &\times \left(1 - \left(1 - \frac{1}{p} \sum_{\varphi=d'_{free}}^{\infty} c_{\varphi} q^{\varphi} \sum_{\delta=0}^{\varphi-1} \binom{\varphi-1+\delta}{\delta} (1-q)^{\delta} \right) \right) \\
 &\times \prod_{s \in \mathfrak{S}_r} \frac{1}{2} \left(1 + \sqrt{\frac{\bar{\gamma}_{sr} R_1}{1 + \bar{\gamma}_{sr} R_1}} \right)^{\frac{\varphi}{2}}, \tag{3.3.9}
 \end{aligned}$$

where q is given by (3.3.7). Analogically, we can obtain the upper bound for the bit error probability of the scheme without the OS by replacing \mathfrak{S}_r with \mathfrak{S} in (3.3.9).

3.4 Code Search

In this section, code criteria are first designed for the proposed scheme and a class of good codes is then constructed.

To achieve multiple interpretations with nested codes, the code design is assumed to satisfy the following criteria:

1. The generators assigned to different sources should be mutually linearly independent.

Table 3.1: Good nested codes			
Rate	Memory Number	Generator Matrices	d_{free}
2/3	2	$\begin{pmatrix} 6 & 5 & 1 \\ 7 & 2 & 5 \end{pmatrix}_8$	5
2/4	2	$\begin{pmatrix} 3 & 7 & 1 & 6 \\ 4 & 7 & 6 & 3 \end{pmatrix}_8$	8
3/4	2	$\begin{pmatrix} 5 & 4 & 3 & 2 \\ 4 & 6 & 5 & 5 \\ 6 & 1 & 4 & 3 \end{pmatrix}_8$	6
4/6	2	$\begin{pmatrix} 5 & 6 & 5 & 6 & 7 & 4 \\ 7 & 0 & 7 & 3 & 6 & 2 \\ 4 & 5 & 2 & 6 & 5 & 0 \\ 6 & 1 & 5 & 7 & 2 & 5 \end{pmatrix}_8$	8

2. The rate of “stacked” generator matrix should be less than 1.
3. For convolutional codes, the “stacked” generator matrix should have large d_{free} so that a desired error performance can be achieved.

According to the designed criteria, several good nested codes are selected from [57], which are presented in Table 3.1. Then, we can choose different rows of one generator matrix as different linearly independent generators. In this chapter, I choose a rate 4/6 code from Table 3.1 for simulations. Table 3.2, shown in the following page, illustrates the code performance of the selected 4/6 code, which is analysed by Matlab.

3.5 Simulation Results

In this section, simulation results are presented to show the performance of the OS and nested codes. In the simulations, the network shown in Fig. 3.1 is considered. All the sources and the relay are assumed with the same transmit power P . All the links are assumed to be quasi-static Rayleigh fading channels. The variance of AWGN

Table 3.2: The performance analysis of the selected 4/6 code.

Rate	Generator Matrices	d_{free}	$\frac{c_\varphi _{\varphi=(d_{free}+i)}}{a_\varphi _{\varphi=(d_{free}+i)}}$						
			$i = 0$	$i = 1$	$i = 2$	$i = 3$	$i = 4$	$i = 5$	$i = 6$
1/6	$\begin{pmatrix} 5 & 6 & 5 & 6 & 7 & 4 \\ 7 & 0 & 7 & 3 & 6 & 2 \end{pmatrix}_8$	12	$\frac{1}{1}$	$\frac{0}{0}$	$\frac{0}{0}$	$\frac{0}{0}$	$\frac{2}{1}$	$\frac{0}{0}$	$\frac{5}{2}$
	$\begin{pmatrix} 7 & 0 & 7 & 3 & 6 & 2 \\ 4 & 5 & 2 & 6 & 5 & 0 \end{pmatrix}_8$	10	$\frac{2}{1}$	$\frac{1}{1}$	$\frac{0}{0}$	$\frac{3}{1}$	$\frac{0}{0}$	$\frac{0}{0}$	$\frac{8}{2}$
	$\begin{pmatrix} 4 & 5 & 2 & 6 & 5 & 0 \\ 6 & 1 & 5 & 7 & 2 & 5 \end{pmatrix}_8$	8	$\frac{1}{1}$	$\frac{0}{0}$	$\frac{0}{0}$	$\frac{0}{0}$	$\frac{2}{1}$	$\frac{0}{0}$	$\frac{2}{1}$
	$\begin{pmatrix} 6 & 1 & 5 & 7 & 2 & 5 \\ 5 & 6 & 5 & 6 & 7 & 4 \end{pmatrix}_8$	11	$\frac{1}{1}$	$\frac{0}{0}$	$\frac{0}{0}$	$\frac{0}{0}$	$\frac{0}{0}$	$\frac{4}{2}$	$\frac{0}{0}$
2/6	$\begin{pmatrix} 5 & 6 & 5 & 6 & 7 & 4 \\ 7 & 0 & 7 & 3 & 6 & 2 \end{pmatrix}_8$	9	$\frac{5}{2}$	$\frac{18}{4}$	$\frac{14}{4}$	$\frac{19}{5}$	$\frac{87}{14}$	$\frac{200}{26}$	$\frac{374}{48}$
	$\begin{pmatrix} 5 & 6 & 5 & 6 & 7 & 4 \\ 4 & 5 & 2 & 6 & 5 & 0 \end{pmatrix}_8$	8	$\frac{3}{2}$	$\frac{0}{0}$	$\frac{10}{3}$	$\frac{0}{0}$	$\frac{40}{12}$	$\frac{0}{0}$	$\frac{131}{28}$
	$\begin{pmatrix} 5 & 6 & 5 & 6 & 7 & 4 \\ 6 & 1 & 5 & 7 & 2 & 5 \end{pmatrix}_8$	9	$\frac{2}{1}$	$\frac{0}{0}$	$\frac{7}{3}$	$\frac{13}{4}$	$\frac{11}{3}$	$\frac{40}{9}$	$\frac{68}{12}$
	$\begin{pmatrix} 7 & 0 & 7 & 3 & 6 & 2 \\ 4 & 5 & 2 & 6 & 5 & 0 \end{pmatrix}_8$	8	$\frac{1}{1}$	$\frac{2}{1}$	$\frac{5}{2}$	$\frac{9}{4}$	$\frac{9}{3}$	$\frac{24}{7}$	$\frac{26}{7}$
	$\begin{pmatrix} 7 & 0 & 7 & 3 & 6 & 2 \\ 6 & 1 & 5 & 7 & 2 & 5 \end{pmatrix}_8$	8	$\frac{2}{1}$	$\frac{0}{0}$	$\frac{4}{2}$	$\frac{16}{6}$	$\frac{24}{6}$	$\frac{24}{6}$	$\frac{28}{6}$
	$\begin{pmatrix} 4 & 5 & 2 & 6 & 5 & 0 \\ 6 & 1 & 5 & 7 & 2 & 5 \end{pmatrix}_8$	8	$\frac{1}{1}$	$\frac{2}{1}$	$\frac{0}{0}$	$\frac{9}{4}$	$\frac{2}{1}$	$\frac{10}{3}$	$\frac{48}{12}$
3/6	$\begin{pmatrix} 5 & 6 & 5 & 6 & 7 & 4 \\ 7 & 0 & 7 & 3 & 6 & 2 \\ 4 & 5 & 2 & 6 & 5 & 0 \end{pmatrix}_8$	8	$\frac{8}{3}$	$\frac{42}{10}$	$\frac{95}{18}$	$\frac{208}{35}$	$\frac{580}{88}$	$\frac{1744}{228}$	$\frac{4971}{570}$
	$\begin{pmatrix} 5 & 6 & 5 & 6 & 7 & 4 \\ 7 & 0 & 7 & 3 & 6 & 2 \\ 6 & 1 & 5 & 7 & 2 & 5 \end{pmatrix}_8$	8	$\frac{2}{1}$	$\frac{29}{7}$	$\frac{102}{19}$	$\frac{162}{30}$	$\frac{349}{55}$	$\frac{1218}{162}$	$\frac{3622}{429}$
	$\begin{pmatrix} 5 & 6 & 5 & 6 & 7 & 4 \\ 4 & 5 & 2 & 6 & 5 & 0 \\ 6 & 1 & 5 & 7 & 2 & 5 \end{pmatrix}_8$	8	$\frac{10}{3}$	$\frac{42}{11}$	$\frac{75}{13}$	$\frac{214}{34}$	$\frac{527}{76}$	$\frac{1612}{205}$	$\frac{4644}{545}$
	$\begin{pmatrix} 7 & 0 & 7 & 3 & 6 & 2 \\ 4 & 5 & 2 & 6 & 5 & 0 \\ 6 & 1 & 5 & 7 & 2 & 5 \end{pmatrix}_8$	8	$\frac{9}{4}$	$\frac{15}{4}$	$\frac{24}{7}$	$\frac{90}{23}$	$\frac{285}{51}$	$\frac{845}{135}$	$\frac{2294}{313}$
4/6	$\begin{pmatrix} 5 & 6 & 5 & 6 & 7 & 4 \\ 7 & 0 & 7 & 3 & 6 & 2 \\ 4 & 5 & 2 & 6 & 5 & 0 \\ 6 & 1 & 5 & 7 & 2 & 5 \end{pmatrix}_8$	8	$\frac{76}{15}$	$\frac{782}{97}$	$\frac{2571}{269}$	$\frac{11049}{973}$	$\frac{49770}{3841}$	$\frac{211356}{14646}$	$\frac{917121}{57026}$

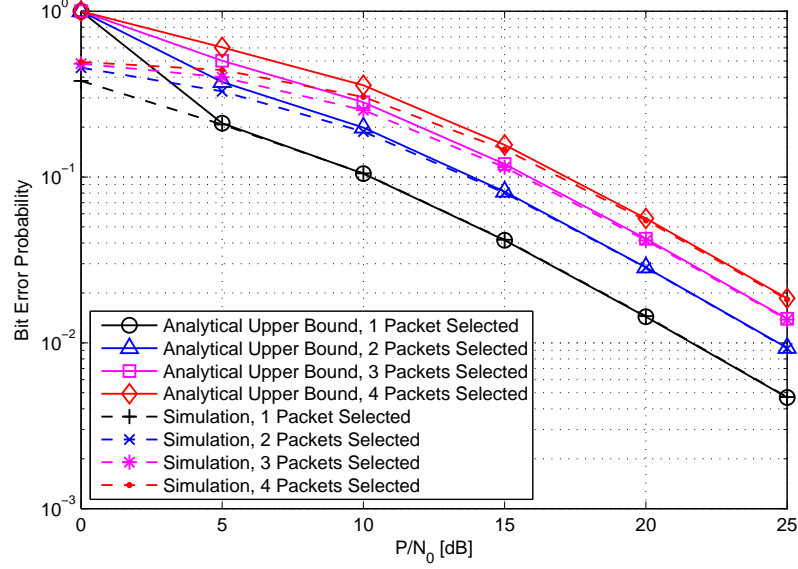


Figure 3.3: The bit error probability of the received network coded packet before the convolutional decoder at a destination under different OS selections.

is normalised to be unit. For the sources A , B , C and D , based on Table 3.2, it is assumed that

$$\begin{aligned}
 \mathbf{G}_A &= [5 \ 6 \ 5 \ 6 \ 7 \ 4]_8, \\
 \mathbf{G}_B &= [7 \ 0 \ 7 \ 3 \ 6 \ 2]_8, \\
 \mathbf{G}_C &= [4 \ 5 \ 2 \ 6 \ 5 \ 0]_8, \\
 \mathbf{G}_D &= [6 \ 1 \ 5 \ 7 \ 2 \ 5]_8.
 \end{aligned} \tag{3.5.1}$$

The rate of RCPC codes is chosen to be $1/3$. To compare the performance of the proposed system to that without the OS, a fixed scheduling with the fixed level $k = 1$ is also considered.

Fig. 3.3 illustrates the derived analytical upper bounds and simulation results on the bit error probability under different OS selections. The bit error probability performance considered here is that of the received network coded packet before the

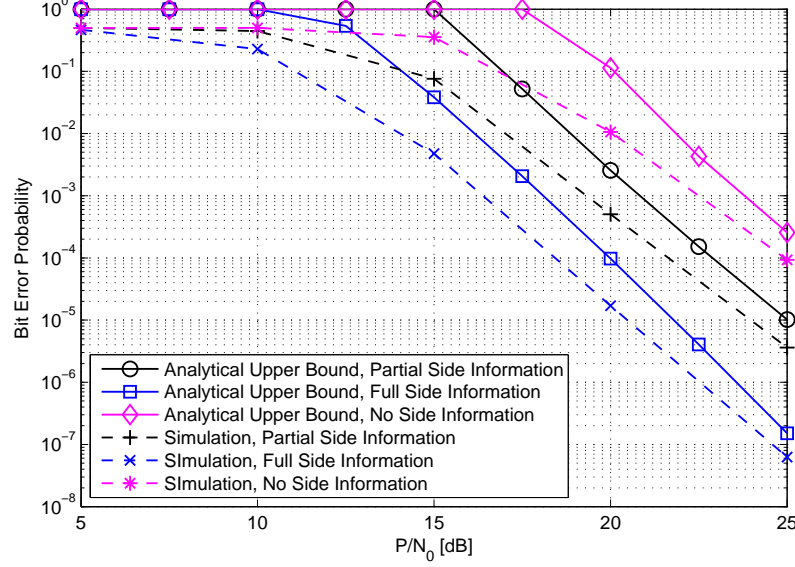


Figure 3.4: The performance of nested codes with different side information when the OS level $k = 1$ and the RCPC code rate is $1/3$.

convolutional decoder at a destination, namely $\mathcal{P}_e^{\text{BSC}}$ in (3.3.1). The different OS selections means that the number of selected packets is different. In general, the larger scheduling level k corresponds to the fewer packets selected by the OS at the relay. It can be observed from Fig. 3.3 that the derived upper bounds are tight at medium and high SNRs. Also, it is shown that the schemes with the OS, i.e., $k > 1$ and less than 4 packets are selected, always have better performance on the bit error probability than that of the case without the OS, i.e., $k = 1$ and 4 packets are selected.

Fig. 3.4 shows the simulation and analytical results when the scheduling level k is fixed to 1, and the RCPC code rate is $1/3$. The bit error probability considered here is $\mathcal{P}_e^{s \rightarrow d}$ in (3.3.9) at a destination. Without loss of generality, we choose an arbitrary destination and assume three different situations for this node, which are full side information, partial side information and no side information. For example, if it is

assumed that the source A transmits to the destination C , then the situation with full side information for the node C means that C has the prior knowledge of \mathbf{i}_B and \mathbf{i}_D . Similarly, partial side information means that C has one of \mathbf{i}_B and \mathbf{i}_D , and no side information means that C only knows its own information \mathbf{i}_C .

It is indicated in Fig. 3.4 that the node with full side information has the best performance on the bit error probability. In contrast, when it only knows its own information, it performs worst. This is due to the correlation between the amount of prior knowledge and the performance of different corresponding generator matrices. Specifically, the destinations with less prior knowledge correspond to the larger “stacking” generator matrices. The larger “stacking” generator matrix generally has a worse error performance. Moreover, it can be observed in Fig. 3.4 that the analytical upper bounds are loose at low SNR and become tight with the increase of SNR.

Chapter 4

Novel Nested Convolutional Lattice Codes for Multi-Way Relaying Systems over Fading Channels

In this chapter, I focus on the realisation of multiple interpretations with a high spectrum efficiency in a multi-way relay channel (MWRC) with fading, where multiple sources communicate with each other with the help of a relay. I first propose a class of nested convolutional lattice codes (NCLC) over a finite field, which can achieve the multiple interpretations for each source in two time slots. Then a theoretical upper bound on word error rate (WER) is derived for the NCLC. I further develop code design criteria by minimising the derived WER. Simulation results show that the proposed code can realise multiple interpretations for each source in two time slots and the derived upper bound is asymptotically tight with the increase of the normalised signal-to-effective-noise ratio ($SENR_{norm}$).

4.1 System Model and Preliminaries

In this section, the system model of a MWRC will be discussed first and then the nested convolutional codes over a finite field are presented.

Consider a network coding group, which consists of one relay node and a set of source nodes, as shown in Fig. 4.1, where r denotes the relay node and $[s_1, s_2, \dots, s_L]$ denote the sources nodes. All sources are receivers as well. The simplified coding process of the proposed scheme is summarised into the following steps:

1. All sources generate different information messages and encode the messages with mutually linearly independent generators.
2. At the transmitter side, each source maps the coded message onto an element of a lattice.
3. The lattice codewords from different source nodes are transmitted within the same frequency band simultaneously in one time slot.
4. The relay observes the superposition of the lattice codewords, and demodulates it to obtain a lattice-based network coded packet.

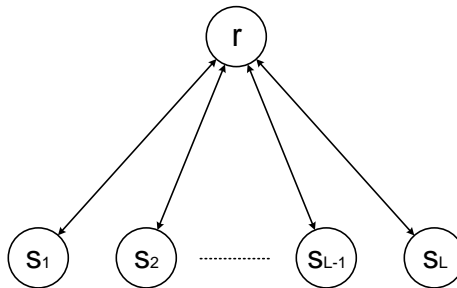


Figure 4.1: The system model of a MWRC.

5. The relay node broadcasts the lattice-based network coded packet to the different source nodes via fading channels in the second time slot.
6. Each source's receiver extracts the information messages of the other sources from the received lattice-based network coded packet forwarded by the relay.

Let \mathbb{R} denote the real number field, let \mathbb{C} denote the complex number field, let \mathbb{Z} denote the integer and let \oplus denote the addition over a finite field. Moreover, let boldface lowercase and uppercase letters denote vectors and matrices, respectively. Let \mathbb{F}_q denote the finite field of size q , where q is assumed to be prime. Let \mathbf{w}_ℓ be the message vector that each of its element is generated independently and uniformly over the \mathbb{F}_q by the source node s_ℓ , $\forall \ell \in \{1, \dots, L\}$. Let \mathbf{G}_ℓ denote the generator matrix with each of its element over \mathbb{F}_q at the source node s_ℓ . Let \mathbf{G}^T denote the transpose of \mathbf{G} .

The nested convolutional codes over \mathbb{F}_q are developed based on the nested codes [8, 58] and non-binary convolutional codes. The mathematical operation of the nested convolutional codes over \mathbb{F}_q can be expressed by

$$\mathbf{w}_1 \mathbf{G}_1 \oplus \mathbf{w}_2 \mathbf{G}_2 \oplus \dots \oplus \mathbf{w}_L \mathbf{G}_L = [\mathbf{w}_1, \mathbf{w}_2, \dots, \mathbf{w}_L] [\mathbf{G}_1, \mathbf{G}_2, \dots, \mathbf{G}_L]^T, \quad (4.1.1)$$

where $\mathbf{G}_1, \mathbf{G}_2, \dots, \mathbf{G}_L$ are mutually linearly independent generators of q -ary convolutional codes.

4.2 Nested Convolutional Lattice Codes (NCLC)

Let w be a complex number so that the ring of integers $\mathbb{Z}[w] \triangleq \{a + bw | a, b \in \mathbb{Z}\}$ is a principle ideal domain. In this chapter, a $\mathbb{Z}[w]$ -lattice is defined as [11],

$$\Lambda = \left\{ \boldsymbol{\lambda} = \mathbf{G}_\Lambda \mathbf{c} : \mathbf{c} \in \mathbb{Z}[w]^N \right\}, \quad (4.2.1)$$

where a lattice generator matrix $\mathbf{G}_\Lambda \in \mathbb{C}^{N \times N}$ is full rank and N is the number of dimensions. Let Λ' denote a coarse lattice, which is a subset of a fine lattice Λ , i.e., $\Lambda' \subset \Lambda$. Let the message space be $\mathcal{W} = \Lambda/\Lambda'$, where Λ/Λ' denotes the set of all the cosets of Λ' in Λ . The message space is a collection of lattice points that the message can be mapped onto. For the NCLC, the coded message $\mathbf{w}_\ell \mathbf{G}_\ell$ is assumed to be uniformly distributed on the lattice points within the message space \mathcal{W} by a mapping process. Besides, let $F_q(\mathbf{w})$ be an operation over \mathbb{F}_q and let $F_{\Lambda'}(\boldsymbol{\lambda})$ be an operation over the fundamental Voronoi region of Λ' (see Chapter 2), denoted by $\mathcal{V}(\Lambda')$, where $\mathbf{w} \in \mathbb{F}_q$ and $\boldsymbol{\lambda} \in \Lambda$. We can have

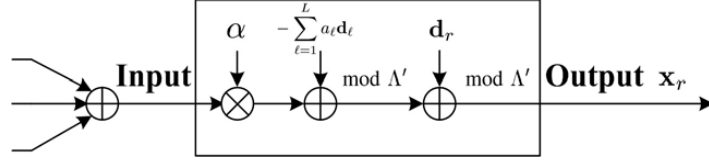
$$\begin{aligned} F_q(\mathbf{w}) &= [\mathbf{w}] \bmod q, \quad F_{\Lambda'}(\boldsymbol{\lambda}) = [\boldsymbol{\lambda}] \bmod \Lambda', \\ F_{\Lambda'}(\boldsymbol{\lambda}) &= \psi(F_q(\mathbf{w})), \quad \text{and} \quad F_q(\mathbf{w}) = \psi^{-1}(F_{\Lambda'}(\boldsymbol{\lambda})), \end{aligned} \quad (4.2.2)$$

where $\psi(\cdot)$ denotes a map labeling the message over \mathbb{F}_q to the points over $\mathcal{V}(\Lambda')$ and $\psi^{-1}(\cdot)$ denotes the inverse process.

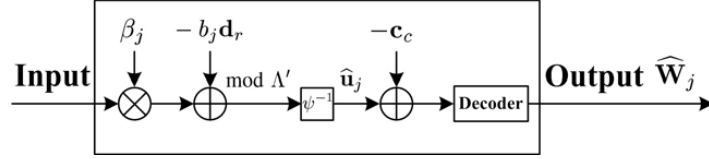
At each transmitter side, we have

$$\mathbf{t}_\ell = \psi(\mathbf{w}_\ell \mathbf{G}_\ell) \quad \text{and} \quad \mathbf{x}_\ell = [\mathbf{t}_\ell + \mathbf{d}_\ell] \bmod \Lambda', \quad (4.2.3)$$

where \mathbf{t}_ℓ denotes the coded message mapped on the fine lattice points. \mathbf{d}_ℓ is a dither vector at the ℓ th node, which is generated independently according to a uniform distribution over $\mathcal{V}(\Lambda')$. \mathbf{x}_ℓ denotes the transmitted lattice signal, which is subject to



(a) The lattice network coding process at the relay node.

(b) The decoding process at the receiver of s_j .Figure 4.2: Processes of the NCLC at the relay node and the source node s_j .

an average power constraint given by

$$\frac{1}{n} \mathbb{E} [\|\mathbf{x}_\ell\|^2] \leq P, \quad (4.2.4)$$

where n is the coded message length.

At the relay node, the input of the relay can be expressed as

$$\mathbf{y}_{sr} = \sum_{\ell=1}^L h_\ell \mathbf{x}_\ell + \mathbf{z}_{sr}. \quad (4.2.5)$$

Fig. 4.2(a) shows the lattice network coding process at the relay node. According to the lattice-partition-based compute-and-forward scheme proposed by Nazer and Gastpar [9], we choose a scale factor $\alpha \in \mathbb{C}$ and a coefficient vector $\mathbf{a} \triangleq (a_1, a_2, \dots, a_L)$

with $\mathbf{a} \in \Lambda$. We then obtain

$$\begin{aligned} \alpha \mathbf{y}_{sr} &= \sum_{\ell=1}^L \alpha h_\ell \mathbf{x}_\ell + \alpha \mathbf{z}_{sr} \\ &= \sum_{\ell=1}^L a_\ell \mathbf{x}_\ell + \underbrace{\sum_{\ell=1}^L (\alpha h_\ell - a_\ell) \mathbf{x}_\ell}_{\mathbf{n}} + \alpha \mathbf{z}_{sr} \\ &= \sum_{\ell=1}^L a_\ell \mathbf{x}_\ell + \mathbf{n}, \end{aligned} \quad (4.2.6)$$

where h_ℓ is the channel coefficient of the link between the source s_ℓ and the relay r

and \mathbf{z}_{sr} represents a vector of AWGN samples, in which each element is an AWGN with a zero mean and one-sided variance σ^2 . Refer to [9], α is derived as

$$\alpha = \frac{P_s \mathbf{h}^H \mathbf{a}}{P_s \|\mathbf{h}\|^2 + N_0}, \quad (4.2.7)$$

where P_s is the transmit power at each source node, \mathbf{h}^H denotes the Hermitian transpose of \mathbf{h} and N_0 is the average noise power. To remove dithers under the power constraint, we have

$$\begin{aligned} & \left[\alpha \mathbf{y}_{sr} - \sum_{\ell=1}^L a_\ell \mathbf{d}_\ell \right] \bmod \Lambda' \\ &= \left[\sum_{\ell=1}^L a_\ell \mathbf{x}_\ell + \mathbf{n} - \sum_{\ell=1}^L a_\ell \mathbf{d}_\ell \right] \bmod \Lambda' \\ &= \left[\sum_{\ell=1}^L a_\ell \mathbf{t}_\ell + \mathbf{n} \right] \bmod \Lambda', \end{aligned} \quad (4.2.8)$$

It is worth pointing out that $\sum_{\ell=1}^L a_\ell \mathbf{t}_\ell$ and \mathbf{n} are independent in the above equation. Now, we have the lattice network coded packet that should be broadcast by the relay to the source nodes under the power constraint, i.e.,

$$\begin{aligned} \mathbf{x}_r &= \left[\left[\sum_{\ell=1}^L a_\ell \mathbf{t}_\ell + \mathbf{n} \right] \bmod \Lambda' + \mathbf{d}_r \right] \bmod \Lambda' \\ &= \left[\sum_{\ell=1}^L a_\ell \mathbf{t}_\ell + \mathbf{n} + \mathbf{d}_r \right] \bmod \Lambda', \end{aligned} \quad (4.2.9)$$

where \mathbf{d}_r is a dither vector generated at the relay, which is made available at each source node. According to [59], since $\sum_{\ell=1}^L a_\ell \mathbf{t}_\ell$ and \mathbf{n} are independent, we can obtain that \mathbf{x}_r and \mathbf{n} are independent.

At the receiver side, as shown in Fig. 4.2(b), a source node s_j , $j \in \{1, \dots, L\} \setminus \ell$, receives the lattice network coded packet from the relay node, i.e.,

$$\begin{aligned} \mathbf{y}_{rs_j} &= h_j \mathbf{x}_r + \mathbf{z}_{rs_j} \\ &= h_j \left(\left[\sum_{\ell=1}^L a_\ell \mathbf{t}_\ell + \mathbf{n} + \mathbf{d}_r \right] \bmod \Lambda' \right) + \mathbf{z}_{rs_j}. \end{aligned} \quad (4.2.10)$$

where h_j is the channel coefficient of the link between the relay r and the source s_j and \mathbf{z}_{rs_j} represents a vector of AWGN samples, in which each element is an AWGN with a zero mean and one-sided variance σ^2 . Then, we remove the dithers at the j th receiver node by choosing a scalar $\beta_j \in \mathbb{C}$ and a coefficient $b_j \in \Lambda$, i.e.,

$$\begin{aligned}
& [\beta_j \mathbf{y}_{rs_j} - b_j \mathbf{d}_r] \bmod \Lambda' \\
&= [\beta_j h_j \mathbf{x}_r + \beta_j \mathbf{z}_{rs_j} - b_j \mathbf{d}_r] \bmod \Lambda' \\
&= [b_j \mathbf{x}_r + (\beta_j h_j - b_j) \mathbf{x}_r + \beta_j \mathbf{z}_{rs_j} - b_j \mathbf{d}_r] \bmod \Lambda' \\
&= \left[b_j \sum_{\ell=1}^L a_\ell \mathbf{t}_\ell + \underbrace{b_j \mathbf{n} + (\beta_j h_j - b_j) \mathbf{x}_r + \beta_j \mathbf{z}_{rs_j}}_{\mathbf{m}_j} \right] \bmod \Lambda' \\
&= \left[b_j \sum_{\ell=1}^L a_\ell \mathbf{t}_\ell + \mathbf{m}_j \right] \bmod \Lambda',
\end{aligned} \tag{4.2.11}$$

where the optimal coefficient b_j should be chosen to be close to the channel coefficient according to [9]. The optimal β_j is given by the following theorem,

Theorem 4.1. *The optimal scale factor β_j should be chosen to maximise the signal-to-effective-noise ratio (SENR) of Eq. (4.2.11). Given the assumption that the minimum mean square error (MMSE) decoder is employed at each receiver, β_j can be obtained by*

$$\beta_j = \frac{b_j P_r h_j}{P_r |h_j|^2 + N_0}, \tag{4.2.12}$$

where P_r is the transmit power from the relay.

Proof. See Appendix A.1. □

Now, we can estimate the desired linearly combination at the source node s_j by

reversely mapping the lattice-based network coded packet to the finite field, i.e.,

$$\begin{aligned}
\hat{\mathbf{u}}_j &= \psi^{-1} \left(\mathcal{Q}_\Lambda \left(\left[b_j \sum_{\ell=1}^L a_\ell \mathbf{t}_\ell + \mathbf{m}_j \right] \bmod \Lambda' \right) \right) \\
&= \psi^{-1} \left(\mathcal{Q}_\Lambda \left(\left[F_{\Lambda'} \left(b_j \sum_{\ell=1}^L a_\ell \mathbf{t}_\ell \right) + \mathbf{m}_j \right] \bmod \Lambda' \right) \right) \\
&= \psi^{-1} \left(\mathcal{Q}_\Lambda \left(F_{\Lambda'} \left(b_j \sum_{\ell=1}^L a_\ell \mathbf{t}_\ell \right) + \mathbf{m}_j - \mathcal{Q}_{\Lambda'}(\Theta) \right) \right) \\
&= \psi^{-1} \left(F_{\Lambda'} \left(b_j \sum_{\ell=1}^L a_\ell \psi(\mathbf{w}_\ell \mathbf{G}_\ell) \right) + \mathcal{Q}_\Lambda(\mathbf{m}_j) - \mathcal{Q}_{\Lambda'}(\Theta) \right) \\
&= F_q \left(p_j \sum_{\ell=1}^L q_\ell \mathbf{w}_\ell \mathbf{G}_\ell \right) + \psi^{-1}(\mathcal{Q}_\Lambda(\mathbf{m}_j)) \\
&= F_q(p_j \mathbf{W} \mathbf{Q} \mathbf{G}) + \psi^{-1}(\mathcal{Q}_\Lambda(\mathbf{m}_j)),
\end{aligned} \tag{4.2.13}$$

where $\mathcal{Q}_\Lambda(\cdot)$ is a quantiser (see Eq. (2.3.6) in Chapter 2), $\mathbf{W} = [\mathbf{w}_1, \mathbf{w}_2, \dots, \mathbf{w}_L]$, $\mathbf{Q} = \text{diag}\{q_1, q_2, \dots, q_L\}$, $\mathbf{G} = [\mathbf{G}_1, \mathbf{G}_2, \dots, \mathbf{G}_L]^T$, $p_j = \psi^{-1}([b_j] \bmod \Lambda')$, $q_\ell = \psi^{-1}([a_\ell] \bmod \Lambda')$, $p_j, q_\ell \in \mathbb{F}_q$, and

$$\Theta = F_{\Lambda'} \left(b_j \sum_{\ell=1}^L a_\ell \mathbf{t}_\ell \right) + \mathbf{m}_j. \tag{4.2.14}$$

Note that the desired linear combination obtained from the lattice-based network coded packet at the source s_j actually is

$$\mathbf{u}_j = F_q \left(p_j \sum_{\ell=1}^L q_\ell \mathbf{w}_\ell \mathbf{G}_\ell \right) = F_q(p_j \mathbf{W} \mathbf{Q} \mathbf{G}). \tag{4.2.15}$$

Therefore, it can be observed from Eqs. (4.2.13) and (4.2.15) that $\hat{\mathbf{u}}_j = \mathbf{u}_j$ if and only if $\psi^{-1}(\mathcal{Q}_\Lambda(\mathbf{m}_j)) = 0$, or equivalently, $\mathcal{Q}_\Lambda(\mathbf{m}_j) \in \Lambda'$.

Furthermore, each source node can reduce the decoding complexity by cancelling its prior known information, if it has, from the desired linear combination. Let \mathcal{K}_j denote the indices of the information prior known to the j th receiver. Let \mathbf{c}_u denote the collection of unknown information and \mathbf{c}_c be the collection of known information.

We have,

$$\begin{aligned}
\mathbf{c}_u &= \mathbf{u}_j \ominus \mathbf{c}_c \\
&= F_q \left(p_j \sum_{\ell=1}^L q_\ell \mathbf{w}_\ell \mathbf{G}_\ell \right) \ominus F_q \left(p_j \sum_{\ell \in \mathcal{K}_j} q_\ell \mathbf{w}_\ell \mathbf{G}_\ell \right) \\
&= F_q \left(p_j \sum_{\ell \notin \mathcal{K}_j} q_\ell \mathbf{w}_\ell \mathbf{G}_\ell \right),
\end{aligned} \tag{4.2.16}$$

where \ominus denotes the subtraction over \mathbb{F}_q .

Given the assumption that all the sources know all the assigned generators a priori and can obtain a sequence of coefficients \mathbf{q} , then, due to the structure of nested codes, each receiver is able to decode all the unknown messages and the multiple interpretations can be realised in two time slots¹.

4.3 Performance Analysis

In this section, I derive a theoretical upper bound on WER for the NCLC and further optimise the NCLC by developing code design criteria that minimises the derived WER.

First, we derive the error probability of $\hat{\mathbf{u}}_j$ at the j th receiver node,

$$\Pr(\hat{\mathbf{u}}_j \neq \mathbf{u}_j) = \Pr(\mathcal{Q}_\Lambda(\mathbf{m}_j) \notin \Lambda'). \tag{4.3.1}$$

¹It should be noted that for the nested code to be an error-correcting code, the number of columns of the “stacked” generator matrix must be larger than the number of rows. This forces the number of columns in each submatrix \mathbf{G}_ℓ to be larger than what would normally be required for a single (non-nested) error-correcting code based on \mathbf{G}_ℓ . Actually, there is a tradeoff between the spectral efficiency advantages and the coding gain of nested codes. If the design of nested codes reduces the spectral efficiency advantages, an additional coding gain could be obtained with the nested code because it results in a longer code length than a single error-correcting code.

With reference to [11], we have

$$\begin{aligned} \Pr(\mathcal{Q}_\Lambda(\mathbf{m}_j) \notin \Lambda') &\leq \Pr(\mathbf{m}_j \notin \mathcal{R}_\nu(\mathbf{0})) \\ &\leq \sum_{\boldsymbol{\lambda} \in \text{Nbr}(\Lambda \setminus \Lambda')} \exp\left(-\frac{v\|\boldsymbol{\lambda}\|^2}{2}\right) \mathbb{E} \left[\exp(v \text{Re}\{\boldsymbol{\lambda}^H \mathbf{m}_j\}) \right], \quad \forall v > 0 \end{aligned} \quad (4.3.2)$$

where $\mathcal{R}_\nu(\mathbf{0})$ denotes the Voronoi region of $\mathbf{0}$ in the set $\{\Lambda \setminus \Lambda'\} \cup \{\mathbf{0}\}$ and $\text{Nbr}(\Lambda \setminus \Lambda')$ is the set of neighbours of $\mathbf{0}$ in $\{\Lambda \setminus \Lambda'\}$.

Subsequently, based on Eqs. (4.2.6) and (4.2.11), we can have

$$\begin{aligned} &\mathbb{E} \left[\exp(v \text{Re}\{\boldsymbol{\lambda}^H \mathbf{m}_j\}) \right] \\ &= \mathbb{E} \left[\exp \left(v \text{Re} \left\{ \boldsymbol{\lambda}^H \left(b_j \sum_{\ell=1}^L (\alpha h_\ell - a_\ell) \mathbf{x}_\ell + b_j \alpha \mathbf{z}_{sr} \right. \right. \right. \right. \\ &\quad \left. \left. \left. + (\beta_j h_j - b_j) \mathbf{x}_r + \beta_j \mathbf{z}_{rs_j} \right) \right\} \right) \right] \\ &= \mathbb{E} \left[\exp \left(v \text{Re}\{\boldsymbol{\lambda}^H (b_j \alpha \mathbf{z}_{sr} + (\beta_j h_j - b_j) \mathbf{x}_r + \beta_j \mathbf{z}_{rs_j})\} \right) \right] \\ &\quad \prod_{\ell} \mathbb{E} \left[\exp(v \text{Re}\{\boldsymbol{\lambda}^H b_j (\alpha h_\ell - a_\ell) \mathbf{x}_\ell\}) \right] \\ &= \exp \left(\frac{1}{2} v^2 \|\boldsymbol{\lambda}\|^2 \left(|b_j|^2 |\alpha|^2 \sigma_{sr}^2 + P_r |\beta_j h_j - b_j|^2 + |\beta_j|^2 \sigma_{rs_j}^2 \right) \right) \\ &\quad \prod_{\ell} \mathbb{E} \left[\exp(v \text{Re}\{\boldsymbol{\lambda}^H b_j (\alpha h_\ell - a_\ell) \mathbf{x}_\ell\}) \right] \\ &= \exp \left(\frac{1}{4} v^2 \|\boldsymbol{\lambda}\|^2 N_0 \left(|b_j|^2 |\alpha|^2 + \frac{P_r}{N_0} |\beta_j h_j - b_j|^2 + |\beta_j|^2 \right) \right) \\ &\quad \prod_{\ell} \mathbb{E} \left[\exp(v \text{Re}\{\boldsymbol{\lambda}^H b_j (\alpha h_\ell - a_\ell) \mathbf{x}_\ell\}) \right]. \end{aligned} \quad (4.3.3)$$

By considering the lattice partition as a hypercube, according to [11], we have

$$\mathbb{E} \left[\exp(\text{Re}\{\mathbf{v}^H \mathbf{x}\}) \right] \leq \exp(\|\mathbf{v}\|^2 \delta^2 / 24), \quad (4.3.4)$$

where $\mathbf{x} \in \mathbb{C}^n$ is a complex random vector uniformly distributed over a hypercube $\delta \mathbf{U} \mathcal{H}_n$, $\delta > 0$ is a scalar factor, \mathbf{U} is any $n \times n$ unitary matrix, and \mathcal{H}_n is a unit hypercube in \mathbb{C}^n defined by $\mathcal{H}_n = ([-1/2, 1/2] + i[-1/2, 1/2])^n$. Note that for a

hypercube, $P = \frac{1}{n} \mathbb{E}[\|\mathbf{x}_\ell\|^2] = \delta^2/6$. Thus, we have

$$\begin{aligned}
& \mathbb{E} [\exp(v \operatorname{Re}\{\boldsymbol{\lambda}^H \mathbf{m}_j\})] \\
&= \exp \left(\frac{1}{4} v^2 \|\boldsymbol{\lambda}\|^2 N_0 \left(|b_j|^2 |\alpha|^2 + \frac{P_r}{N_0} |\beta_j h_j - b_j|^2 + |\beta_j|^2 \right) \right) \\
& \quad \prod_{\ell} \mathbb{E} [\exp(v \operatorname{Re}\{\boldsymbol{\lambda}^H b_j (\alpha h_\ell - a_\ell) \mathbf{x}_\ell\})] \\
&\leq \exp \left(\frac{1}{4} v^2 \|\boldsymbol{\lambda}\|^2 N_0 \left(|b_j|^2 |\alpha|^2 + \frac{P_r}{N_0} |\beta_j h_j - b_j|^2 + |\beta_j|^2 \right) \right) \\
& \quad \prod_{\ell} \exp (\|\boldsymbol{\lambda} b_j (\alpha h_\ell - a_\ell)\|^2 P_s/4) \\
&= \exp \left(\frac{1}{4} v^2 \|\boldsymbol{\lambda}\|^2 N_0 \left(|b_j|^2 |\alpha|^2 + \frac{P_r}{N_0} |\beta_j h_j - b_j|^2 + |\beta_j|^2 \right) \right. \\
& \quad \left. + \frac{1}{4} v^2 \|\boldsymbol{\lambda}\|^2 |b_j|^2 \|\alpha \mathbf{h} - \mathbf{a}\|^2 P_s \right) \\
&= \exp \left(\frac{1}{4} v^2 \|\boldsymbol{\lambda}\|^2 N_0 Q(\alpha, \mathbf{a}, \beta_j, b_j) \right), \tag{4.3.5}
\end{aligned}$$

where the quantity $Q(\alpha, \mathbf{a}, \beta_j, b_j)$ is defined as

$$Q(\alpha, \mathbf{a}, \beta_j, b_j) = \frac{P_s}{N_0} |b_j|^2 \|\alpha \mathbf{h} - \mathbf{a}\|^2 + |b_j|^2 |\alpha|^2 + \frac{P_r}{N_0} |\beta_j h_j - b_j|^2 + |\beta_j|^2. \tag{4.3.6}$$

Hence, by choosing $v = 1/(N_0 Q(\alpha, \mathbf{a}, \beta_j, b_j))$, we obtain

$$\begin{aligned}
& \Pr(\hat{\mathbf{u}}_j \neq \mathbf{u}_j) = \Pr(\mathcal{Q}_\Lambda(\mathbf{m}_j) \notin \Lambda') \\
&\leq \sum_{\boldsymbol{\lambda} \in \text{Nbr}(\Lambda \setminus \Lambda')} \exp \left(-\frac{v \|\boldsymbol{\lambda}\|^2}{2} + \frac{1}{4} v^2 \|\boldsymbol{\lambda}\|^2 N_0 Q(\alpha, \mathbf{a}, \beta_j, b_j) \right) \\
&= \sum_{\boldsymbol{\lambda} \in \text{Nbr}(\Lambda \setminus \Lambda')} \exp \left(-\frac{\|\boldsymbol{\lambda}\|^2}{4 N_0 Q(\alpha, \mathbf{a}, \beta_j, b_j)} \right) \\
&\approx K(\Lambda/\Lambda') \exp \left(-\frac{d^2(\Lambda/\Lambda')}{4 N_0 Q(\alpha, \mathbf{a}, \beta_j, b_j)} \right) \\
&= K(\Lambda/\Lambda') \exp \left(-\frac{3 \text{SENR}_{\text{norm}} \gamma_c(\Lambda/\Lambda')}{2} \right), \tag{4.3.7}
\end{aligned}$$

where $\gamma_c(\Lambda/\Lambda')$, $d^2(\Lambda/\Lambda')$, and $K(\Lambda/\Lambda')$ denote the nominal coding gain, the squared minimum inter-coset distance, and the number of the nearest neighbours with $d^2(\Lambda/\Lambda')$

of the lattice partition Λ/Λ' , respectively. Refer to [60] and we have the $\text{SENR}_{\text{norm}}$ as

$$\text{SENR}_{\text{norm}} = \frac{\text{SENR}}{2^R} = \frac{P}{2^R N_0 Q(\alpha, \mathbf{a}, \beta_j, b_j)}. \quad (4.3.8)$$

Let $V(\Lambda)$ denote the volume of the Voronoi region of Λ . The nominal coding gain [61] can be expressed by

$$\gamma_c(\Lambda/\Lambda') = \frac{d^2(\Lambda/\Lambda')}{V(\Lambda)^{1/N}}, \quad (4.3.9)$$

where the number of dimensions N is equivalent to the coded message length n .

Next, we consider the WER of $\widehat{\mathbf{W}}_j$ at the j th node. To obtain the error probability of the information matrix \mathbf{W}_j from the desired linear combination \mathbf{u}_j , we can regard $\Pr(\widehat{\mathbf{u}}_j \neq \mathbf{u}_j)$ as the crossover probability of a BSC channel. Thus, according to [56, 58], we can obtain,

$$\Pr(\widehat{\mathbf{W}}_j \neq \mathbf{W}_j) < \sum_{d=d_{free}^2}^{\infty} a_d (4\Pr(\widehat{\mathbf{u}}_j \neq \mathbf{u}_j) (1 - \Pr(\widehat{\mathbf{u}}_j \neq \mathbf{u}_j)))^{\sqrt{d}/2}, \quad (4.3.10)$$

where d_{free}^2 and a_d denote the minimum squared Euclidian distance and the number of paths at a squared Euclidian distance d from the all-zero path of the convolutional code corresponding to the “stacked” generator matrix \mathbf{G} in (4.2.13), respectively.

The cancellation process at each receiver node actually will not change the degree of error. Therefore, the crossover probability is still $\Pr[\widehat{\mathbf{u}}_j \neq \mathbf{u}_j]$ after the cancellation process. In other words, the cancellation process will not affect the performance of the derived upper bound.

Finally, based on (4.3.6), (4.3.7) and (4.3.10), we have the code design criteria for the proposed scheme as follows

1. The scalars α and β_j should be chosen such that $Q(\alpha, \mathbf{a}, \beta_j, b_j)$ is minimised.
2. The lattice partition Λ/Λ' should be designed such that $K(\Lambda/\Lambda')$ is minimised and $d^2(\Lambda/\Lambda')$ is maximised.

3. The “stacked” convolutional generator matrix should be designed such that d_{free}^2 is maximised and a_d is minimised.

4.4 Simulation Results

In this section, we consider a MWRC with three sources and one relay, and assign different linearly independent q -ary convolutional generators with a rate $1/3$ and memory 1 for all the sources. It is assumed that all the sources and the relay have the same maximum transmit power P , the lattice partition is chosen as a typical Gaussian integer $\mathcal{W} \cong \mathbb{Z}[i]/\delta\mathbb{Z}[i]$, where $\delta = 2 + 3i$, and the finite field is chosen as \mathbb{F}_{13} with the size $q = 13$. Thus, $\mathcal{W} \cong \mathbb{F}_{13}$, the shaping is a rotated hypercube in \mathbb{C}^N , and the message rate $R = \frac{1}{n} \log_2 13$. Besides, all the links between sources and the relay are assumed to be quasi-static Rayleigh fading channels.

Without loss of generality, we select the source node s_3 as an example node. That is, we focus on the realisation of multiple interpretations at s_3 by extracting the information of s_1 and s_2 from the lattice-based network coded packet sent by the relay. Specifically, s_3 inversely maps each received message from the relay to the corresponding non-binary convolutional codeword in \mathbb{F}_{13} , subtracts its own information based on the cancellation process shown in Eq. (4.2.16), and decodes the desired information by stacking the generator matrices of s_1 and s_2 as a rate $2/3$ generator matrix. Based on the code design criteria described in the previous section, we obtain a good generator matrix with the code rate $2/3$ given by

$$\begin{bmatrix} \mathbf{G}_1 \\ \mathbf{G}_2 \end{bmatrix} = \begin{bmatrix} 8 + 2D & 6 + 5D & 2 + 4D \\ 7 + 12D & 0 & 7D \end{bmatrix}, \quad (4.4.1)$$

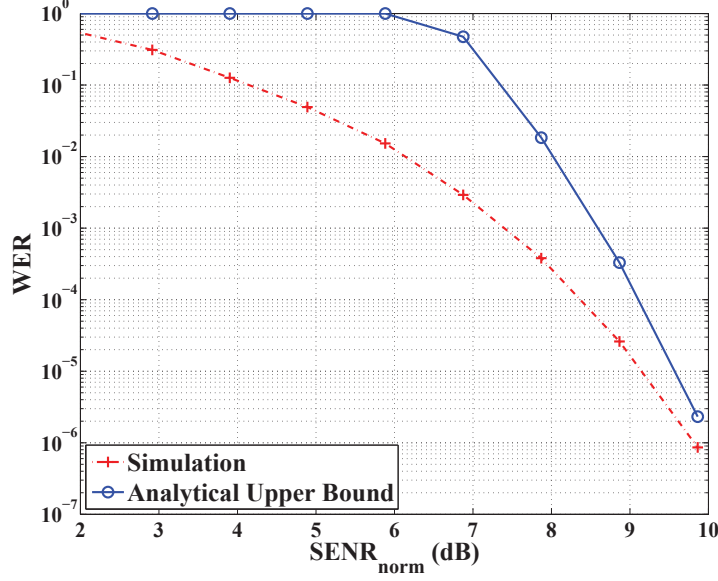


Figure 4.3: The Monte-Carlo simulation result and the analytical upper bound.

with

$$d_{free}^2 = 9 \text{ and } a_{d|d=d_{free}^2} = 24. \quad (4.4.2)$$

Next, the WER of s_3 , i.e., $\Pr(\widehat{\mathbf{W}}_3 \neq \mathbf{W}_3)$, is investigated based on the code profile given in Eq. (4.4.1). We have $\mathbf{W}_3 = [\mathbf{w}_1, \mathbf{w}_2]$, where \mathbf{W}_3 is the desired information matrix at the source node s_3 , and is composed by the information $\mathbf{w}_1, \mathbf{w}_2$ from the source nodes s_1 and s_2 . Fig. 4.3 illustrates the Monte-Carlo simulation result and the analytical upper bound on WER. The dotted and solid curves denote the simulation result and analytical upper bound, respectively. We can observe that the analytical upper bound is asymptotically tight to the simulation result with the increase of the $\text{SEN R}_{\text{norm}}$.

Chapter 5

Network Coded Non-Binary LDGM Codes Based on Lattices for a Multi-Access Relay System

In this chapter, I propose a network coded non-binary low-density generator matrix (LDGM) code structure based on lattices with a low complexity decoder for a multi-access relay system, where multiple sources transmit to a destination with the help of a relay. Specifically, a network coded non-binary LDGM code structure is developed by considering lattice-signal transmissions at both the sources and the relay. Then I derive the achievable computation rate (ACR) for the proposed system and select the key parameters in the proposed structure to maximise the ACR. Furthermore, I optimise the network coded non-binary LDGM codes based on lattices to approach the ACR. Simulation results show that the optimal setting of the parameters is consistent with that obtained from the analysis and the proposed code outperforms the designed reference scheme.

5.1 System Model

Consider a multi-access relay system with L sources, a single relay and a destination, as shown in Fig. 5.1 on the following page, where the relay receives transmissions from the L sources and forwards a network coded message to the destination. The transmission process is conducted in two time slots. Let boldface lowercase and uppercase letters denote vectors and matrices, respectively. In the first time slot, messages are transmitted from their respective sources to the relay, i.e.,

$$\mathbf{y}_{sr} = \sum_{\ell=1}^L h_{\ell} \mathbf{x}_{\ell} + \mathbf{z}_{sr}, \quad (5.1.1)$$

where \mathbf{y}_{sr} is the received signal at the relay from all the sources, h_{ℓ} is the complex channel coefficient of the link between the ℓ th source and the relay, \mathbf{x}_{ℓ} is the transmitted message from the ℓ th source, and \mathbf{z}_{sr} represents a vector of AWGN samples, in which each element is an AWGN with a zero mean and one-sided variance σ^2 . The transmit power at the ℓ th source is subject to the constraint $\frac{1}{n} \mathbb{E} [\|\mathbf{x}_{\ell}\|^2] \leq P$, where n denotes the message length. In the second time slot, the network coded message is transmitted from the relay to the destination, i.e.,

$$\mathbf{y}_{rd} = h_{rd} \mathbf{x}_r + \mathbf{z}_{rd}, \quad (5.1.2)$$

where \mathbf{y}_{rd} is the received signal at the destination from the relay, h_{rd} is the complex channel coefficient of the link between the relay and the destination, \mathbf{x}_r is the transmitted message from the relay, and \mathbf{z}_{rd} is a vector of AWGN samples, in which each element is an AWGN with a zero mean and one-sided variance σ^2 . The transmit power at the relay is subject to the constraint $\frac{1}{n} \mathbb{E} [\|\mathbf{x}_r\|^2] \leq P$. We define the SNR as $\gamma = P/(2\sigma^2)$.

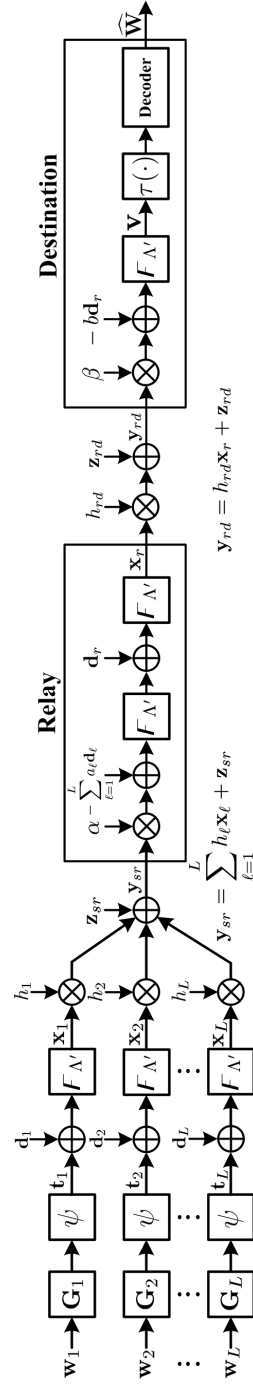


Figure 5.1: A multi-access relay network model with multiple sources, one relay and one destination.

5.2 Nested LDGM Codes Based on Lattices

In this section, we first review the mapping relationships between the values in a finite field and the points on a lattice. Then, we design the coding rules for the non-binary nested codes. At last, we elaborate the code structure of the nested LDGM codes based on lattices.

Let Λ' denote a coarse lattice, which is a subset of a fine lattice Λ , i.e., $\Lambda' \subset \Lambda$. Let the message space be $\mathcal{W} = \Lambda/\Lambda'$, where Λ/Λ' denotes the set of all the cosets of Λ' in Λ . Let \mathbb{F}_q denote a finite field of size q , where q is a positive prime integer and $q > 2$. Let $F_q(\mathbf{w})$ be an operation over \mathbb{F}_q and let $F_{\Lambda'}(\boldsymbol{\lambda})$ be an operation over the fundamental Voronoi region of Λ' [9], denoted by $\mathcal{V}(\Lambda')$, where $\mathbf{w} \in \mathbb{F}_q^k$ and $\boldsymbol{\lambda} \in \Lambda$. Thus,

$$\begin{aligned} F_q(\mathbf{w}) &= [\mathbf{w}] \bmod q, \quad F_{\Lambda'}(\boldsymbol{\lambda}) = [\boldsymbol{\lambda}] \bmod \Lambda', \\ F_{\Lambda'}(\boldsymbol{\lambda}) &= \psi(F_q(\mathbf{w})), \text{ and } F_q(\mathbf{w}) = \psi^{-1}(F_{\Lambda'}(\boldsymbol{\lambda})), \end{aligned} \quad (5.2.1)$$

where $\psi(\cdot)$ denotes a map labeling the message over \mathbb{F}_q to the points over $\mathcal{V}(\Lambda')$ and $\psi^{-1}(\cdot)$ denotes the inverse process [62].

Let \mathbf{w}_ℓ denote the message vector that each of its element is generated independently and uniformly over \mathbb{F}_q by the ℓ th source and let \mathbf{G}_ℓ denote the generator matrix with each of its element over \mathbb{F}_q at the ℓ th source. The mathematical operation of nested codes over \mathbb{F}_q can be expressed by

$$F_q\left(\sum_{\ell=1}^L \mathbf{w}_\ell \mathbf{G}_\ell\right) = F_q(\mathbf{W}\mathbf{G}), \quad (5.2.2)$$

where $\mathbf{W} = [\mathbf{w}_1, \mathbf{w}_2, \dots, \mathbf{w}_L]$, $\mathbf{G} = [\mathbf{G}_1^T, \mathbf{G}_2^T, \dots, \mathbf{G}_L^T]^T$ and $\mathbf{G}_1, \dots, \mathbf{G}_L$ are mutually linearly independent generators at different sources.

For the nested non-binary LDGM codes based on lattices, the finite field \mathbb{F}_q of the nested non-binary LDGM codes is regarded as the message space \mathcal{W} of the lattices.

Thus, the coded message $\mathbf{w}_\ell \mathbf{G}_\ell$ is uniformly distributed over the message space \mathcal{W} . The message rate for each source is defined to be the same as $R_\ell \triangleq \frac{1}{n} \log_2 |\mathcal{W}| = r_\ell \log_2 q$, where r_ℓ is the LDGM code rate at the ℓ th source.

At the ℓ th source, let \mathbf{t}_ℓ denote the coded message on Λ and let \mathbf{d}_ℓ denote a dither generated independently according to a uniform distribution over $\mathcal{V}(\Lambda')$. Then, we have

$$\mathbf{t}_\ell = \psi(\mathbf{w}_\ell \mathbf{G}_\ell) \text{ and } \mathbf{x}_\ell = F_{\Lambda'}(\mathbf{t}_\ell + \mathbf{d}_\ell). \quad (5.2.3)$$

At the relay, as in [9], we optimise the system performance by choosing a scale factor α and a coefficient vector $\mathbf{a} \triangleq (a_1, a_2, \dots, a_L)$, where $\alpha \in \mathbb{C}$, \mathbb{C} denotes the complex field, and $\mathbf{a} \in \Lambda$. It is worth noting that, to guarantee the successful decoding of all the messages at the destination, it is assumed that $a_\ell \neq 0, \forall \ell \in \{1, 2, \dots, L\}$. Then, we obtain

$$F_{\Lambda'} \left(\alpha \mathbf{y}_{sr} - \sum_{\ell=1}^L a_\ell \mathbf{d}_\ell \right) = F_{\Lambda'} \left(\sum_{\ell=1}^L a_\ell \mathbf{t}_\ell + \mathbf{n} \right), \quad (5.2.4)$$

where $\mathbf{n} = \sum_{\ell=1}^L (\alpha h_\ell - a_\ell) \mathbf{x}_\ell + \alpha \mathbf{z}_{sr}$.

Thus, the transmitted network coded message from the relay to the destination is $\mathbf{x}_r = F_{\Lambda'} \left(\sum_{\ell=1}^L a_\ell \mathbf{t}_\ell + \mathbf{n} + \mathbf{d}_r \right)$, where \mathbf{d}_r is a dither generated independently according to a uniform distribution over $\mathcal{V}(\Lambda')$ at the relay.

At the destination, we remove the dither by choosing scalars $\beta \in \mathbb{C}$ and $b \in \Lambda$, and obtain the received lattice signal \mathbf{v} (see Fig. 5.1) given by

$$\begin{aligned} \mathbf{v} &= F_{\Lambda'} (\beta \mathbf{y}_{rd} - b \mathbf{d}_r) = F_{\Lambda'} \left(b \sum_{\ell=1}^L a_\ell \mathbf{t}_\ell + \mathbf{m} \right) \\ &= F_{\Lambda'} (\mathbf{u} + \mathbf{m}), \end{aligned} \quad (5.2.5)$$

where the effective noise $\mathbf{m} = b \mathbf{n} + (\beta h_{rd} - b) \mathbf{x}_r + \beta \mathbf{z}_{rd}$.

Then, we define a function $\tau(\cdot)$ that converts the received i th lattice signal $v_i, v_i \in$

\mathbf{v} in (5.2.5), into the log-likelihood ratio vector $\mathbf{L}(u_i)$ as the input of the decoder, i.e.,

$$\mathbf{L}(u_i) = \tau(v_i), \quad \forall i \in \{1, \dots, n\}, \quad u_i \in \mathbf{u}, \quad v_i \in \mathbf{v}, \quad (5.2.6)$$

where $\mathbf{L}(u_i) \triangleq [L(u_i = \lambda^{(1)}), \dots, L(u_i = \lambda^{(q-1)})]$. Let $\lambda^{(\xi)}$ denote the ξ th non-zero fine lattice point in $\mathcal{V}(\Lambda')$, and we have

$$L(u_i = \lambda^{(\xi)}) \triangleq \ln \frac{\Pr(u_i = \lambda^{(\xi)})}{\Pr(u_i = 0)}, \quad \forall \xi \in \{1, \dots, q-1\}. \quad (5.2.7)$$

The detailed process of $\tau(\cdot)$ function is given as follows. First, we expand (5.2.5), corresponding to the i th signal, as

$$\begin{aligned} v_i &= F_{\Lambda'}(u_i + m_i) \\ &= F_{\Lambda'}(u_{i,rl} + ju_{i,im} + m_{i,rl} + jm_{i,im}) \\ &= F_{\Lambda'}(v_{i,rl} + jv_{i,im}), \quad m_i \in \mathbf{m}, \end{aligned} \quad (5.2.8)$$

where $m_{i,rl}$ and $m_{i,im}$ are approximated as the realisations of Gaussian random variables with the same variance σ_m^2 . The joint probability density function of $v_{i,rl}$, $v_{i,im}$ is

$$\begin{aligned} &p(v_i|u_i) \\ &= \frac{1}{2\pi\sigma_m^2} \sum_{k_1=-\infty}^{k_1=\infty} \sum_{k_2=-\infty}^{k_2=\infty} \exp\left(-\frac{(v_{i,rl} - u_{i,rl} - qk_1)^2}{2\sigma_m^2} - \frac{(v_{i,im} - u_{i,im} - qk_2)^2}{2\sigma_m^2}\right), \end{aligned} \quad (5.2.9)$$

where q is the size of the finite field, as well as the number of fine lattice points over $\mathcal{V}(\Lambda')$.

Second, according to the Bayes' theorem, we have

$$\begin{aligned} \Pr(u_i|v_i) &= \frac{p(v_i|u_i)\Pr(u_i)}{\Pr(v_i)} \\ &= g_i \sum_{k_1=-\infty}^{k_1=\infty} \sum_{k_2=-\infty}^{k_2=\infty} \exp\left(-\frac{(v_{i,rl} - u_{i,rl} - qk_1)^2}{2\sigma_m^2} - \frac{(v_{i,im} - u_{i,im} - qk_2)^2}{2\sigma_m^2}\right), \end{aligned} \quad (5.2.10)$$

where $g_i = \Pr(u_i)/(2\pi\sigma_m^2\Pr(v_i))$ is a constant if all the signals in $\mathcal{V}(\Lambda')$ are transmitted with equal probability. The normalised constant g_i ensures $\Pr(u_i = 0|v_i) +$

$\sum_{\xi=1}^{q-1} \Pr(u_i = \lambda^{(\xi)} | v_i) = 1$. Based on (5.2.10), we have the function $\tau(\cdot)$ as

$$\tau(v_i) = \mathbf{L}(u_i) = \left[\ln \frac{\Pr(u_i = \lambda^{(1)} | v_i)}{\Pr(u_i = 0 | v_i)}, \dots, \ln \frac{\Pr(u_i = \lambda^{(q-1)} | v_i)}{\Pr(u_i = 0 | v_i)} \right]. \quad (5.2.11)$$

Hence, given the assumption that the destination knows all the assigned generators a priori and can obtain a sequence of corresponding coefficients, according to (5.2.2), it can extract all the messages from all the sources. It should be noticed that the proposed code structure is significantly different from that in [9]. Following the analysis in [9], only with sufficiently linear combinations of the transmitted signals sent from multiple relays, can the destination decode the messages individually. However, due to the joint design of the nested LDGM codes and lattices, the destination in the proposed code structure can decode all the messages from one network coded signal forwarded by the relay. Interested readers can refer to [58, 62] for further information regarding such a nested code structure.

5.3 Achievable Computation Rate (ACR)

In this section, we will analyse the ACR and select the key parameters α , \mathbf{a} , β and b in the proposed code structure to maximise the ACR. The ACR is defined as follows: a message rate R_ℓ is said to be achievable if and only if for any $\epsilon > 0$ and n large enough, can the destination recover all the messages with an average probability of error ϵ .

Theorem 5.1. *For the complex-valued channels, the ACR of the proposed system can be expressed by*

$$\mathcal{R}(\mathbf{h}, \mathbf{a}, h_{rd}, b) = \log^+ \left(\frac{\gamma}{|b|^2 \|\alpha \mathbf{h} - \mathbf{a}\|^2 \gamma + |b|^2 |\alpha|^2 + |\beta h_{rd} - b|^2 \gamma + |\beta|^2} \right), \quad (5.3.1)$$

where $\log^+(x) \triangleq \max(\log_2(x), 0)$.

Proof. See Appendix B.1. □

To maximise the ACR, the related parameters α , \mathbf{a} , β and b are optimised by the following propositions.

Proposition 5.2. *The parameters α and β that maximise the ACR are given by*

$$\alpha = \frac{\mathbf{a}\gamma\mathbf{h}^H}{\gamma\|\mathbf{h}\|^2 + 1} \text{ and } \beta = \frac{b\gamma h_{rd}^H}{\gamma|h_{rd}|^2 + 1}, \quad (5.3.2)$$

where \mathbf{a} is chosen by a greedy approach to maximise the ACR and \mathbf{h}^H denotes the Hermitian transpose of \mathbf{h} .

Proof. See Appendix B.2. □

Proposition 5.3. *Given channel coefficient parameters \mathbf{h} and h_{rd} , the ACR is maximised by choosing the lattice network coding coefficient b to be the closest point to the origin on Λ .*

Proof. See Appendix B.3. □

The ACR is derived and used as a theoretical limit for the optimisation of the proposed codes. Here, different from [9], which only considers the optimisation of parameters α and \mathbf{a} at the relay, I consider a different system model and optimise all the parameters α , \mathbf{a} , β and b by maximising the ACR for the entire system at the destination. If the chosen parameters can achieve a better ACR, then the performance of the proposed codes can be improved with the corresponding parameters.

5.4 Code Optimisation

To optimise the proposed nested non-binary LDGM codes based on lattices, we first develop a corresponding low complexity decoder. Note that a conventional low

complexity decoding algorithm, such as the fast fourier transform (FFT), requires that the size of the finite field should be a power of two. However, in the case of the proposed code structure, the size of the finite field q is a prime. Therefore, I employ and expand the extended min-sum algorithm in [63] to a lattice-based extended min-sum (L-EMS) algorithm, where the size of the finite field is a prime. The initialised channel input of the L-EMS decoder is estimated on the lattice by (5.2.11) and the exchanged messages between variable nodes and check nodes are truncated vectors with a length $n_m \leq q$. With the L-EMS decoder, the computational complexity is dominated by $\mathcal{O}(n_m \log_2(n_m))$, compared with that of the Belief Propagation (BP) algorithm denominated by $\mathcal{O}(q^2)$ [64].

We then optimise the proposed codes with the L-EMS decoder. It should be noted that the structure of the nested non-binary LDGM codes based on lattices is identical to that of a single “stacked” non-binary LDGM code based on lattices. In particular, we consider only the average column weight \bar{w}_c of the single “stacked” non-binary LDGM code, because it is intractable to locate the optimal code among a huge irregular LDGM matrix set. For a given LDGM code rate, \bar{w}_c will be optimised with respect to SNR under a certain symbol error rate. Formally, we write

$$\bar{w}_{c,opt} = \arg \min_{\bar{w}_c} \{\gamma(\bar{w}_c)\}. \quad (5.4.1)$$

As stated in [65], simulation based approaches have to be used to solve the optimisation problem (5.4.1). In this chapter, a lattice-based Monte Carlo method is employed, where the initialised channel input on lattices is estimated as (5.2.11).

5.5 Reference Scheme

This section presents a reference scheme based on amplify-and-forward (AF) protocol¹ to compare with the proposed code structure. For the AF, the received signal at the relay is still (5.1.1) and the received signal at the destination can be written as

$$\mathbf{y}_d = h_{rd}\mathcal{A} \left(\sum_{\ell=1}^L h_{\ell}\mathbf{x}_{\ell} + \mathbf{z}_{sr} \right) + \mathbf{z}_{rd}, \quad (5.5.1)$$

where \mathcal{A} is the amplification factor given by $\mathcal{A} = \sqrt{\frac{\gamma}{\gamma\|\mathbf{h}\|^2+1}}$. Then, to successfully decode the messages at the destination, analogue to the proposed code structure, we introduce a scale factor $\rho \in \mathbb{C}$ as well as a coefficient vector $\mathbf{c} \triangleq (c_1, c_2, \dots, c_L)$, where $\mathbf{c} \in \Lambda$ and $c_{\ell} \neq 0$, and then obtain

$$F_{\Lambda'} \left(\rho\mathbf{y}_d - \sum_{\ell=1}^L c_{\ell}\mathbf{d}_{\ell} \right) = F_{\Lambda'} \left(\sum_{\ell=1}^L c_{\ell}\mathbf{t}_{\ell} + \mathbf{n}_{AF} \right), \quad (5.5.2)$$

where $\mathbf{n}_{AF} = \sum_{\ell=1}^L (\rho h_{rd}\mathcal{A}h_{\ell} - c_{\ell})\mathbf{x}_{\ell} + \rho h_{rd}\mathcal{A}\mathbf{z}_{sr} + \rho\mathbf{z}_{rd}$.

Based on Proposition 5.2, the scale factor ρ can be obtained as

$$\rho = \frac{\mathcal{A}\mathbf{c}\gamma\mathbf{h}^H h_{rd}^H}{\mathcal{A}^2\gamma\|\mathbf{h}\|^2|h_{rd}|^2 + \mathcal{A}^2|h_{rd}|^2 + 1}, \quad (5.5.3)$$

where \mathbf{c} can be readily obtained via a greedy approach. Thus, based on Theorem 5.1, the ACR of the reference scheme based on AF, denoted by \mathcal{R}_{AF} , can be obtained as

$$\mathcal{R}_{AF} = \log^+ \left(\frac{\gamma}{\|\rho h_{rd}\mathcal{A}\mathbf{h} - \mathbf{c}\|^2\gamma + |\rho|^2|h_{rd}|^2\mathcal{A}^2 + |\rho|^2} \right). \quad (5.5.4)$$

5.6 Simulation Results

In the simulations, a multi-access relay system with two sources, one relay and one destination is considered. As in [11], the channels are set as $h_1 = -1.17 + 2.15j$,

¹Decode-and-forward (DF) protocol is not considered for comparison because, to the best knowledge of the author, there is not a feasible method except the proposed code structure that can be implemented to decode the messages at the relay.

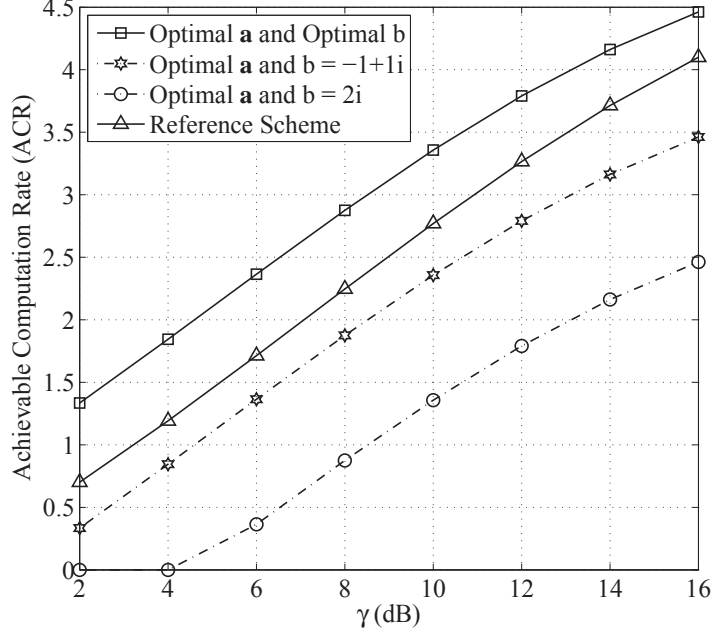


Figure 5.2: The ACR performance of the proposed system with an optimal \mathbf{a} and different choices of \mathbf{b} , compared with that of the reference scheme.

$h_2 = 1.25 - 1.63j$ and $h_{rd} = 0.77 + 1.12j$. The lattice partition is chosen to be a typical Gaussian integer $\mathcal{W} \cong \mathbb{Z}[i]/\delta\mathbb{Z}[i]$ as in [60], where $\delta = 2 + 3i$. The finite field is \mathbb{F}_{13} . The LDGM code rate for each source is set as 0.25 and the LDGM code length is 2000. Thus the message rate $R_\ell = 0.25 \log_2 13$. According to Propositions 5.2 and 5.3, the optimal lattice network coding coefficients² for the proposed code structure are computed by $\mathbf{a} = [-1, 1]$ and $\mathbf{b} = 1$. For the reference scheme, we have $\mathbf{c} = [-1, 1]$. Using the lattice-based Monte Carlo method, we obtain an optimal average column weight $\bar{w}_c = 2.4$ for the proposed codes over \mathbb{F}_{13} . Subsequently, we construct the generator matrix \mathbf{G} of the corresponding single “stacked” LDGM code. To assign

²Note that the optimal lattice network coding coefficients are the points on the fine lattice and there are multiple choices for optimal \mathbf{a} or \mathbf{b} that maximise the ACR. Here I just present one optimal result of \mathbf{a} or \mathbf{b} .

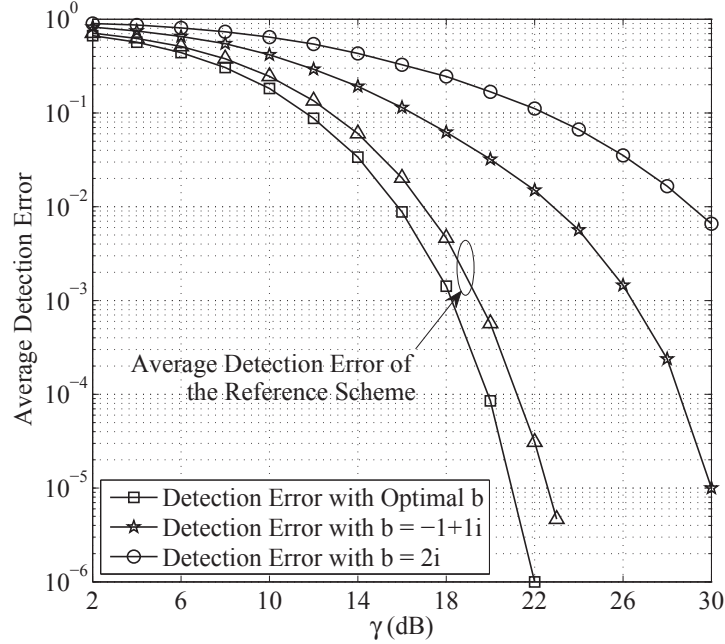


Figure 5.3: The average detection error performance with different values of b .

each source with different linearly independent LDGM codes, we divide the generator matrix of the single “stacked” LDGM code as³

$$\mathbf{G}^{1000 \times 2000} = \begin{bmatrix} \mathbf{G}_1^{500 \times 2000} \\ \mathbf{G}_2^{500 \times 2000} \end{bmatrix}.$$

Fig. 5.2 shows the ACR performance of the proposed system with an optimal \mathbf{a} and different choices of b , and that of the reference scheme is also plotted for comparison. It is illustrated that the curve with the optimal b achieves higher ACR than that with $b = -1 + 1i$ and $b = 2i$, respectively, which validates the result in Proposition 5.3 that b should be the closet point to the origin on Λ . It also can be observed that the proposed system with optimal lattice network coding coefficients performs better

³Here, I simulate symmetric case only where the rates for \mathbf{G}_1 and \mathbf{G}_2 are equal. However, it can be readily extended to asymmetric scenarios by assigning \mathbf{G}_1 and \mathbf{G}_2 with different rates.

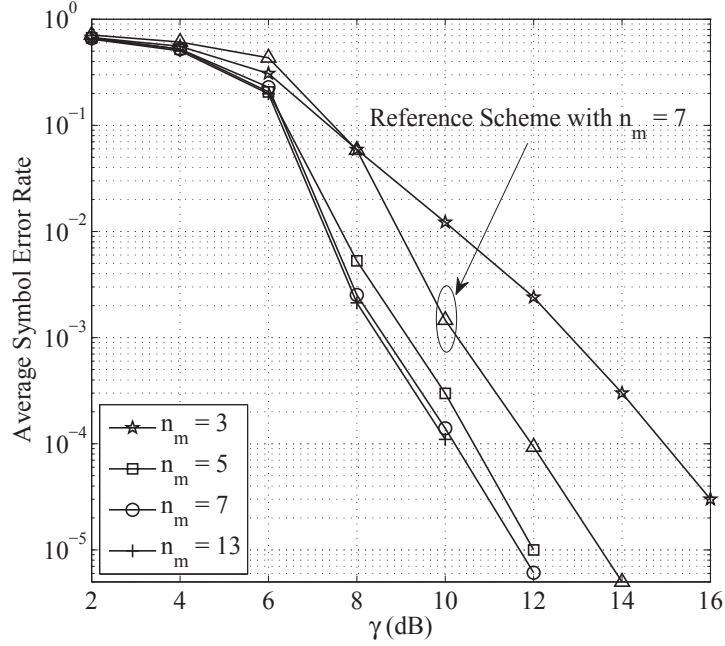


Figure 5.4: The average symbol error performance of the proposed codes.

than the reference scheme.

Fig. 5.3 shows the average detection error performance of the proposed system with the lattice network coding coefficients chosen as $b = 1$, $b = -1 + 1i$, and $b = 2i$, respectively. Each curve hereafter is obtained by averaging over 1000 runs. The detection error is defined as the average symbol error rate at the input of the decoder (i.e., the output of the function $\tau(\cdot)$, see Fig. 5.1). Fig. 5.3 shows that the best average detection error performance is realised by choosing optimal $b = 1$ compared with $b = -1 + 1i$ and $b = 2i$, which is consistent with the result of Proposition 5.3 and the analysis for Fig. 5.2. Besides, the average detection error performance of the reference scheme is also shown for comparison, which reveals a worse performance than that of the proposed system.

In Fig. 5.4, the average symbol error performance of the optimised codes via Section 5.4 with the L-EMS decoder are depicted with the truncated message length $n_m = 3, 5, 7$, and 13, respectively. A tradeoff exists between the code performance corresponding to the value of n_m and the decoding complexity. It is shown that a further increase of n_m from $n_m = 7$ to 13 only results in a marginal performance improvement, which indicates that $n_m = 7$ can be a good choice for the codes. Concerning the complexity, based on the analysis in Section 5.4, the L-EMS decoder with $n_m = 13$ is 2.44 times more complex than the L-EMS decoder with $n_m = 7$. Furthermore, the performance of the reference scheme based on AF protocol with $n_m = 7$ are also simulated in Fig. 5.4 for comparison. The reference scheme employs the same codes adopted by the proposed system. It is shown that the SNR required by the proposed code structure to achieve an average symbol rate of 10^{-4} is about 2dB less than that required by the reference scheme to achieve the same error rate.

Chapter 6

Distributed and Optimal Resource Allocation for Power Beacon-Assisted Wireless-Powered Communications

In this chapter, the optimal resource allocation is investigated in a power beacon-assisted wireless-powered communication network (PB-WPCN), which consists of a set of hybrid access point (AP)-source pairs and a power beacon (PB). Both cooperative and non-cooperative scenarios are considered based on whether the PB is cooperative with the APs or not. For the cooperative scenario, a social welfare maximisation problem is formulated to maximise the weighted sum-throughput of all AP-source pairs, which is subsequently solved by a water-filling based distributed algorithm. In the non-cooperative scenario, I formulate an auction game and propose an auction based distributed algorithm by considering the PB as the auctioneer and the APs as the bidders. Finally, numerical results are performed to validate the convergence of both the proposed algorithms and demonstrate the impacts of various system parameters.

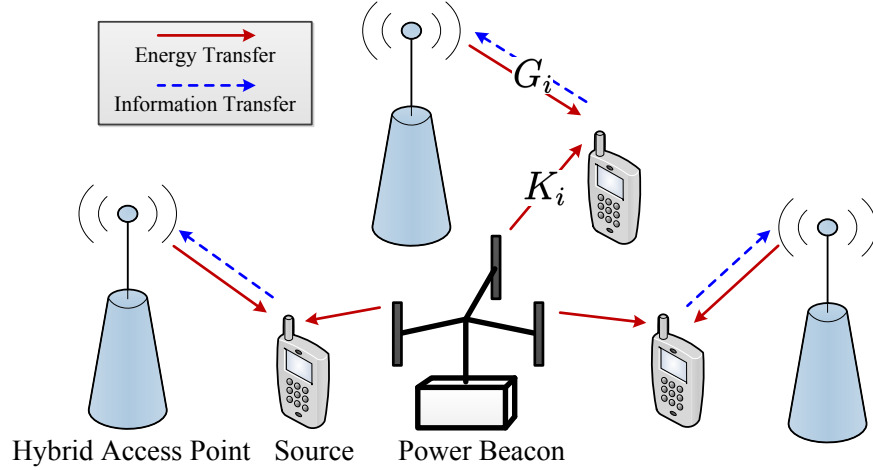


Figure 6.1: System model for the proposed PB-WPCN.

6.1 System Model

In this chapter, as shown in Fig. 6.1, we consider a PB-WPCN with one PB and N APs associated with N (information) sources. The considered network setup is very likely to find its applications in the practical scenario of small cells, such as picocells (range from 10 to 100 meters) and femtocells (WiFi-like range), which has been regarded as one of the key enabling technologies of the upcoming 5G cellular networks [23]. It is considered that the APs and the PB are connected to constant power supplies. Each AP aims to collect the information from its associated source. Denote by $\mathcal{N} = \{1, \dots, N\}$ the set of AP-source pairs. The i th AP-source pair consists of the i th AP and the i th (associated) source, $\forall i \in \mathcal{N}$. We consider that each source has no fixed energy supplies and thus needs to replenish energy from the signal¹ sent by its AP and/or the PB. It is also considered that all APs are connected

¹Note that the energy signal could be designed as a zero-mean pseudo-random signal with arbitrary distribution as long as its power spectral density satisfies certain regulations on radio signal radiation for the operating band of interest since it does not carry any intentional information [66].

with the PB via backhaul but they are not connected with each other directly. We assume that all the AP-source pairs work on orthogonal frequency bands, while the PB can work on all frequency bands. All AP-source pairs work in the half-duplex mode. The APs and sources are each equipped with one single antenna and the PB is equipped with $M > 1$ antennas. Full CSI is assumed to be available at the transmitter side.

We exploit the “harvest-then-transmit” protocol proposed in [28]. Specifically, each source first harvests energy from RF signals broadcast by its associated AP and/or the PB in the DL and then uses the harvested energy for information transmission in the UL. By considering that the sources may be low-cost, low-complexity and low-energy devices, it is assumed that an integrated architecture is adopted at each source, where the energy harvesting component and the information processing component are integrated together by using one rectifier circuit² [67]. In this context, each source can only harvest energy from the RF signals with the frequency inside its working band, which means that each source can only harvest energy from its own AP and/or the PB.

As illustrated in Fig. 6.2, it is assumed that all APs and PB perform WET to sources simultaneously from the beginning of each transmission block \mathcal{T} . Denote by τ_i the fraction of a transmission block \mathcal{T} for DL WET from the i th AP to the i th source. Denote by τ'_i the fraction for DL WET from the PB to the i th source. Then the DL

²Note that if the sources are advanced enough such that they are equipped with separated front-end hardware for the energy harvesting unit and the information processing unit, it is also interesting to consider the case that the RF energy transfer is performed in a wideband manner and the sources can harvest energy over all frequency bands. However, the design of such a system with wideband energy transfer would be quite different from and much more complicated than the one considered with narrowband energy transfer. Thus, as with the initial effort towards the design of the PB-WPCN, I choose to focus on the case with narrowband energy transfer in this chapter and I would like to consider the design of another interesting setup with wideband energy transfer as future work.

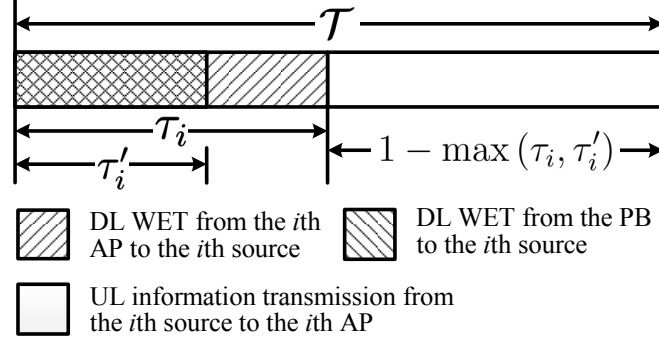


Figure 6.2: An illustration of the time diagram for i th AP-source pair in a transmission block \mathcal{T} .

WET time for the i th source is thus given by $\max(\tau_i, \tau_i') \mathcal{T}$. During the remaining time $(1 - \max(\tau_i, \tau_i')) \mathcal{T}$, the i th source uses the harvested energy to transmit its information to its corresponding AP in the UL. For convenience and without loss of generality, it is assumed that $\mathcal{T} = 1$ in the sequel of this chapter.

We assume that the DL and UL channels are reciprocal. Let scalar g_i denote the complex channel between the i th AP and the i th source and let $\mathbf{k}_i \in \mathbb{C}^{M \times 1}$ denote the complex channel vector between the PB and the i th source, where $\mathbb{C}^{M \times 1}$ denotes a set of all complex vectors of size $M \times 1$. Besides, we use $\mathbf{w}_i \in \mathbb{C}^{M \times 1}$ to denote the beamforming vector at the PB applied to the energy signal transmitted to the i th source with $\|\mathbf{w}_i\|^2 = 1$, where $\|\mathbf{w}_i\|$ is the Euclidean norm of \mathbf{w}_i . It is assumed that the i th AP transmits with power p_i to the i th source and the PB transmits to each source on different frequency bands³ with the same power p_b . Furthermore, the PB is constrained by a total energy during each transmission block, denoted by E_b^{tot} , which leads to a total energy constraint⁴ $\sum_{i \in \mathcal{N}} \tau_i' p_b \leq E_b^{tot}$.

³Multi-input single-output and orthogonal frequency division multiplexing (MISO-OFDM) can be adopted at the PB to power the sources on different frequency bands via multiple antennas.

⁴Generally, an energy consumption constraint should also be imposed to each AP as that to the

Then, during the DL WET phase, the received signal at the i th source, denoted by y_i , can be expressed as follows when both the i th AP and the PB perform WET to the i th source,

$$y_i = \sqrt{p_i}g_i x_{i,AP} + \sqrt{p_b} \mathbf{k}_i^H \mathbf{w}_i x_{i,PB} + n_i, \quad (6.1.1)$$

where $x_{i,AP}$ and $x_{i,PB}$ are the transmitted signals from the i th AP and the PB to the i th source, respectively, with $\mathbb{E}[|x_{i,AP}|^2] = 1$ and $\mathbb{E}[|x_{i,PB}|^2] = 1$. $\mathbb{E}[\cdot]$ denotes the expectation. $(\cdot)^H$ is the Hermitian transpose. n_i is the AWGN with a zero mean and variance σ^2 . Note that the first or the second term on the right-hand side of (6.1.1) should be removed when only the PB or the i th AP transfers energy to the i th source.

Since the multi-antenna PB transmits energy signal to a single-antenna source and full CSI is available at the PB, the optimal energy beamforming vector at the PB should be maximum ratio transmission (MRT) [41, 68]. We thus have $\mathbf{w}_i = \frac{\mathbf{k}_i}{\|\mathbf{k}_i\|}$. Therefore, at the end of WET phase, the amount of energy harvested by the i th source, denoted by E_i^s , can be written by

$$E_i^s = \eta (\tau_i p_i G_i + \tau'_i p_b K_i), \quad (6.1.2)$$

where $0 < \eta < 1$ is the energy conversion efficiency, $G_i \triangleq |g_i|^2$ is the channel power gain between the i th AP and the i th source, $K_i \triangleq \|\mathbf{k}_i\|^2$ is the equivalent channel power gain between the PB and the i th source, and the harvested energy from the noise is ignored since it is negligible in practice [67]. It is also defined that $\mathbf{G} \triangleq$

PB. However, the energy consumption requirement at the APs could be easily satisfied because we consider that the APs are connected to constant power supplies and only serve their own source with fixed transmit power. In contrast, the PB needs to transmit wireless energy to multiple sources and its energy consumption constraint could be frequently violated when the number of sources becomes large. Moreover, it is worth mentioning that the proposed distributed algorithm elaborated in Section 6.2 can readily be extended to solve the problem with additional energy constraints for the APs. For the purpose of exposition, in this chapter I choose to ignore the energy constraint at each AP.

$[G_1, \dots, G_N]^H$ and $\mathbf{K} \triangleq [K_1, \dots, K_N]^H$, respectively. Note that the derivation from (6.1.1) to (6.1.2) is carried out based on the assumption that the signals transmitted by the AP and PB are mutually independent as in [69–71].

After the source replenishes its energy in the DL, it then transmits its information to the AP in the UL. It is assumed that the harvested energy is exhausted by the source for information transmission. The effect of energy storage and energy consumption of the circuit is disregarded for clarity as in [28, 29]. The transmit power of the i th source, denoted by q_i , is thus equal to

$$q_i = \frac{E_i^s}{1 - \max\{\tau_i, \tau'_i\}} = \frac{\eta(\tau_i p_i G_i + \tau'_i p_b K_i)}{1 - \max(\tau_i, \tau'_i)}. \quad (6.1.3)$$

Then, the achievable throughput at the i th AP can be written as

$$\begin{aligned} R_i(\tau_i, \tau'_i) &= (1 - \max(\tau_i, \tau'_i)) W \log_2 \left(1 + \frac{G_i q_i}{\sigma^2} \right) \\ &= (1 - \max(\tau_i, \tau'_i)) W \log_2 \left(1 + \frac{G_i \eta(\tau_i p_i G_i + \tau'_i p_b K_i)}{(1 - \max(\tau_i, \tau'_i)) \sigma^2} \right), \end{aligned} \quad (6.1.4)$$

where W is the bandwidth and σ^2 is the noise power, which are assumed to be the same for all AP-source pairs, without loss of generality. It can be observed from (6.1.4) that the achievable throughput for the i th source to its AP can be increased with the assistance of the PB.

In this chapter, both cooperative and non-cooperative scenarios are considered based on whether the PB is cooperative with the APs or not. In the cooperative scenario, the PB and the APs cooperate to maximise the network social welfare, defined as the weighted sum-throughput of all AP-source pairs. In contrast, the PB and the APs are considered to be self-interested in the non-cooperative scenario. More specifically, the PB will request a monetary compensation for its wireless charging service and each AP-source pair will value its benefits with its payment to the PBs. Note that the cooperative scenario can correspond to the situation that APs and

the PB are deployed by the same operator as the one considered in [26]. The non-cooperative scenario could be used to model the case that the APs and the PB are installed by different operators. In the following sections, the resource allocation schemes for these two scenarios will be designed, respectively.

6.2 Cooperative Scenario

In this section, a social welfare maximisation problem is first formulated for the cooperative scenario and then it is solved by a water-filling based algorithm in a distributed manner.

6.2.1 Problem Formulation

Consider a weight $\lambda_i > 0$ for the i th AP, which represents a gain per unit throughput from the i th source to its AP. Then, the social welfare maximisation problem can be formulated as

$$\begin{aligned} & \max_{\{\tau_i\}, \{\tau'_i\}} \sum_{i \in \mathcal{N}} \lambda_i R_i(\tau_i, \tau'_i), \\ & \text{s.t. } \tau_i, \tau'_i \geq 0, \quad 0 < \max(\tau_i, \tau'_i) < 1, \quad \forall i \in \mathcal{N}, \end{aligned} \quad (6.2.1)$$

$$\sum_{i \in \mathcal{N}} \tau'_i p_b \leq E_b^{\text{tot}},$$

where the constraint $0 < \max(\tau_i, \tau'_i) < 1$ guarantees that the weighted sum-throughput is larger than zero. By observing the objective function of problem (6.2.1), we obtain the following lemma:

Lemma 6.1. *The function $R_i(\tau_i, \tau'_i)$ in (6.1.4) can be rewritten as*

$$R_i(\tau_i, E_i) = (1 - \tau_i) W \log_2 \left(1 + \frac{G_i \eta (\tau_i p_i G_i + E_i K_i)}{(1 - \tau_i) \sigma^2} \right), \quad (6.2.2)$$

where $E_i \triangleq \tau'_i p_b$ is the amount of energy that the PB allocates to the i th source.

Proof. We first prove that $\max\{\tau_i, \tau'_i\} = \tau_i$ by contradiction. If $\tau_i < \tau'_i$, then $\max\{\tau_i, \tau'_i\} = \tau'_i$ and (6.1.4) becomes

$$R_i(\tau_i, \tau'_i) = (1 - \tau'_i) W \log_2 \left(1 + \frac{G_i \eta (\tau_i p_i G_i + \tau'_i p_b K_i)}{(1 - \tau'_i) \sigma^2} \right). \quad (6.2.3)$$

We can easily see that the right-hand side of (6.2.3) is a monotonically increasing function of τ_i . This means that the achievable throughput R_i can always be enhanced by increasing the value of τ_i to that of τ'_i . This contradicts the assumption that $\tau_i < \tau'_i$. We thus have $\tau_i \geq \tau'_i$, i.e., $\max\{\tau_i, \tau'_i\} = \tau_i$. Furthermore, for the ease of presentation, it is defined that $E_i \triangleq \tau'_i p_b$, which is the amount of energy that the PB allocates to the i th source. Applying these two operations into (6.1.4), we can rewrite it as (6.2.2), which completes this proof. \square

Based on Lemma 6.1, we can reformulate the problem (6.2.1) as

$$\begin{aligned} \max_{\boldsymbol{\tau}, \mathbf{E}} \quad & \sum_{i \in \mathcal{N}} \lambda_i R_i(\tau_i, E_i), \\ \text{s.t.} \quad & \mathbf{0} \prec \boldsymbol{\tau} \prec \mathbf{1}, \\ & \mathbf{0} \preceq \mathbf{E} \preceq \boldsymbol{\tau} p_b, \\ & \sum_{i \in \mathcal{N}} E_i \leq E_b^{tot}, \end{aligned} \quad (6.2.4)$$

where $\boldsymbol{\tau} \triangleq [\tau_1, \dots, \tau_N]^T$ and $\mathbf{E} \triangleq [E_1, \dots, E_N]^T$, the symbols \prec or \preceq represent the element-wise inequality, $\mathbf{0}$ or $\mathbf{1}$ is a vector of zeros or ones that has the same size as $\boldsymbol{\tau}$ and \mathbf{E} , and the constraint of \mathbf{E} is derived based on $E_i = \tau'_i p_b$ and $0 \leq \tau'_i \leq \tau_i$. Moreover, we denote by $(\boldsymbol{\tau}^*, \mathbf{E}^*)$ the optimal solution to the problem (6.2.4).

We can see from (6.2.4) that the social welfare can only be maximised by jointly designing the DL WET time of each AP and the energy allocation of the PB. It is

worth noting that $\boldsymbol{\tau}$ and \mathbf{E} are mutually interdependent and the achievable throughput of all APs are coupled together due to the total energy constraint $\sum_{i \in \mathcal{N}} E_i \leq E_b^{tot}$.

6.2.2 Optimal Solution and Distributed Algorithm

The convexity of the objective function in problem (6.2.4) can readily be checked by introducing a new optimisation variable $\theta_i = 1 - \max\{\tau_i, \tau'_i\}$, $\forall i \in \mathcal{N}$. Substituting θ_i into (6.1.4), we can observe that $R_i(\tau_i, \tau'_i)$ is jointly concave on τ_i , τ'_i and θ_i , since θ_i is the perspective variable of the log. Accordingly, the problem (6.2.4) is convex and could be solved by applying standard convex optimisation approaches. However, these approaches are normally done in a centralised manner. In practice, a distributed approach is of more interest because it can significantly reduce the network overhead. Motivated by this, I propose a distributed method with three steps to resolve it in this section. In step 1, we first find the optimal relationship between τ_i and E_i by expressing τ_i as a function of E_i . Then, the problem (6.2.4) can be reformulated as a problem with only \mathbf{E} as a variable. In step 2, we investigate the properties of the reformulated problem. Finally, a water-filling based algorithm is proposed to find the optimal solution of the new problem in step 3. I present the details of these three steps in the following subsections.

Step 1. Problem Reformulation

We first derive the expression of τ_i as a function of E_i for each AP. With a given \mathbf{E} that satisfies $\mathbf{0} \preceq \mathbf{E} \prec \mathbf{1}p_b$ and $\sum_{i \in \mathcal{N}} E_i \leq E_b^{tot}$, the problem (6.2.4) is decoupled and we can have the following optimisation problem for each AP regarding τ_i ,

$$\max_{\tau_i} \mathcal{S}_i(\tau_i), \text{ s.t. } 0 < \tau_i < 1, \tau_i \geq \frac{E_i}{p_b}, \quad (6.2.5)$$

where $\mathcal{S}_i(\tau_i)$ can be expressed by

$$\mathcal{S}_i(\tau_i) = \lambda_i R_i(\tau_i, E_i) = \lambda_i W(1 - \tau_i) \log_2 \left(1 + \frac{G_i \eta (\tau_i p_i G_i + E_i K_i)}{(1 - \tau_i) \sigma^2} \right). \quad (6.2.6)$$

We denote by $\tau_i(E_i)$ the optimal solution of (6.2.5), which is given in the following proposition.

Proposition 6.2. *Given $E_i \in [0, p_b]$, the optimal solution $\tau_i(E_i)$ to the problem (6.2.5) can be expressed by*

$$\tau_i(E_i) = \begin{cases} \frac{(z_i^\dagger - 1)\sigma^2 - G_i \eta E_i K_i}{(z_i^\dagger - 1)\sigma^2 + G_i^2 \eta p_i}, & \text{if } 0 \leq E_i \leq E_i^{lim}, \\ \frac{E_i}{p_b}, & \text{if } E_i^{lim} < E_i < p_b, \end{cases} \quad (6.2.7)$$

where

$$E_i^{lim} \triangleq \frac{p_b (z_i^\dagger - 1) \sigma^2}{(z_i^\dagger - 1) \sigma^2 + G_i \eta (p_i G_i + p_b K_i)}, \quad (6.2.8)$$

and $z_i^\dagger > 1$ can be expressed by

$$z_i^\dagger = \exp \left(\mathcal{W} \left(\frac{G_i^2 \eta p_i - \sigma^2}{\sigma^2 \exp(1)} \right) + 1 \right), \quad (6.2.9)$$

in which $\mathcal{W}(x)$ is the Lambert \mathcal{W} function that is the solution to the equality $x = \mathcal{W} \exp(\mathcal{W})$.

Proof. See Appendix C.1. □

Then, by replacing τ_i in $\mathcal{S}_i(\tau_i)$ with $\tau_i(E_i)$ given in Proposition 6.2, we have a function $\mathcal{S}_i(E_i)$ with only E_i as the variable given by the following Lemma.

Lemma 6.3. *$\mathcal{S}_i(E_i)$ can be expressed by*

$$\mathcal{S}_i(E_i) = \begin{cases} \frac{\lambda_i W G_i \eta (p_i G_i + E_i K_i)}{z_i^\dagger \sigma^2 \ln 2}, & \text{if } 0 \leq E_i \leq E_i^{lim}, \\ \lambda_i W \left(1 - \frac{E_i}{p_b} \right) \log_2 \left(1 + \frac{X_i E_i}{p_b - E_i} \right), & \text{if } E_i^{lim} < E_i < p_b, \end{cases} \quad (6.2.10)$$

where $X_i \triangleq \frac{G_i \eta (p_i G_i + p_b K_i)}{\sigma^2}$.

Proof. See Appendix C.2. □

Hence, we now can reformulate the problem (6.2.4) with only \mathbf{E} as the variable as follows

$$\max_{\mathbf{E}} \sum_{i \in \mathcal{N}} \mathcal{S}_i(E_i), \text{ s.t. } \mathbf{0} \preceq \mathbf{E} \prec \mathbf{1}p_b, \sum_{i \in \mathcal{N}} E_i \leq E_b^{tot}. \quad (6.2.11)$$

Note that we can solve the problem (6.2.11) to obtain \mathbf{E}^* , and then we can calculate $\boldsymbol{\tau}^*$ based on (6.2.7), thereby solving the original problem (6.2.4).

Step 2. Property Characterisation

To solve the problem (6.2.11), we first characterise the properties of the objective function $\sum_{i \in \mathcal{N}} \mathcal{S}_i(E_i)$. Since $\sum_{i \in \mathcal{N}} \mathcal{S}_i(E_i)$ is a positive summation of N independent functions with the same structure, we then first investigate the property of any function $\mathcal{S}_i(E_i)$, which is summarised in the following proposition:

Proposition 6.4. *When $0 \leq E_i < p_b$, $\mathcal{S}_i(E_i)$ is differentiable and the gradient of $\mathcal{S}_i(E_i)$, denoted by $\nabla \mathcal{S}_i(E_i)$, is continuous. $\nabla \mathcal{S}_i(E_i)$ is derived as*

$$\nabla \mathcal{S}_i(E_i) = \begin{cases} \alpha_i, & \text{if } 0 \leq E_i \leq E_i^{lim}, \\ \beta_i(E_i), & \text{if } E_i^{lim} < E_i < p_b, \end{cases} \quad (6.2.12)$$

where α_i is a constant given by

$$\alpha_i = \frac{\lambda_i W G_i \eta K_i}{z_i^\dagger \sigma^2 \ln 2}, \quad (6.2.13)$$

and $\beta_i(E_i)$ is strictly decreasing, which is expressed as

$$\beta_i(E_i) = -\frac{\lambda_i W}{p_b} \log_2 \left(1 + \frac{X_i E_i}{p_b - E_i} \right) + \frac{\lambda_i W X_i}{(p_b - E_i + X_i E_i) \ln 2}. \quad (6.2.14)$$

Proof. See Appendix C.2. □

Therefore, based on Proposition 6.4, it is easy to show that $\mathcal{S}_i(E_i)$ is a concave function of E_i when $0 \leq E_i < p_b$. Then, by letting the first-order derivative of $\mathcal{S}_i(E_i)$ be equal to zero, i.e., $\beta_i(E_i) = 0$, we obtain the stationary point that maximises $\mathcal{S}_i(E_i)$, denoted by E_i^o , given by

$$E_i^o = \frac{p_b (z_i^\dagger - 1) \sigma^2}{(z_i^\dagger - 1) \sigma^2 + G_i \eta (p_i G_i + p_b K_i)}, \quad (6.2.15)$$

where $z_i^\dagger > 1$ can be expressed as

$$z_i^\dagger = \exp \left(\mathcal{W} \left(\frac{G_i \eta (p_i G_i + p_b K_i) - \sigma^2}{\sigma^2 \exp(1)} \right) + 1 \right). \quad (6.2.16)$$

Note that E_i^o has the same structure as E_i^{lim} given in (6.2.8). The only differences between them are the parameters z_i^\dagger and z_i^\dagger . Furthermore, we can easily observe that $z_i^\dagger > z_i^\dagger > 1$ based on the property of the equation (C.1.2) in Appendix C.1. We divide both the top and the bottom of the right-hand side in (6.2.15) by $(z_i^\dagger - 1) \sigma^2$ (in (6.2.8) by $(z_i^\dagger - 1) \sigma^2$). We thus can obtain that $E_i^{lim} < E_i^o < p_b$. Now, we have an important property of $\mathcal{S}_i(E_i)$: it is increasing when $0 \leq E_i \leq E_i^o$ and decreasing when $E_i^o < E_i < p_b$. The PB will at most allocate the amount of energy that is equal to E_i^o to the i th AP to achieve the maximisation of the social welfare. We thus only need to focus on the interval $0 \leq E_i \leq E_i^o$ for each AP. We now can update the property of the function $\mathcal{S}_i(E_i)$ over the interval $0 \leq E_i \leq E_i^o$ in the following proposition:

Proposition 6.5. *For $0 \leq E_i \leq E_i^o$, $\mathcal{S}_i(E_i)$ is differentiable, increasing and concave, and $\nabla \mathcal{S}_i(E_i)$ is continuous. $\nabla \mathcal{S}_i(E_i)$ is constant when $0 \leq E_i \leq E_i^{lim}$ while strictly decreasing when $E_i^{lim} < E_i < E_i^o$ and equal to zero when $E_i = E_i^o$.*

For the ease of understanding, functions $\tau_i(E_i)$, $\mathcal{S}_i(E_i)$ and $\nabla \mathcal{S}_i(E_i)$, given in (6.2.7), (6.2.10) and (6.2.12), respectively, are graphically interpreted in Fig. 6.3. We use the black and red curves to characterise the functions in the intervals $0 \leq E_i \leq$

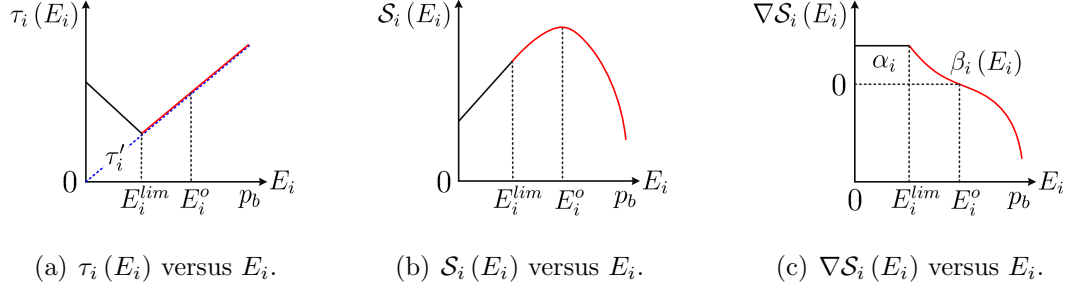


Figure 6.3: Graphical interpretations for the functions (6.2.7), (6.2.10) and (6.2.12) in the proposed cooperative scenario.

E_i^{lim} and $E_i^{lim} < E_i < p_b$, respectively. We can see from Fig. 6.3(a) that $\tau_i(E_i)$ linearly decreases in the interval $0 \leq E_i \leq E_i^{lim}$, but linearly increases when $E_i^{lim} < E_i < p_b$. The harvesting time from the PB $\tau'_i = \frac{E_i}{p_b}$ is also shown in Fig. 6.3(a) using the blue dashed line, which is always linearly increasing in the whole interval and coincides with the red curve in the interval $E_i^{lim} < E_i < p_b$. It can be observed in Fig. 6.3(b) that $S_i(E_i)$ is linearly increasing in the interval $0 \leq E_i \leq E_i^{lim}$, which corresponds to the observation in Fig. 6.3(c) that $\nabla S_i(E_i)$ is constant for $0 \leq E_i \leq E_i^{lim}$. With the increase of E_i , $S_i(E_i)$ is maximised at the point E_i^o , where $\nabla S_i(E_i)$ equals zero. Finally, when $E_i^o < E_i < p_b$, $S_i(E_i)$ keeps decreasing and $\nabla S_i(E_i)$ is shown to be always negative.

Step 3. A Distributed Algorithm

Based on the analysis in step 2, the optimisation problem (6.2.11) can be written as

$$\begin{aligned}
 & \max_{\mathbf{E}} \sum_{i \in \mathcal{N}} S_i(E_i), \\
 & \text{s.t. } \mathbf{0} \preceq \mathbf{E} \preceq \mathbf{E}^o, \\
 & \sum_{i \in \mathcal{N}} E_i \leq E_b^{tot},
 \end{aligned} \tag{6.2.17}$$

where $\mathbf{E}^o \triangleq [E_1^o \cdots, E_N^o]^T$. Based on the property of $\mathcal{S}_i(E_i)$ summarised in Proposition 6.5, we then can solve the problem (6.2.17) using a water-filling based approach [72]. It should be noted that when $E_b^{tot} \geq \sum_{i \in \mathcal{N}} E_i^o$, the optimisation problem (6.2.17) has a trivial solution that $E_i^* = E_i^o, \forall i \in \mathcal{N}$. We thus only consider the case that $E_b^{tot} < \sum_{i \in \mathcal{N}} E_i^o$, namely, the PB's energy will be exhausted to enhance the social welfare. The optimal solution \mathbf{E}^* to the problem (6.2.17) can be presented by the following proposition.

Proposition 6.6. *The optimal solution to the problem (6.2.17) is given by $\mathbf{E}^* = [E_1^*, \cdots, E_N^*]^T$ with*

$$E_i^* = \begin{cases} \gamma_i(\nu), & \text{if } 0 \leq \nu < \alpha_i, \\ E_b^{tot} - \sum_{j \in \mathcal{N} \setminus \{i\}} E_j^*, & \text{if } \nu = \alpha_i \\ 0, & \text{if } \nu > \alpha_i, \end{cases} \quad (6.2.18)$$

where $\nu \geq 0$ is a constant chosen to meet the total energy constraint $\sum_{i \in \mathcal{N}} E_i^* = E_b^{tot}$ and $\gamma_i(\nu)$ is a strictly decreasing function on $0 \leq \nu < \alpha_i$ given by

$$\gamma_i(\nu) = \frac{p_b (z_i^{\S} - 1) \sigma^2}{(z_i^{\S} - 1) \sigma^2 + G_i \eta (p_i G_i + p_b K_i)}, \quad (6.2.19)$$

where $z_i^{\S} > 1$ is the unique solution of the equation

$$z_i \ln(z_i) + \left(\frac{\nu p_b \ln 2}{\lambda_i W} - 1 \right) z_i + 1 = \frac{G_i \eta (p_i G_i + p_b K_i)}{\sigma^2}. \quad (6.2.20)$$

Proof. See Appendix C.3. □

According to Proposition 6.5 and Proposition 6.6, there exists a unique ν to meet the total energy constraint. However, from Proposition 6.6, if $\nu = \alpha_i$, then E_i^* has a unique solution only under the assumption that each AP corresponds to a different $\alpha_i, \forall i \in \mathcal{N}$. This is because $E_j^*, \forall j \in \mathcal{N} \setminus \{i\}$ is unique when $\nu \neq \alpha_j$. If there is at least

another AP, say the k th AP, $k \in \mathcal{N} \setminus \{i\}$, and $\nu = \alpha_k = \alpha_i$, then the optimality can be achieved with multiple solutions. Based on the proof of Proposition 6.6, the solutions of E_i^* and E_k^* can be any combination, which is subject to that $0 \leq E_i^* \leq E_i^{lim}$, $0 \leq E_k^* \leq E_k^{lim}$ and $E_i^* + E_k^* = E_b^{tot} - \sum_{j \in \mathcal{N} \setminus \{i,k\}} E_j^*$.

Next, we propose a water-filling based distributed algorithm to obtain \mathbf{E}^* by finding the constant ν . Note that we only consider the case that each AP corresponds to a different α_i , which can be readily modified to adapt to the case that multiple APs have the same α_i . For convenience and without loss of generality, we assume that $\alpha_1 > \alpha_2 > \dots > \alpha_N$. As ν is unique and $\nu \geq 0$, a possible value of ν could be α_i , $\forall i \in \mathcal{N}$, or between an interval (α_{i+1}, α_i) , where $\alpha_{N+1} \triangleq 0$. Note that when the optimal ν falls into an interval between any two adjacent α_i 's, we need to apply the iterative water-filling algorithm [73] to achieve it. Specifically, after the PB releases the current energy price in each round, all the APs update their bids in parallel and feed them back to the PB within the current round.

We now elaborate the steps in Algorithm 1. Each AP first provides its α_i to the PB, then the PB constructs a descending sequence $\{\alpha_i\}_{i \in \mathcal{N}}$, sets $i = 1$ and announces $\nu^{(i)}$, which is equal to each α_i , sequentially. Then, with $\nu^{(i)}$, the j th AP, $\forall j \in \mathcal{N} \setminus \{i\}$, computes the response, here denoted by $E_j^{(i)}$, according to (6.2.18), while⁵ the i th AP responds that $E_i^{(i)} = E_i^{lim}$. Then, by comparing the aggregate of all the responses, computed by $E_{agg}^{(i)} = \sum_{j \in \mathcal{N} \setminus \{i\}} E_j^{(i)} + E_i^{(i)}$, with E_b^{tot} , the PB can decide on the value of ν as listed in Algorithm 1. Note that if ν exists in an interval, then a bisection

⁵According to Proposition 6.6, given $\nu = \alpha_i$, the response energy for the i th AP is that $E_i^* = E_b^{tot} - \sum_{j \in \mathcal{N} \setminus \{i\}} E_j^*$. However, this happens only when ν is found to meet the total energy constraint. As proved in Appendix C.3, given $\nu = \alpha_i$, under the assumption that the i th AP does not know the total energy constraint, the possible value of E_i^* exists in an interval $[0, E_i^{lim}]$. Therefore, in this case, the i th AP is set to respond that $E_i^{(i)} = E_i^{lim}$ to the PB. Then the PB knows the interval of the i th AP, which will help it to make decisions in the following steps.

Algorithm 1 Water-filling based distributed algorithm

- 1: Each AP reflects its α_i to the PB.
 - 2: The PB constructs a descending sequence $\{\alpha_i\}_{i \in \mathcal{N}}$, sets $i = 1$ and repeats:
 1. The PB announces $\nu^{(i)} = \alpha_i$ to all APs.
 2. The j th AP responds an optimal $E_j^{(i)}$ to the PB according to Proposition 6.6, $\forall j \in \mathcal{N} \setminus \{i\}$, while the i th AP responds $E_i^{(i)} = E_i^{lim}$.
 3. The PB computes that $E_{agg}^{(i)} = \sum_{j \in \mathcal{N} \setminus \{i\}} E_j^{(i)} + E_i^{(i)}$ and compares $E_{agg}^{(i)}$ with E_b^{tot} :
 - (a) If $E_{agg}^{(i)} < E_b^{tot}$, then set $i = i + 1$ and continue.
 - (b) Elseif $E_{agg}^{(i)} \geq E_b^{tot}$ and $E_{agg}^{(i)} - E_i^{lim} \leq E_b^{tot}$, then $\nu = \alpha_i$, $E_j^* = E_j^{(i)}$, and $E_i^* = E_b^{tot} - \sum_{j \in \mathcal{N} \setminus \{i\}} E_j^{(i)}$.
 - (c) Else, the unique $\nu \in (\alpha_i, \alpha_{i-1})$, which can be readily found via a bisection method.
-

method [74] can be employed to find the unique value. The implementation of the bisection method is simple and thus omitted. It can be observed that Algorithm 1 can always find the exact value or the existing interval of ν with at most N iterations, since ν is unique and $0 \leq \nu \leq \max_{i \in \mathcal{N}} \{\alpha_i\}$.

According to Algorithm 1, each AP first needs to measure the (equivalent) channel power gains G_i and K_i , and acquire the transmit power p_b from the PB. The values calculated by each AP and forwarded to the PB should be α_i given in (6.2.13), E_i^{lim} defined in (6.2.8) and the optimal response obtained by (6.2.18). With these signals from the APs, the PB announces $\nu_i^{(i)}$ at the end of each iteration and the allocated energy E_i^* finally to each AP.

Finally, with the value of ν achieved via Algorithm 1 and (6.2.18), we can obtain \mathbf{E}^* . Subsequently, based on (6.2.7) given in Proposition 6.2, we have $\tau_i^* = \tau_i(E_i^*)$ and $\boldsymbol{\tau}^* = [\tau_1^*, \dots, \tau_N^*]^T$. Therefore, we have already found the optimal solution $(\boldsymbol{\tau}^*, \mathbf{E}^*)$ of the original problem (6.2.4).

6.3 Non-Cooperative Scenario

This section investigates the non-cooperative scenario, where the multiple APs and the PB are assumed to be rational and self-interested. We adopt an auction model to characterise the conflicting interactions among the APs and the PB, where the APs are bidders and the PB is the auctioneer. Note that auction theory [75] has been well investigated and widely applied for designing the resource allocation in cognitive radio networks [76], D2D communication networks [77] and cooperative communication networks [78], as well as energy harvesting networks [69, 79]. A cooperative network with multiple source-destination pairs and a relay was considered in [69], where an auction based power allocation scheme was proposed to allocate the harvested energy of the relay in a distributed manner. [79] formulated a non-cooperative game to model the competitive WET bidding of the users in a WPCN with one AP and multiple users, where the AP adopted an auction mechanism for DL WET. Both [69] and [79] adopted the concept of Nash equilibrium to evaluate the strategic interactions between bidders only. In contrast, in this chapter we adopt a different auction mechanism to study the hierarchical interaction between the PB (auctioneer) and the AP-source pairs (bidders). In particular, we employ a well-known Ausubel auction [80], which constructs an ascending-bid version of the Vickrey-Clarke-Groves (VCG) auction and induces truthful bidding⁶ as well as achieving the maximum social welfare, i.e., the global optimum [75, 80–82]. In the sequel, we first define the utility functions of both APs and the PB. Then we formulate an auction game, in which an auction based distributed algorithm is proposed. Last, we analyse the formulated game and prove

⁶Truthful bidding means that reporting true optimal demand at every iteration is the mutually best response for each bidder [75].

convergence of the proposed algorithm.

6.3.1 Utility Functions

We first present the utility functions of APs and the PB, respectively.

The Utility Function of Each AP

Given the unit price of the PB's energy, denoted by μ , the payment from the i th AP can be written by

$$\Gamma_i = \mu E_i. \quad (6.3.1)$$

Therefore, with (6.2.2) and (6.3.1), the utility function of the i th AP can be defined as

$$\begin{aligned} \mathcal{U}_i(\tau_i, E_i, \mu) &= \lambda_i R_i(\tau_i, E_i) - \Gamma_i \\ &= \lambda_i(1 - \tau_i)W \log_2 \left(1 + \frac{G_i \eta (\tau_i p_i G_i + E_i K_i)}{(1 - \tau_i) \sigma^2} \right) - \mu E_i. \end{aligned} \quad (6.3.2)$$

The Utility Function of the PB

Recall that $\mathbf{E} = [E_1, \dots, E_N]^T$. Then, the utility of the PB can be expressed as

$$\mathcal{U}_b(\mu, \mathbf{E}) = \sum_{i \in \mathcal{N}} \Gamma_i = \mu \sum_{i \in \mathcal{N}} E_i. \quad (6.3.3)$$

Note that there is a reserve price for the PB, denoted by $\mu^{(0)}$. It is assumed that if the outcome price of an auction game is larger than $\mu^{(0)}$, the PB would benefit from the trade. *Otherwise, it would not participate in the trade* [76, 82].

6.3.2 Auction Game

Now, we are ready to formulate an auction game, where the APs are bidders and the PB is the auctioneer. Each AP submits bids to compete for the PB's energy, in

order to maximise its utility defined in (6.3.2). On the other hand, the PB aims to maximise its revenue in (6.3.3) by increasing its energy's unit price. In particular, the auctioneer first announces an initial price $\mu = \mu^{(0)}$, and the bidders respond to the auctioneer with their optimal demands, i.e., the bids. Then, the auctioneer raises the price μ until the aggregate demands meet the total energy constraint, and at that point, the auctioneer concludes the auction and decides the final allocated energy to each bidder.

In the formulated game, at each round $t \geq 0$, with a given price $\mu^{(t)}$, the i th AP has an optimisation problem as

$$\max_{\tau_i, E_i} \mathcal{U}_i(\tau_i, E_i, \mu^{(t)}), \text{ s.t. } 0 < \tau_i < 1, 0 \leq E_i \leq \tau_i p_b. \quad (6.3.4)$$

We denote by $(\tau_i^{(t)}, E_i^{(t)})$ the optimal solution of (6.3.4). That is

$$(\tau_i^{(t)}, E_i^{(t)}) = \arg \max_{\tau_i, E_i} \mathcal{U}_i(\tau_i, E_i, \mu^{(t)}). \quad (6.3.5)$$

Thus the bid of the i th AP is $E_i^{(t)}$ given $\mu^{(t)}$. We also denote by \tilde{E}_i^* and $\tilde{\Gamma}_i^*$ the final allocated energy and the final payment of the i th AP when the PB concludes the auction. With \tilde{E}_i^* and $\tilde{\Gamma}_i^*$, the utility of the i th AP in (6.3.2) becomes

$$\mathcal{U}_i(\tau_i) = \lambda_i(1 - \tau_i)W \log_2 \left(1 + \frac{G_i \eta (\tau_i p_b G_i + \tilde{E}_i^* K_i)}{(1 - \tau_i) \sigma^2} \right) - \tilde{\Gamma}_i^*. \quad (6.3.6)$$

We then have an optimisation problem regarding τ_i as

$$\max_{\tau_i} \mathcal{U}_i(\tau_i), \text{ s.t. } 0 < \tau_i < 1, \tau_i \geq \frac{\tilde{E}_i^*}{p_b}. \quad (6.3.7)$$

We use $\tilde{\tau}_i^*$ to denote the optimal solution to problem (6.3.7), which is the optimal harvesting time of the i th source from its own AP. Analogue to the proof of Proposition 6.2, we can readily get $\tilde{\tau}_i^* = \tau_i(\tilde{E}_i^*)$, where $\tau_i(\cdot)$ is given by (6.2.7).

Algorithm 2 elaborates the auction steps. Before starting the auction, the PB sets

Algorithm 2 Auction based distributed algorithm

-
- 1: Given E_b^{tot} , price step $\Delta > 0$, and $t = 0$, the PB initialises the asking price $\mu^{(0)}$.
 - 2: With $\mu^{(0)}$, each AP computes and submits its optimal bid $E_i^{(0)}$ with (6.3.5).
 - 3: The PB sums up all bids that $\mathcal{E}^{(0)} = \sum_{i \in \mathcal{N}} E_i^{(0)}$ and compares $\mathcal{E}^{(0)}$ with E_b^{tot} :
 1. If $\mathcal{E}^{(0)} \leq E_b^{tot}$, then the PB ends the auction and quits the trade.
 2. Else, then the PB computes the cumulative clinches $\{\mathcal{C}_i^{(0)}\}_{i \in \mathcal{N}}$ by (6.3.8), sets $\mu^{(t+1)} = \mu^{(t)} + \Delta$, $t = t + 1$, and repeats:
 - (a) The PB announces $\mu^{(t)}$ to all APs.
 - (b) Given $\mu^{(t)}$, each AP updates its optimal bid $E_i^{(t)}$ obtained by (6.3.5).
 - (c) The PB sums up all bids that $\mathcal{E}^{(t)} = \sum_{i \in \mathcal{N}} E_i^{(t)}$ and compares $\mathcal{E}^{(t)}$ with E_b^{tot} :
 - i. If $\mathcal{E}^{(t)} > E_b^{tot}$, then the PB records the cumulative clinches $\{\mathcal{C}_i^{(t)}\}_{i \in \mathcal{N}}$ and sequentially sets $\mu^{(t+1)} = \mu^{(t)} + \Delta$, $t = t + 1$. The auction continues.
 - ii. Else, then by setting $T = t$, the PB concludes the auction and computes $\{\mathcal{C}_i^{(T)}\}_{i \in \mathcal{N}}$ with (6.3.9). Then, the PB allocates $\tilde{E}_i^* = \mathcal{C}_i^{(T)}$ to the i th AP.
-

up the iteration index $t = 0$, the constant price step⁷ $\Delta > 0$, and the initial price $\mu^{(0)}$. The price will be announced to all APs, and each AP will submit its optimal bid $E_i^{(0)}$ based on the optimal response given by (6.3.5). Then the PB sums up all bids that $\mathcal{E}^{(0)} \triangleq \sum_{i \in \mathcal{N}} E_i^{(0)}$, and compares $\mathcal{E}^{(0)}$ with E_b^{tot} . If $\mathcal{E}^{(0)} \leq E_b^{tot}$, then the PB ends the auction and quits the trade. Otherwise, the PB first computes a cumulative clinch [80] for each AP, which is the amount of the PB's energy that each AP is guaranteed to be allocated. The cumulative clinch for the i th AP at the round $t \geq 0$ is given by

$$\mathcal{C}_i^{(t)} = \max \left\{ 0, E_b^{tot} - \sum_{j \in \mathcal{N} \setminus \{i\}} E_j^{(t)} \right\}. \quad (6.3.8)$$

⁷Note that the constant step normally introduces errors to the convergence point [83]. However, this is not a problem for the considered auction mechanism with the proportional rationing rule (PRR) [84] given in (6.3.9), which guarantees that the total energy of the PB can be entirely allocated at last.

Then, the PB sets $\mu^{(t+1)} = \mu^{(t)} + \Delta$, $t = t + 1$ and updates $\mu^{(t)}$ to all APs.

With the updated $\mu^{(t)}$, each AP submits its optimal bid $E_i^{(t)}$ based on the optimal response $(\tau_i^{(t)}, E_i^{(t)})$ obtained by (6.3.5). By comparing the aggregate bids $\mathcal{E}^{(t)} \triangleq \sum_{i \in \mathcal{N}} E_i^{(t)}$ with E_b^{tot} , if $\mathcal{E}^{(t)} > E_b^{tot}$, then the PB records the cumulative clinches $\{\mathcal{C}_i^{(t)}\}_{i \in \mathcal{N}}$ and sequentially sets $\mu^{(t+1)} = \mu^{(t)} + \Delta$, $t = t + 1$. The auction continues till $\mathcal{E}^{(t)} \leq E_b^{tot}$. By setting $T = t$, the PB concludes the auction and computes the cumulative clinches $\{\mathcal{C}_i^{(T)}\}_{i \in \mathcal{N}}$ according to the proportional rationing rule (PRR) [84] by

$$\mathcal{C}_i^{(T)} = E_i^{(T)} + \frac{E_i^{(T-1)} - E_i^{(T)}}{\sum_{i \in \mathcal{N}} E_i^{(T-1)} - \sum_{i \in \mathcal{N}} E_i^{(T)}} \left(E_b^{tot} - \sum_{i \in \mathcal{N}} E_i^{(T)} \right), \quad (6.3.9)$$

where $\mathcal{C}_i^{(T)}$ is actually the finally allocated energy to the i th AP and it is a sum of its last energy bid and a proportion of the remaining energy $(E_b^{tot} - \sum_{i \in \mathcal{N}} E_i^{(T)})$. Then, the PB allocates $\tilde{E}_i^* = \mathcal{C}_i^{(T)}$ to the i th AP. With \tilde{E}_i^* , the i th AP can decide its final harvesting time $\tilde{\tau}_i^*$. Hence, the utility of the i th AP can be expressed by

$$\mathcal{U}_i(\tilde{\tau}_i^*, \tilde{E}_i^*) = \lambda_i (1 - \tilde{\tau}_i^*) W \log_2 \left(1 + \frac{G_i \eta (\tilde{\tau}_i^* p_i G_i + \tilde{E}_i^* K_i)}{(1 - \tilde{\tau}_i^*) \sigma^2} \right) - \tilde{\Gamma}_i^*, \quad (6.3.10)$$

where the payment from the i th AP $\tilde{\Gamma}_i^*$ is given by

$$\tilde{\Gamma}_i^* = \mu^{(0)} \mathcal{C}_i^{(0)} + \sum_{t=1}^T \mu^{(t)} (\mathcal{C}_i^{(t)} - \mathcal{C}_i^{(t-1)}). \quad (6.3.11)$$

Notice that the term $(\mathcal{C}_i^{(t)} - \mathcal{C}_i^{(t-1)})$ in (6.3.11) is actually the amount of energy that the i th AP is guaranteed to be allocated with the announced price $\mu^{(t)}$. Their product will be the corresponding payment of the i th AP at the current round. By accumulating these payments generated at each round (from $t = 0$ to $t = T$), we can achieve the total payment of the i th AP given in (6.3.11). The utility of the PB thus

is written by

$$\mathcal{U}_b = \sum_{i \in \mathcal{N}} \tilde{\Gamma}_i^* = \sum_{i \in \mathcal{N}} \left(\mu^{(0)} \mathcal{C}_i^{(0)} + \sum_{t=1}^T \mu^{(t)} \left(\mathcal{C}_i^{(t)} - \mathcal{C}_i^{(t-1)} \right) \right). \quad (6.3.12)$$

6.3.3 Analysis of the Formulated Game

In this subsection, we analyse the formulated auction game. We first derive the optimal solution to problem (6.3.4) given in the following proposition.

Proposition 6.7. *Given a price $\mu^{(t)}$ by the PB, the optimal solution to problem (6.3.4) can be expressed as*

$$\left(\tau_i^{(t)}, E_i^{(t)} \right) = \begin{cases} \left(\frac{(z_i^\dagger - 1)\sigma^2}{(z_i^\dagger - 1)\sigma^2 + G_i^2 \eta p_i}, 0 \right), & \text{if } \mu^{(t)} \geq \mu_i^{lim}, \\ \left(\frac{\gamma_i(\mu^{(t)})}{p_b}, \gamma_i(\mu^{(t)}) \right), & \text{if } \mu^{(t)} < \mu_i^{lim}, \end{cases} \quad (6.3.13)$$

where μ_i^{lim} is defined as the maximum acceptable price for the i th AP, which is equal to α_i in (6.2.13), z_i^\dagger and $\gamma_i(\cdot)$ are expressed in (6.2.9) and (6.2.19), respectively.

Proof. See Appendix C.4. □

Next, we prove that the proposed auction based distributed algorithm has the following convergence property.

Proposition 6.8. *The proposed auction based distributed algorithm converges within a finite number of iterations.*

Proof. Recall that $\mathcal{E}^{(t)} = \sum_{i \in \mathcal{N}} E_i^{(t)}$ and the auction concludes when $\mathcal{E}^{(t)} \leq E_b^{tot}$. According to Proposition 6.7, if the asking price $\mu^{(t)} \geq \mu_i^{lim}$, then the i th AP will drop from the auction with $E_i^{(t)} = 0$. If the asking price $\mu^{(t)} < \mu_i^{lim}$, then the i th AP always submits a non-zero bid $E_i^{(t)} = \gamma_i(\mu^{(t)})$. By referring to Proposition 6.6,

we can show that $\gamma_i(\mu^{(t)})$ is a strictly decreasing function when $0 \leq \mu^{(t)} < \mu_i^{lim}$ and when $\mu(t)$ approaches μ_i^{lim} , we can get

$$\lim_{\mu \rightarrow \mu_i^{lim}} E_i^{(t)} = E_i^{lim}. \quad (6.3.14)$$

We denote by n the number of iterations when the proposed auction concludes. Recall that the price step is Δ . Thus $\mu^{(T)} = \Delta \times n + \mu^{(0)}$. When n grows, $\mu^{(T)}$ increases. Since $E_i^{(T)}$ is a decreasing function of $\mu^{(T)}$, the summation of bids $\mathcal{E}^{(T)} = \sum_{i \in \mathcal{N}} E_i^{(T)}$ will decrease as $\mu^{(T)}$ increases. Therefore, there always exists an $\mathcal{E}^{(T)}$ that satisfies $\mathcal{E}^{(T)} \leq E_b^{tot}$ such that the PB concludes the auction. Hence, the number of iterations n is finite, which completes this proof. \square

Last, we analyse the required signaling for the computations in the non-cooperative scenario. According to Algorithm 2, each AP first needs to measure the (equivalent) channel power gains G_i and K_i , and acquire the transmit power p_b from the PB. The only value calculated by each AP and forwarded to the PB is the optimal bid $E_i^{(t)}$ obtained by (6.3.13). With all the bids from the APs, the PB announces the price $\mu^{(t)}$ at the end of each iteration and the allocated energy \tilde{E}_i^* finally to each AP.

6.4 Numerical Results

In this section, numerical results are presented to illustrate and compare the performance of both the proposed cooperative and non-cooperative scenarios. Let $d_{A_i S_i}$ and $d_{P S_i}$ denote the distance between the i th source and its AP, and the distance between the i th source and the PB, respectively, $\forall i \in \mathcal{N}$. It is assumed that all the channels experience quasi-static Rayleigh fading and adopt a distance-dependent path loss model such as $L_{d_{XY}} = 10^{-3} (d_{XY})^{-\zeta}$, where d_{XY} denotes $d_{A_i S_i}$ or $d_{P S_i}$ and

Table 6.1: System parameters

The bandwidth W	100KHz
The noise power σ^2	-80dBm
The path-loss factor ζ	2
The transmit power of the PB p_b	2Watt
The transmit power of each AP p_i	1Watt
The gain per unit throughput for each AP λ_i	10/Mbps
The distance between the i th source and its AP $d_{A_i S_i}$	10m
The distance between the i th source and the PB $d_{P S_i}$	10m
The number of antennas at the PB	4
The energy conversion efficiency η	0.5
The reserve price for the PB $\mu^{(0)}$	0.001
The price step Δ	0.01

$\zeta \in [2, 5]$ is the path-loss factor [85]. Notice that a 30dB average signal power attenuation is assumed at a reference distance of 1m in the above channel model [28]. The system parameters used in the following simulations are listed in Table 6.1.

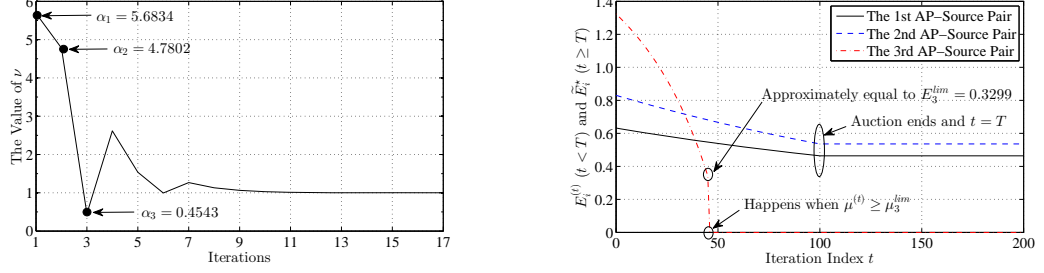
The curves in Figs. 6.4-6.5 correspond to a network setup consisting of three AP-source pairs with one randomly generated channel realisation, where the channel power gains between the APs and sources and the equivalent channel power gains between the PB and the sources are

$$\mathbf{G} = \begin{bmatrix} 0.0446 \\ 0.1569 \\ 0.8628 \end{bmatrix} \times 10^{-5}, \quad \mathbf{K} = \begin{bmatrix} 0.1616 \\ 0.6486 \\ 0.4379 \end{bmatrix} \times 10^{-4}. \quad (6.4.1)$$

With these parameters, we thus can compute $[\alpha_1, \alpha_2, \alpha_3] = [\mu_1^{lim}, \mu_2^{lim}, \mu_3^{lim}] = [5.6834, 4.7802, 0.4543]$, $[E_1^{lim}, E_2^{lim}, E_3^{lim}] = [0.1676, 0.0989, 0.3299]$ and $[E_1^o, E_2^o, E_3^o] = [0.6325, 0.8307, 1.3247]$ based on (6.2.13), (6.2.8) and (6.2.15), respectively.

Fig. 6.4 illustrates the convergence properties in the case $E_b^{tot} = 1\text{Joule}$ ⁸ for both the proposed water-filling based distributed algorithm in Algorithm 1 and the auction

⁸We consider $\mathcal{T} = 1\text{s}$ to guarantee the consistency of all physical units.

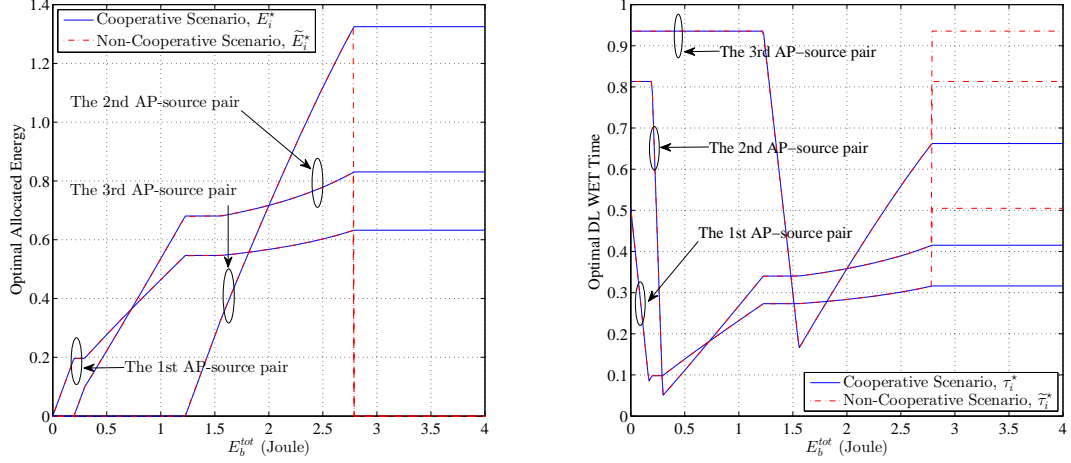


(a) Convergence of the water-filling based distributed algorithm. (b) Convergence of the auction based distributed algorithm.

Figure 6.4: The convergence properties of both the proposed algorithms when $N = 3$.

based distributed algorithm in Algorithm 2. It is shown in Fig. 6.4(a) that the value of ν starts from $\nu = \max_{i \in \mathcal{N}} \{\alpha_i\} = \alpha_1 = 5.6834$, turns to $\nu = \alpha_2 = 4.7802$ and $\nu = \alpha_3 = 0.4543$. Then it is confirmed that ν exists between α_3 and α_2 . With the bisection method, the proposed water-filling based distributed algorithm converges within few iterations and the desired ν is achieved. In Fig. 6.4(b), with the increasing price $\mu^{(t)}$ (as the iteration index t increases), the third AP-source pair first quits the auction when $\mu^{(t)} \geq \mu_3^{lim}$ and its last bid is approximately equal to $E_3^{lim} = 0.3299$ (when the price step Δ is sufficiently small). When the price $\mu^{(t)}$ continues to rise, the bids of the first and the second AP-source pairs will decrease till the summation of the bids is smaller than E_b^{tot} . Then the PB concludes the auction, sets $t = T$ and allocates the energy to each AP-source pair based on (6.3.9), which validates the convergence of the proposed auction based distributed algorithm.

Fig. 6.5 shows the optimal allocated energy and optimal DL WET time for each AP-source pair versus E_b^{tot} in the case of $N = 3$ for both the proposed cooperative and non-cooperative scenarios. It can be observed in Fig. 6.5(a) that the first AP-source pair, which has the largest $\alpha_1 = 5.6834$, is first allocated energy by the PB. Then the



(a) The optimal allocated energy to each AP-source pair versus E_b^{tot} in the case of $N = 3$ for both the proposed scenarios. (b) The optimal DL WET time to each source pair versus E_b^{tot} in the case of $N = 3$ for both the proposed scenarios.

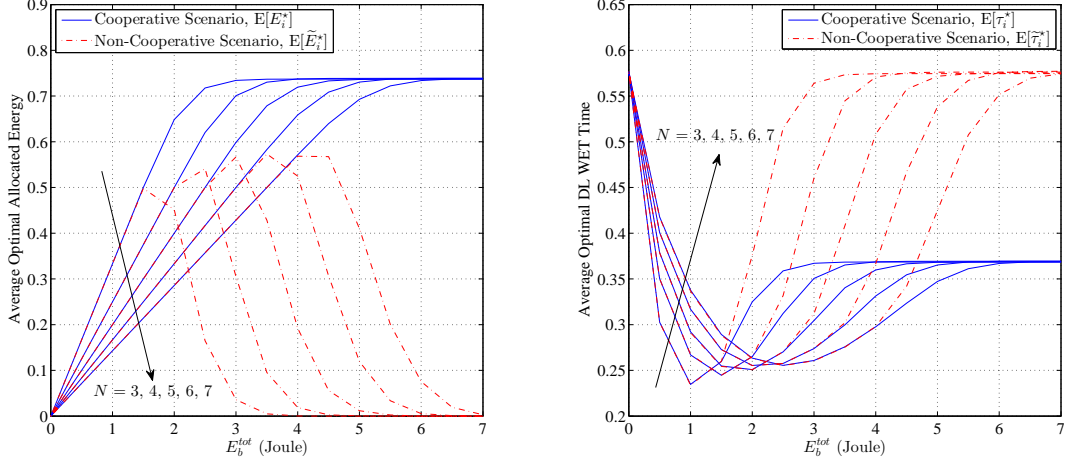
Figure 6.5: The optimal allocated energy and optimal DL WET time for each AP-source pair versus E_b^{tot} for both cooperative and non-cooperative scenarios.

second and the third AP-source pairs with $\alpha_2 = 4.7802$ and $\alpha_3 = 0.4543$ are allocated energy by the PB subsequently. With the increase of E_b^{tot} , the optimal allocated energy E_i^* for each AP-source pair in the cooperative scenario converges to E_i^o and equals E_i^o when $E_b^{tot} \geq \sum_{i \in \mathcal{N}} E_i^o$. Meanwhile, as expected, the final allocated energy \tilde{E}_i^* for each AP-source pair in the non-cooperative scenario can efficiently match that in the cooperative scenario (i.e., E_i^*), when E_b^{tot} is small. But \tilde{E}_i^* plummets to zero since the value of E_b^{tot} exceeds that of $\sum_{i \in \mathcal{N}} E_i^{(0)}$, which is due to the quitting of the PB in the adopted auction mechanism. Note that when $\mu^{(0)}$ is sufficiently small, the energy payment of each AP to the PB can be ignored in its own utility function. In this case, the non-cooperative scenario can be approximated to the cooperative scenario. Thus, the optimal bid $E_i^{(0)}$ from each AP should approximately equal to E_i^o , which leads to $\sum_{i \in \mathcal{N}} E_i^{(0)} \approx \sum_{i \in \mathcal{N}} E_i^o$. Therefore, the approach of E_i^* to E_i^o and

the plummeting of \tilde{E}_i^* to zero occur almost simultaneously, as depicted in Fig. 6.5(a).

Fig. 6.5(b) shows the trends of both τ_i^* and $\tilde{\tau}_i^*$ versus E_b^{tot} . By increasing E_b^{tot} , the optimal DL WET time of the first AP-source pair first decreases and then increases while others remain the same. This is because the first AP-source pair is allocated energy first. When E_b^{tot} is small, the harvested energy for the source mainly comes from its associated AP, which corresponds to the case $\tau_i > \tau_i'$ (see Proposition 6.2). But, with the assistance of the PB, the AP can shorten its DL WET time, which leads to the decrease of τ_i^* (or $\tilde{\tau}_i^*$). When E_b^{tot} continually increases, the source can harvest more energy from the PB, which corresponds to the case that the DL WET time is dominated by the PB, i.e., $\tau_i = \tau_i'$ (see Proposition 6.2). In this case, the value of τ_i^* (or $\tilde{\tau}_i^*$) grows as the value of E_b^{tot} increases. Moreover, we can observe the same tendency in the second and the third AP-source pairs when they are allocated energy. When $E_i^{tot} \geq \sum_{i \in \mathcal{N}} E_i^o$, τ_i^* of each AP-source pair in the cooperative scenario becomes constant as $E_i^* = E_i^o$, almost at the same time, $\tilde{\tau}_i^*$ for each AP-source pair in the non-cooperative scenario equals that in the case each source only harvests energy from its own AP, which is caused by the quitting of the PB.

Now we show the average performance of both the proposed scenarios and each curve hereafter is averaged over 10^4 randomly generated channel realisations. Fig. 6.6 demonstrates the average allocated energy and average DL WET time for each AP-source pair versus E_b^{tot} in both the proposed cooperative and non-cooperative scenarios. $\mathbb{E}[E_i^*]$, $\mathbb{E}[\tilde{E}_i^*]$, $\mathbb{E}[\tau_i^*]$ and $\mathbb{E}[\tilde{\tau}_i^*]$ are averaged for each AP-source pair and averaged over 10^4 channel realisations. It can be observed in Fig. 6.6(a) that the optimal allocated energy in the cooperative scenario $\mathbb{E}[E_i^*]$ rises with the increase of E_b^{tot} . However, $\mathbb{E}[E_i^*]$ decreases with the increment of the number of participating



(a) The average allocated energy from the PB to each AP-source pair versus E_b^{tot} for both the proposed scenarios. (b) The average DL WET time to each source versus E_b^{tot} for both the proposed scenarios.

Figure 6.6: The average allocated energy and average DL WET time for each AP-source pair versus E_b^{tot} for both cooperative and non-cooperative scenarios.

AP-source pairs with a given E_b^{tot} because $\mathbb{E}[E_i^*]$ is averaged for each AP-source pair. All $\mathbb{E}[E_i^*]$ s corresponding to different N converge to a constant value with the increase of E_b^{tot} , because the larger E_b^{tot} is, the larger is the probability of $E_b^{tot} \geq \sum_{i \in \mathcal{N}} E_i^o$ in each simulation block with one channel realisation. For the non-cooperative scenario, $\mathbb{E}[\tilde{E}_i^*]$ closely matches $\mathbb{E}[E_i^*]$ when E_b^{tot} is small, but converges to zero when E_b^{tot} is sufficiently large due to the quitting of the PB. Fig. 6.6(b) depicts both $\mathbb{E}[\tau_i^*]$ and $\mathbb{E}[\tilde{\tau}_i^*]$ versus E_b^{tot} . When E_b^{tot} increases, both $\mathbb{E}[\tau_i^*]$ and $\mathbb{E}[\tilde{\tau}_i^*]$ decrease first and then increase, and they converge to different values for the reason shown in Fig. 6.5(b). Besides, when the number of participating AP-source pairs rises, the turning point of the corresponding curve appears later. The reason is that the more AP-source pairs, the less energy allocated to each source from the PB. Then, a larger value of E_b^{tot} is needed to make the DL WET time at each source dominated by the PB.

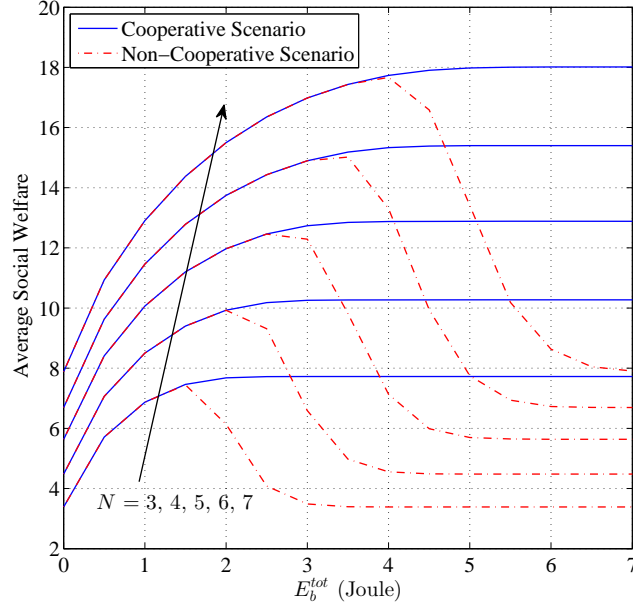


Figure 6.7: The average social welfare (i.e., the weighted sum throughput) of both the proposed cooperative and non-cooperative scenarios versus E_b^{tot} in the case of different number of participating AP-source pairs.

Fig. 6.7 presents the average social welfare of both the proposed cooperative and non-cooperative scenarios versus E_b^{tot} in the case of different number of participating AP-source pairs. The social welfare in the non-cooperative scenario is assumed to be the aggregate of the utilities of all the AP-source pairs and the PB. It can be observed that the network setup with a larger N in either proposed scenario achieves a better social welfare performance due to the energy resource brought by the newly joined AP-source pairs. The average social welfare of the cooperative scenario increases as E_b^{tot} grows and approaches a constant value when E_b^{tot} is large enough. This is because when $E_b^{tot} \geq \sum_{i \in \mathcal{N}} E_i^o$, as shown in Fig. 6.5(a), the allocated energy to each source will be a constant value and independent of E_b^{tot} , which leads to the saturation of the social welfare performance. In the non-cooperative scenario, as

E_b^{tot} increases, the average social welfare performance closely matches that in the cooperative scenario when E_b^{tot} is small, but then deteriorates due to the quitting of the PB when $E_b^{tot} \geq \sum_{i \in \mathcal{N}} E_i^{(0)}$. Notice that when $E_b^{tot} = 0$, i.e., without the PB, the average social welfare performance is always the worst.

Chapter 7

Distributed Power Control in Interference Channel with SWIPT: A Game-Theoretic Approach

This chapter develops a new distributed power control scheme for a power splitting-based interference channel (IFC) with simultaneous wireless information and power transfer (SWIPT). The considered IFC consists of multiple source-destination pairs. Each pair adjusts its transmit power and power splitting ratio to meet both signal-to-interference-plus-noise ratio (SINR) and energy harvesting (EH) constraints at its corresponding destination. To characterise rational behaviours of source-destination pairs, I formulate a non-cooperative game for the considered system, where each pair is modeled as a strategic player who aims to minimise its own transmit power under both SINR and EH constraints at the destination. I derive a sufficient condition for the existence and uniqueness of the Nash equilibrium (NE) for the formulated game. The best response strategy of each player is derived and then the NE can be achieved iteratively. Numerical results show that the proposed game-theoretic approach can achieve a near-optimal performance under various SINR and EH constraints.

7.1 System Model and Game Formulation

In this section, I first describe the system model and then formulate a non-cooperative game for the considered network.

7.1.1 System Model

Consider an IFC consisting of N source-destination pairs. I use $\mathcal{N} = \{1, \dots, n, \dots, N\}$ to denote the index set of source-destination pairs, in which the n th pair consists of the n th source and the n th destination. All pairs are assumed to share the same frequency band and thus they interfere with each other. It is assumed that all sources and destinations are equipped with one antenna and operate in a half-duplex mode. Each destination is equipped with a power splitting [33] device so that it is able to decode the information as well as harvest energy from the received signal at the same time. Besides, it is considered that the links between all nodes experience slow and frequency-flat fading.

Let h_{nn} and h_{mn} denote the channel gain from the n th source to the n th destination and that from the m th source to the n th destination, respectively. At the n th destination, the received signal before power splitting can be expressed as

$$y_n = h_{nn}\sqrt{p_n}x_n + \sum_{m \in \mathcal{N}/\{n\}} h_{mn}\sqrt{p_m}x_m + z_n, \quad (7.1.1)$$

where p_n and p_m are transmit powers of the n th source and m th source, respectively. x_n and x_m denote the unit-energy symbols transmitted by the n th source and m th source. $z_n \sim \mathcal{CN}(0, \delta_n^2)$ is the additive noise introduced by the receiver antenna at the n th destination.

The n th destination splits the received signal into two streams with a power

splitting ratio α_n . The fraction $\sqrt{\alpha_n}$ of the received signal is used for EH, while the remaining $\sqrt{1 - \alpha_n}$ fraction is passed to the ID unit. The ID unit at each receiver will introduce an additional baseband noise to the signal stream passed to the ID circuit. It is assumed that this additional baseband noise is an additive Gaussian random variable with zero mean and variance σ_n^2 and it should be independent of the antenna noise z_n . Accordingly, we can express the respective harvested energy and received SINR at the n th destination by

$$E_n(p_n, \alpha_n; \mathbf{p}_{-n}) = \eta \alpha_n \sum_{m \in \mathcal{N}} p_m G_{mn}, \quad (7.1.2)$$

$$\text{SINR}_n(p_n, \alpha_n; \mathbf{p}_{-n}) = \frac{(1 - \alpha_n) p_n G_{nn}}{(1 - \alpha_n) \left(\sum_{m \in \mathcal{N}/\{n\}} p_m G_{mn} + \delta_n^2 \right) + \sigma_n^2}, \quad (7.1.3)$$

where $\mathbf{p}_{-n} \triangleq [p_1, \dots, p_{n-1}, p_{n+1}, \dots, p_N]^T$, $G_{nn} \triangleq |h_{nn}|^2$, $G_{mn} \triangleq |h_{mn}|^2$, and $0 < \eta < 1$ is the energy conversion efficiency. The notation $(p_n, \alpha_n; \mathbf{p}_{-n})$ indicates that p_n and α_n are variables given \mathbf{p}_{-n} . Note that in (7.1.2), the amount of energy harvested from the antenna noise is ignored since it is normally below the sensitivity of the energy harvesting device in practice [67].

7.1.2 Game Formulation

I follow [37, 38] and assume that each destination is subject to strict QoS and EH constraints. The QoS constraint requires that the received SINR at the n th destination, i.e., SINR_n given in (7.1.3), should be no less than a predefined threshold γ_n , while the EH constraint imposes the condition that the value of E_n defined in (7.1.2) should be larger than or equal to the energy threshold \mathcal{E}_n . In contrast to [37, 38], which assume that all source-destination pairs are cooperative to minimise the network total transmit power, I consider an alternative non-cooperative scenario in which

the source-destination pairs are all rational and self-interested so that they only want to minimise their respective transmit powers under their individual SINR and EH constraints. In this case, the results presented in [37, 38] by minimising the network total transmit power may no longer be applicable for the considered non-cooperative scenario. In this regard, I model the considered system by the well-established game theory [86]. Specifically, I formulate the following non-cooperative game:

- *Players*: The N source-destination pairs.
- *Actions*: Each pair determines its source transmit power and the power splitting ratio at the destination, i.e., (p_n, α_n) , to minimise its transmit power under the SINR and EH constraints at the destination.
- *Utilities*: The source transmit powers p_n .

We notice that each player's strategy (p_n, α_n) only depends on the transmit powers of the others \mathbf{p}_{-n} , as the power splitting ratio of each player only operates at the destination side. Thus, given the transmit powers of the others \mathbf{p}_{-n} , the best response strategy of the n th pair (player) is the solution to the following optimisation problem,

$$\begin{aligned}
 & \min_{\{p_n, \alpha_n\}} p_n, \\
 & \text{s.t. C1 : } 0 \leq \alpha_n \leq 1, \\
 & \text{C2 : } p_n \geq 0, \\
 & \text{C3 : } \frac{(1 - \alpha_n) p_n G_{nn}}{(1 - \alpha_n) \left(\sum_{m \in \mathcal{N}/\{n\}} p_m G_{mn} + \delta_n^2 \right) + \sigma_n^2} \geq \gamma_n, \\
 & \text{C4 : } \eta \alpha_n \sum_{m \in \mathcal{N}} p_m G_{mn} \geq \mathcal{E}_n.
 \end{aligned} \tag{7.1.4}$$

We denote by (p_n^*, α_n^*) the optimal solution to the optimisation problem (7.1.4). It is straightforward to verify that (7.1.4) always has a feasible solution. Considering

that p_n and α_n should be jointly optimised and they are all dependent on \mathbf{p}_{-n} , we can rewrite α_n as a function of p_n and \mathbf{p}_{-n} , i.e., $\alpha_n = f_n(p_n, \mathbf{p}_{-n})$. Then, we denote by $\mathcal{P}_n(\mathbf{p}_{-n})$ the feasible power policies of the n th pair given the others' power strategies, which can be expressed as

$$\begin{aligned} \mathcal{P}_n(\mathbf{p}_{-n}) \triangleq \{p_n > 0 : \text{SINR}_n(p_n, f_n(p_n, \mathbf{p}_{-n}); \mathbf{p}_{-n}) \geq \gamma_n, \\ E_n(p_n, f_n(p_n, \mathbf{p}_{-n}); \mathbf{p}_{-n}) \geq \mathcal{E}_n\}. \end{aligned} \quad (7.1.5)$$

Now, we define $\mathbf{p}^* = [p_1^*, \dots, p_N^*]^T$ and $\boldsymbol{\alpha}^* = [\alpha_1^*, \dots, \alpha_N^*]^T$ and denote by $(\mathbf{p}^*, \boldsymbol{\alpha}^*)$ the solution (if exists) to the formulated non-cooperative game, which is well-known as the NE [86]. A NE for the formulated game is a feasible profile $(\mathbf{p}^*, \boldsymbol{\alpha}^*)$ that satisfies

$$\begin{cases} p_n^* \leq p_n \\ \alpha_n^* = f_n(p_n^*, \mathbf{p}_{-n}^*) \end{cases}, \quad \forall p_n \in \mathcal{P}_n(\mathbf{p}_{-n}^*), \quad \forall n \in \mathcal{N}. \quad (7.1.6)$$

7.2 Existence and Uniqueness of the NE

In this section, I first analyse the best response strategy of each source-destination pair by solving the optimisation problem (7.1.4). Then, I derive a sufficient condition that guarantees the existence and uniqueness for the NE of the formulated game.

7.2.1 The Best Response Strategy

Now, we calculate the best response strategy (p_n^*, α_n^*) for the n th pair by solving the optimisation problem (7.1.4), which is described in the following proposition,

Proposition 7.1. *Given \mathbf{p}_{-n} , the optimal response strategy of the n th pair can be expressed as*

$$\begin{cases} p_n^* = \frac{-X_n + Y_n + \gamma_n X_n + \gamma_n \sigma_n^2 + \sqrt{\Delta_n}}{2G_{nn}}, \\ \alpha_n^* = \frac{X_n + Y_n + \gamma_n X_n + \gamma_n \sigma_n^2 - \sqrt{\Delta_n}}{2(X_n + \gamma_n X_n)}, \end{cases} \quad (7.2.1)$$

where $X_n = \sum_{m \in \mathcal{N}/\{n\}} p_m G_{mn} + \delta_n^2$, $Y_n = \frac{\varepsilon_n}{\eta}$ and $\Delta_n = (X_n - Y_n + \gamma_n X_n + \gamma_n \sigma_n^2)^2 + 4\gamma_n Y_n \sigma_n^2$.

Proof. See Appendix D.1. □

The best response strategy given in Proposition 7.1 confirms the discussion that the choice of α_m^* , $\forall m \in \mathcal{N}/\{n\}$, of the others will not affect the decision of the n th pair. Therefore, the competitive interaction among the players is actually proceeded by adjusting their own power allocation strategy. We thus define the best response function at the n th pair as

$$p_n^* = \mathcal{B}_n(\mathbf{p}_{-n}) = \frac{-X_n + Y_n + \gamma_n X_n + \gamma_n \sigma_n^2 + \sqrt{\Delta_n}}{2G_{nn}}, \quad \forall n \in \mathcal{N}. \quad (7.2.2)$$

Besides, based on (7.2.1), we have

$$f_n(p_n, \mathbf{p}_{-n}) = \frac{X_n + Y_n + \gamma_n X_n + \gamma_n \sigma_n^2 - \sqrt{\Delta_n}}{2(X_n + \gamma_n X_n)}. \quad (7.2.3)$$

The NE for the non-cooperative game can now be redefined as

$$\begin{cases} p_n^* = \mathcal{B}_n(\mathbf{p}_{-n}^*) \\ \alpha_n^* = f_n(p_n^*, \mathbf{p}_{-n}^*) \end{cases}, \quad \forall n \in \mathcal{N}, \quad (7.2.4)$$

which can be readily achieved with the well-known *best-response dynamics* [71] if its existence and uniqueness are guaranteed. It is worth mentioning that the adopted best-response dynamics has a low implementation and computation complexity to achieve the NE of the formulated game. In particular, each link only needs to measure its own channel gain (i.e., G_{nn}) and the power of the interference from all other links and the antenna noise (i.e., X_n denoted in Proposition 7.1). With these measurements, each link can easily compute its best response strategy based on (7.2.1), and the NE of the formulated non-cooperative game can be readily achieved by the proposed algorithm. In the next subsection, I will derive a sufficient condition to

guarantee the existence and uniqueness for the NE of the formulated game.

7.2.2 A Sufficient Condition

The best-response dynamics, i.e., the iterative behaviours of each player with its best response strategy, can be regarded as a mapping process [87, 88]. A sufficient condition to guarantee the existence and uniqueness of the NE is equivalent to the condition to guarantee the mapping process as a contraction, which then implies that the mapping has a unique fixed point [88]. We then refer to the contraction mapping theorem [87], i.e.,

Theorem 7.2. *A mapping $f(x)$, $\mathbb{R}^N \rightarrow \mathbb{R}^N$ (\mathbb{R} is the set of real numbers) is a contraction if and only if $\|f(x_1) - f(x_2)\| \leq \beta \|x_1 - x_2\|$, $\forall x_1, x_2$, $\beta < 1$.*

Note that the well-known contraction mapping theorem has been widely adopted in open literature due to its following advantages [89]. First, it can guarantee not only the existence of the NE but also the uniqueness of the NE. Second, it does not require that the space being mapped onto itself is convex or bounded. Third, it has the inherent convergence property. Additionally, it is also pointed out in [89] that the contraction mapping theorem provides a quite general condition for the mapping to have a unique fixed point. Then, we can have the following proposition regarding the existence and uniqueness of the NE:

Proposition 7.3. *The existence and uniqueness of the NE of the non-cooperative game is guaranteed if the spectral radius¹ $\rho(\mathbf{\Omega}) < 1$, where the square matrix $\mathbf{\Omega} \in$*

¹The spectral radius of the matrix $\mathbf{\Omega}$ is defined as the largest absolute eigenvalue of $\mathbf{\Omega}$, i.e., $\rho(\mathbf{\Omega}) \triangleq \max_i (|\lambda_i|)$, where λ_i 's are eigenvalues of $\mathbf{\Omega}$ [90].

$\mathbb{R}^{N \times N}$ is defined as

$$[\mathbf{\Omega}]_{n,m} = \begin{cases} 0, & \text{if } m = n, \\ \frac{G_{mn}\gamma_n}{G_{nn}}, & \text{if } m \neq n. \end{cases} \quad (7.2.5)$$

Proof. See Appendix D.2. □

It is interesting to observe that *the sufficient condition obtained in Proposition 7.3 is also that for the power minimisation problem in conventional IFCs with only rate constraint, which was given and proved in [91]*. This indicates that the introduction of EH constraints does not lead to a stricter sufficient condition for the existence and uniqueness of the NE.

7.3 Numerical Results

In this section, I provide numerical results to validate the above theoretical analysis. Let d_{mn} denote the inter-link distance between the m th source and the n th destination, $\forall m \in \mathcal{N}/\{n\}$, and let d_{nn} denote the inner-link distance between the n th source and the n th destination. All channels are assumed to experience quasi-static Rayleigh fading. I adopt a channel model with $\mathbb{E}[G_{mn}] = 10^{-3}(d_{mn})^{-\zeta}$ and $\mathbb{E}[G_{nn}] = 10^{-3}(d_{nn})^{-\zeta}$, where $\zeta \in [2, 5]$ is the path-loss factor [85] and a 30dB average signal power attenuation is assumed with reference distance of 1m. In all simulations, I set $d_{mn}/d_{nn} = 2$, $\eta = 0.5$, $\zeta = 2$, $\delta_n^2 = -60\text{dBm}$, and $\sigma_n^2 = -50\text{dBm}$, $\forall n \in \mathcal{N}$. To evaluate the performance of the formulated non-cooperative game, the sufficient condition $\rho(\mathbf{\Omega}) < 1$ is assumed to be satisfied in the sequel.

First, I demonstrate the convergence of best-response dynamics in the formulated non-cooperative game for a four-pair setup with one randomly generated channel

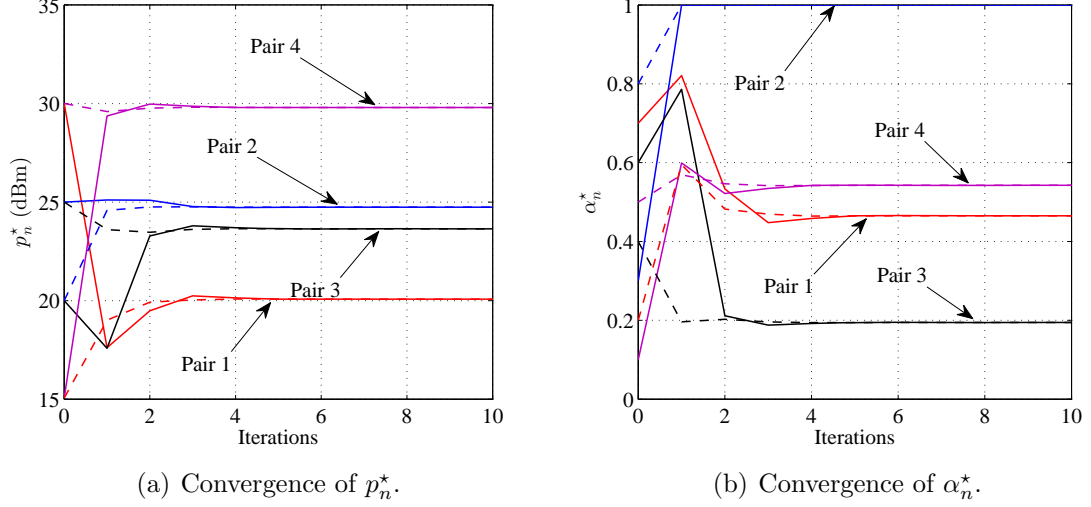


Figure 7.1: The convergence of best-response dynamics in the formulated non-cooperative game with four source-destination pairs starting from two different sets of initial points, which are distinguished by solid lines and dash lines.

realisation as well as SINR and EH constraints. The pairs 1-4 are assumed with SINR constraints 0dB, 0dB, 10dB, 10dB, and EH constraints -20dBm , -10dBm , -20dBm , -10dBm , respectively. Fig. 7.1(a) and Fig. 7.1(b) show the transmit power and the power splitting ratio of each pair versus the number of iterations, respectively. Two cases starting from two random sets of initial points are presented, which are distinguished by dash and solid lines, respectively. It can be observed from this figure that both p_n^* and α_n^* can converge quickly to the same stationary values (i.e., the NE) from different starting points. Also, as the minimum p_n^* is about 20dBm , the signal-to-noise ratio (SNR) region is over 70dB ($\sigma_n^2 = -50\text{dBm}$), which is practical for energy harvesting devices. Note that I only show results in Fig. 7.1 for one random realisation of channel gains and the constraints, although similar results can also be shown for other realisations. This validates the effectiveness of the derived sufficient condition of the NE.

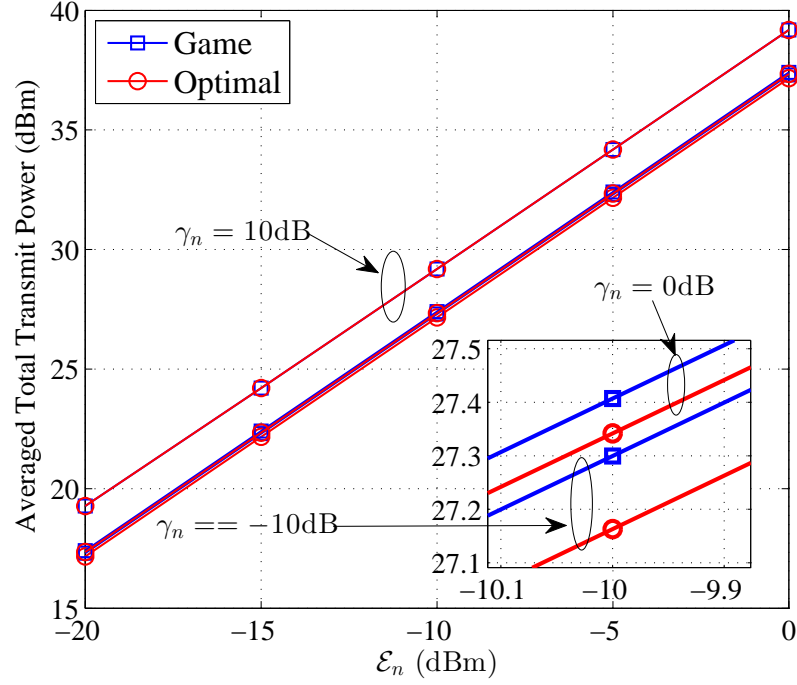


Figure 7.2: Averaged total transmit power versus the EH constraint with different SINR constraints in a two-pair network.

Fig. 7.2 illustrates the averaged total transmit power versus the EH constraints with different SINR constraints in a two-pair network setup. The SINR and EH constraints for two pairs are assumed to be the same, respectively. Each curve is obtained by averaging over 10^4 independent channel realisations. The averaged total transmit power obtained by the proposed game-theoretic approach is compared with an optimal strategy calculated via an exhaustive search. The optimal strategy is conducted based on the assumption that all source-destination pairs cooperate with each other to minimise the averaged total transmit power. Note that the optimal scheme here is actually consistent with the problems considered in [37] and [38]. It can be observed from Fig. 7.2 that the averaged total transmit power of the proposed

game-theoretic method can closely match that of the optimal results. Note that the proposed strategy cannot perfectly coincide with the optimal strategy due to the rational and selfish behaviours of source-destination pairs in the game formulation. In addition, it is also shown that with the increasing of γ_n or \mathcal{E}_n , the averaged total transmit power increases accordingly to meet the higher SINR and EH constraints.

Chapter 8

Conclusions

In this thesis, I proposed new network coding schemes with designed network coded structures and investigated resource allocations for the RF energy transfer schemes with game theoretical approaches. In the following, I summarise the key results and findings of this thesis.

In Chapter 3, I proposed a multi-source multi-destination wireless relay network coded scheme combining the merits of nested codes and the OS. I presented the detailed coding process of the proposed scheme, and derived upper bounds on bit error probability for the schemes with and without the OS. The code search was also carried out based on the designed criteria. In the simulation results, the theoretical upper bounds were validated and it was shown that the designed network coded scheme outperforms the scheme without the OS on the bit error probability.

In Chapter 4, I proposed a novel NCLC for a MWRC over fading to achieve a high spectrum efficiency. In particular, the detailed coding process of the proposed scheme was first presented. Then a theoretical upper bound on WER was derived for the NCLC and code design criteria were developed by minimising the derived WER. Simulation results showed that the NCLC can realise multiple interpretations for each

source in two time slots, and the derived upper bound is asymptotically tight with the increase of $\text{SENR}_{\text{norm}}$.

In Chapter 5, I proposed a class of nested non-binary LDGM codes based on lattices for a multi-access relay system. Specifically, I first constructed these novel codes by considering lattice-signal transmissions at both the sources and the relay. Besides, I derived the ACR and optimised related parameters to maximise the ACR for the proposed system. Furthermore, the proposed codes were optimised by using a lattice-based Monte Carlo method to approach the ACR with a low complexity L-EMS decoder. Finally, simulation results showed that the optimal setting of the parameters is consistent with that suggested in the analysis and the proposed code performs 2dB better than the reference scheme at an average symbol error rate of 10^{-4} .

Chapter 6 investigated the joint time and energy allocation of a PB-assisted WPCN with multiple AP-source pairs and a PB. I considered both cooperative and non-cooperative scenarios corresponding to situations in which either the PB provides wireless charging service to each AP-source pair for free or not. Moreover, the social welfare was maximised in the proposed cooperative scenario and the respective utility of each AP and the PB was maximised in the non-cooperative scenario. The numerical results validated the convergence of both the proposed water-filling based and auction based distributed algorithms. It was demonstrated that the average social welfare of the cooperative scenario improves as either the number of participating AP-source pairs or the total energy of the PB increases, but saturates when the total energy of the PB is sufficiently large. Moreover, the average social welfare performance of the non-cooperative scenario closely matches that in the cooperative scenario when the total energy of the PB is small, but deteriorates when the total energy of the

PB is sufficiently large, which is caused by the quitting of the PB in the adopted auction mechanism.

Finally, in Chapter 7, I developed a game-theoretic framework to tackle the distributed joint power and power splitting ratio problem in an IFC with SWIPT. A non-cooperative game was formulated for the considered system, where each source-destination pair is modeled as a selfish and rational player who aims to minimise its own transmit power under both SINR and EH constraints. The best response strategy of each player was derived and thus the NE can be obtained iteratively. The numerical results validated the sufficient condition and showed that the performance of the proposed game-theoretic approach can closely match the optimal strategy on averaged total transmit power under various SINR and EH constraints.

In addition to the key results and findings summarised above, there are still some research problems to be investigated in the future. In the short term, comparisons between the proposed code constructions in Chapters 3 and 4, and that in the state of the art will be tried to make. Finding a fair way to compare the results in Chapters 3, 4 and 5 will also be considered. Besides, more interesting results related to the SWIPT in the IFC will be provided as well. In the long term, further research on the proposed code structures in Chapters 3, 4 and 5 will be conducted to apply the findings in the upcoming 5G cellular network. Moreover, practical applications of RF energy transfer will be considered to support the theoretical results that have been obtained.

Appendix A

Proofs for Chapter 4. Novel Nested Convolutional Lattice Codes for Multi-Way Relaying Systems over Fading Channels

A.1 Proof of Theorem 4.1

First, I show that maximising the SENR is equivalent to minimising \mathbf{m}_j/b_j . From Eq. (4.2.11), we have

$$\begin{aligned} & \left[b_j \sum_{\ell=1}^L a_\ell \mathbf{t}_\ell + \mathbf{m}_j \right] \bmod \Lambda' \\ &= \left[b_j \left(\sum_{\ell=1}^L a_\ell \mathbf{t}_\ell + \frac{\mathbf{m}_j}{b_j} \right) \right] \bmod \Lambda' \\ &= b_j \left(\sum_{\ell=1}^L a_\ell \mathbf{t}_\ell + \frac{\mathbf{m}_j}{b_j} \right) - \mathcal{Q}_{\Lambda'}(\Theta), \end{aligned} \tag{A.1.1}$$

where

$$\Theta = b_j \sum_{\ell=1}^L a_\ell \mathbf{t}_\ell + \mathbf{m}_j. \tag{A.1.2}$$

Because $\mathcal{Q}_{\Lambda'}(\Theta)$ is the point on the coarse lattice Λ' and $\psi^{-1}(\mathcal{Q}_{\Lambda'}(\Theta)) = 0$, we can regard $\mathcal{Q}_{\Lambda'}(\Theta)$ as a regular shift of the signal. Hence, β_j should be chosen to minimise

\mathbf{m}_j/b_j , which is equivalent to maximising the SENR.

It is assumed that the MMSE detector is employed at each receiver node. Let $f(\beta_j) = \mathbb{E} [|\mathbf{m}_j/b_j|^2]$, from Eqs. (4.2.6) and (4.2.11), we have,

$$f(\beta_j) = \|\alpha \mathbf{h} - \mathbf{a}\|^2 P_s + |\alpha|^2 N_0 + P_r \left| \frac{\beta_j}{b_j} h_j - 1 \right|^2 + \left| \frac{\beta_j}{b_j} \right|^2 N_0. \quad (\text{A.1.3})$$

It is apparent that $f(\beta_j)$ is convex. By deriving $\frac{\partial f(\beta_j)}{\partial \beta_j} = 0$, we have,

$$\beta_j = \frac{b_j P_r h_j}{P_r |h_j|^2 + N_0}. \quad (\text{A.1.4})$$

This completes the proof of Theorem 4.1.

Appendix B

Proofs for Chapter 5. Network Coded Non-Binary LDGM Codes Based on Lattices for a Multi-Access Relay System

B.1 Proof of Theorem 5.1

Let $\mathbf{h} = [h_1, \dots, h_\ell, \dots, h_L]$. The ACR is obtained based on the observation that the destination can decode the message with arbitrary coefficients \mathbf{a} and b on Λ/Λ' . Therefore, the message rate is within the ACR as

$$R_\ell < \min_{\mathbf{a}, b \neq 0} \mathcal{R}(\mathbf{h}, \mathbf{a}, h_{rd}, b). \quad (\text{B.1.1})$$

The effective noise observed at the destination is expressed by $\mathbf{m} = b\mathbf{n} + (\beta h_{rd} - b)\mathbf{x}_r + \beta \mathbf{z}_{rd}$. Thus, the average power of the effective noise is

$$\begin{aligned} N_e &= \mathbb{E} [\|\mathbf{m}\|^2 | \mathbf{h}, h_{rd}] \\ &= |b|^2 \|\alpha \mathbf{h} - \mathbf{a}\|^2 P + 2\sigma^2 |b|^2 |\alpha|^2 + |\beta h_{rd} - b|^2 P + 2\sigma^2 |\beta|^2. \end{aligned} \quad (\text{B.1.2})$$

The rate that can be achieved by the lattice code is less than that in [9]

$$R_\ell < \min_{\mathbf{a}, b \neq 0} \frac{1}{2} \log^+ \left(\frac{P}{G(\Lambda) 4\pi e \sigma_m^2} \right), \quad (\text{B.1.3})$$

where σ_m^2 is the one-side variance of the effective noise \mathbf{m} , $G(\Lambda)$ is the normalised second moment of the lattice Λ and

$$\lim_{N \rightarrow \infty} G(\Lambda^{(N)}) = \frac{1}{2\pi e}. \quad (\text{B.1.4})$$

With $\forall \delta > 0$, as the dimension N is large enough, we have that $G(\Lambda)2\pi e < (1 + \delta)$. Meanwhile, $2\sigma_m^2$ converges to N_e . It follows that for N large enough, $2\sigma_m^2 < (1 + \delta)N_e$. Thus, by choosing δ small enough, for the complex-valued channels, the ACR is given by (5.3.1), which completes the proof.

B.2 Proof of Proposition 5.2

First, I show that maximising the ACR is equivalent to minimising N_e . From (5.2.5), we have

$$F_{\Lambda'} \left(b \sum_{\ell=1}^L a_\ell \mathbf{t}_\ell + \mathbf{m} \right) = \Theta - \mathcal{Q}_{\Lambda'}(\Theta), \quad (\text{B.2.1})$$

where $\Theta = b \sum_{\ell=1}^L a_\ell \mathbf{t}_\ell + \mathbf{m}$ and the mapping $\mathcal{Q}_{\Lambda'}(\Theta) \triangleq \arg \min_{\boldsymbol{\lambda}' \in \Lambda'} \|\Theta - \boldsymbol{\lambda}'\|$. Since $\mathcal{Q}_{\Lambda'}(\Theta)$ is a point on the coarse lattice Λ' and $\psi^{-1}(\mathcal{Q}_{\Lambda'}(\Theta)) = 0$, we can regard $\mathcal{Q}_{\Lambda'}(\Theta)$ as a regular shift of the signal. Hence, α and β should be chosen to minimise N_e , which is equivalent to maximising the ACR.

It is apparent that N_e is jointly convex in α and β . By solving $\frac{\partial N_e}{\partial \alpha} = 0$ and $\frac{\partial N_e}{\partial \beta} = 0$, we complete the proof.

B.3 Proof of Proposition 5.3

Inserting the expressions of α and β into (5.3.1), we have another expression of the ACR. Then maximising $\mathcal{R}(\mathbf{h}, \mathbf{a}, h_{rd}, b)$ can be regarded as an equivalent to the

following minimisation problem,

$$\min_{b \neq 0} \left\{ |b|^2 \|\mathbf{a}\|^2 - \frac{|b|^2 \gamma |\mathbf{h}^H \mathbf{a}|^2}{1 + \gamma \|\mathbf{h}\|^2} + |b|^2 - \frac{|b|^2 \gamma |h_{rd}^H|^2}{1 + \gamma |h_{rd}|^2} \right\}. \quad (\text{B.3.1})$$

By extracting $|b|^2$, as $b \in \Lambda$, it is optimum to choose b as the closest point to the origin on the fine lattice Λ and this completes the proof.

Appendix C

Proofs for Chapter 6. Distributed and Optimal Resource Allocation for Power Beacon-Assisted Wireless-Powered Communications

C.1 Proof of Proposition 6.2

To proceed, I first derive the second-order derivative of $\mathcal{S}_i(\tau_i)$ with respect to τ_i . After some simplifications, we have

$$\frac{\partial^2 \mathcal{S}_i(\tau_i)}{\partial \tau_i^2} = -\frac{\lambda_i W (A_i + B_i)^2}{(1 - \tau_i) (1 - \tau_i + A_i \tau_i + B_i)^2 \ln 2}. \quad (\text{C.1.1})$$

where $A_i = \frac{G_i^2 \eta p_i}{\sigma^2}$ and $B_i = \frac{G_i \eta E_i K_i}{\sigma^2}$. Since $\frac{\partial^2 \mathcal{S}_i(\tau_i)}{\partial \tau_i^2} < 0$, $\mathcal{S}_i(\tau_i)$ is a concave function of τ_i . Thus, the optimal solution can be obtained by setting the first-order derivative of $\mathcal{S}_i(\tau_i)$ equal to zero and comparing the obtained stationary points with the constraints. That is, $\frac{\partial \mathcal{S}_i(\tau_i)}{\partial \tau_i} = 0$. After some algebraic manipulations, we have

$$z_i \ln(z_i) - z_i + 1 = A_i, \quad (\text{C.1.2})$$

where $z_i = 1 + \frac{A_i \tau_i + B_i}{1 - \tau_i}$. Note that $z_i > 1$ as $A_i > 0$ and $0 < \tau_i < 1$. With reference to [28], $f(z_i) = z_i \ln(z_i) - z_i + 1$ is strictly increasing when $z_i > 1$ and $f(1) = 0$.

We then can deduce that there exists a unique solution, denoted by $z_i^\dagger > 1$, to the equality $f(z_i) = A_i$. After some manipulations, we obtain

$$z_i^\dagger = \exp \left(\mathcal{W} \left(\frac{A_i - 1}{\exp(1)} \right) + 1 \right), \quad (\text{C.1.3})$$

in which $\mathcal{W}(x)$ is the Lambert \mathcal{W} function that is the solution to the equality $x = \mathcal{W} \exp(\mathcal{W})$. Let τ_i^\dagger denote the optimal solution to the equation (C.1.2). Then, we have $1 + \frac{A_i \tau_i^\dagger + B_i}{1 - \tau_i^\dagger} = z_i^\dagger$. Rearranging this equality, we obtain

$$\tau_i^\dagger = \frac{z_i^\dagger - 1 - B_i}{z_i^\dagger - 1 + A_i}. \quad (\text{C.1.4})$$

Recall the constraints on τ_i in the optimisation problem (6.2.5) that $0 < \tau_i < 1$ and $\tau_i \geq \frac{E_i}{p_b}$, we have

$$\tau_i(E_i) = \max \left\{ \tau_i^\dagger, \frac{E_i}{p_b} \right\}, \quad (\text{C.1.5})$$

since it is easy to check that $\tau_i^\dagger < 1$ and $\tau_i^\dagger > 0$ when $E_i = 0$. To further expand (C.1.5), we compare the two terms τ_i^\dagger and E_i/p_b and obtain that $\tau_i^\dagger < E_i/p_b$ only if

$$E_i > \frac{p_b (z_i^\dagger - 1) \sigma^2}{(z_i^\dagger - 1) \sigma^2 + G_i \eta (p_i G_i + p_b K_i)}, \quad (\text{C.1.6})$$

which is obtained by substituting the expression of A_i and B_i into (C.1.4). Therefore, the optimal solution $\tau_i(E_i)$ to the problem (6.2.5) can be further expressed as

$$\tau_i(E_i) = \begin{cases} \tau_i^\dagger, & \text{if } 0 \leq E_i \leq E_i^{lim}, \\ \frac{E_i}{p_b}, & \text{if } E_i^{lim} < E_i < p_b, \end{cases} \quad (\text{C.1.7})$$

where E_i^{lim} is defined as the right-hand side of (C.1.6). This completes the proof.

C.2 Proof of Lemma 6.3 and Proposition 6.4

When $0 \leq E_i \leq E_i^{lim}$, by replacing τ_i in (6.2.6) with $\tau_i(E_i)$, with careful simplification, we have

$$\begin{aligned} \mathcal{S}_i(E_i) &= \lambda_i W \frac{G_i \eta (p_i G_i + E_i K_i)}{(z_i^\dagger - 1) \sigma^2 + G_i^2 \eta p_i} \log_2(z_i^\dagger) \\ &= \lambda_i W \frac{G_i \eta (p_i G_i + E_i K_i)}{(z_i^\dagger - 1) \sigma^2 + G_i^2 \eta p_i} \frac{(z_i^\dagger - 1) \sigma^2 + G_i^2 \eta p_i}{z_i^\dagger \sigma^2 \ln 2} \\ &= \frac{\lambda_i W G_i \eta (p_i G_i + E_i K_i)}{z_i^\dagger \sigma^2 \ln 2}. \end{aligned} \quad (\text{C.2.1})$$

where the second equality is based on that $z_i^\dagger \ln(z_i^\dagger) - z_i^\dagger + 1 = \frac{G_i^2 \eta p_i}{\sigma^2}$ (please refer to the proof in Appendix C.1). Thus, the gradient of $\mathcal{S}_i(E_i)$ is a constant, denoted by α_i , given by

$$\alpha_i = \frac{\partial \mathcal{S}_i(E_i)}{\partial E_i} = \frac{\lambda_i W G_i \eta K_i}{z_i^\dagger \sigma^2 \ln 2} > 0. \quad (\text{C.2.2})$$

When $E_i^{lim} < E_i < p_b$, by inserting the expression of τ_i into (6.2.6), we have

$$\mathcal{S}_i(E_i) = \lambda_i W \left(1 - \frac{E_i}{p_b} \right) \log_2 \left(1 + \frac{X_i E_i}{p_b - E_i} \right), \quad (\text{C.2.3})$$

where $X_i \triangleq \frac{G_i \eta (p_i G_i + p_b K_i)}{\sigma^2}$. By deriving the first-order derivative of $\mathcal{S}_i(E_i)$, we have

the gradient of $\mathcal{S}_i(E_i)$ when $E_i^{lim} < E_i < p_b$, denoted by $\beta_i(E_i)$, as

$$\beta_i(E_i) = \frac{\partial \mathcal{S}_i(E_i)}{\partial E_i} = -\frac{\lambda_i W}{p_b} \log_2 \left(1 + \frac{X_i E_i}{p_b - E_i} \right) + \frac{\lambda_i W X_i}{(p_b - E_i + X_i E_i) \ln 2}. \quad (\text{C.2.4})$$

Moreover, we derive the second-order derivative of $\mathcal{S}_i(E_i)$ and obtain

$$\frac{\partial^2 \mathcal{S}_i(E_i)}{\partial E_i^2} = -\frac{\lambda_i W X_i^2 p_b}{(p_b - E_i + X_i E_i)^2 (p_b - E_i) \ln 2} < 0. \quad (\text{C.2.5})$$

Thus, when $E_i^{lim} < E_i < p_b$, $\beta_i(E_i)$ is strictly decreasing.

Furthermore, by inserting the expression of E_i^{lim} , given by (6.2.8), into $\beta_i(E_i)$,

with simplification, we have

$$\begin{aligned}\beta_i(E_i^{lim}) &= \frac{\lambda_i W}{z_i^\dagger p_b \ln 2} \left(X_i - \left(z_i^\dagger \ln(z_i^\dagger) - z_i^\dagger + 1 \right) \right) \\ &= \frac{\lambda_i W}{z_i^\dagger p_b \ln 2} \left(\frac{G_i \eta (p_i G_i + p_b K_i)}{\sigma^2} - \frac{G_i^2 \eta p_i}{\sigma^2} \right) = \alpha_i.\end{aligned}\tag{C.2.6}$$

Hence, on $0 \leq E_i < p_b$, $\mathcal{S}_i(E_i)$ is differentiable and the gradient of $\mathcal{S}_i(E_i)$ is continuous. This completes the proof.

C.3 Proof of Proposition 6.6

According to Proposition 6.5, the Karush-Kuhn-Tucker (KKT) conditions are both necessary and sufficient for the optimality of the problem (6.2.17). To proceed, we first discuss the solution of a problem without the condition $\mathbf{0} \preceq \mathbf{E} \preceq \mathbf{E}^o$. By removing $\mathbf{0} \preceq \mathbf{E} \preceq \mathbf{E}^o$, we have the Lagrangian as

$$\mathcal{L} = \sum_{i \in \mathcal{N}} \mathcal{S}_i(E_i) - \nu \left(\sum_{i \in \mathcal{N}} E_i - E_b^{tot} \right), \tag{C.3.1}$$

Taking the stationarity condition, we have

$$\nabla \mathcal{S}_i(E_i) - \nu = 0, \tag{C.3.2}$$

and the KKT conditions are

$$\nu \left(\sum_{i \in \mathcal{N}} E_i - E_b^{tot} \right) = 0, \tag{C.3.3a}$$

$$\nu \geq 0. \tag{C.3.3b}$$

Recall that the gradient of $\mathcal{S}_i(E_i)$ is subject to that $0 \leq \nabla \mathcal{S}_i(E_i) \leq \alpha_i$ when $0 \leq E_i \leq E_i^o$, on that basis, we begin to discuss the following cases.

Case 1: When $E_i^{lim} < E_i \leq E_i^o$, $\nabla \mathcal{S}_i(E_i) = \beta_i(E_i)$, $\beta_i(E_i)$ is strictly decreasing and $0 \leq \beta_i(E_i) < \alpha_i$. Therefore, given $0 \leq \nu < \alpha_i$, there always exists a unique E_i^*

satisfying (C.3.2). By solving that $\beta(E_i^*) = \nu$ with (6.2.14), we have

$$z_i \ln(z_i) + \left(\frac{\nu p_b \ln 2}{\lambda_i W} - 1 \right) z_i + 1 = X_i, \quad (\text{C.3.4})$$

where $X_i = \frac{G_i \eta (p_i G_i + p_b K_i)}{\sigma^2}$, $z_i = 1 + \frac{X_i E_i^*}{p_b - E_i^*}$ and $z_i > 1$ as $X_i > 0$ and $E_i^{lim} < E_i^* \leq E_i^o$.

We denote by $z_i^{\S} > 1$ the solution of (C.3.4). Then, we denote $E_i^* = \gamma_i(\nu)$ and obtain $\gamma_i(\nu)$ by solving $z_i^{\S} = 1 + \frac{X_i E_i^*}{p_b - E_i^*}$ as

$$\gamma_i(\nu) = \frac{p_b (z_i^{\S} - 1) \sigma^2}{(z_i^{\S} - 1) \sigma^2 + G_i \eta (p_i G_i + p_b K_i)}. \quad (\text{C.3.5})$$

We then prove that z_i^{\S} is unique. We first define a function that $g(z_i) = z_i \ln(z_i) + (Y_i - 1) z_i + 1$, which is the left-hand side of (C.3.4) and $Y_i = \frac{\nu p_b \ln 2}{\lambda_i W}$. By deriving the first-order derivative of $g(z_i)$, we have

$$\frac{\partial g(z_i)}{\partial z_i} = \ln z_i + Y_i. \quad (\text{C.3.6})$$

Therefore, as $Y_i \geq 0$, $g(z_i)$ is monotonically increasing when $z_i > 1$. When $z_i = 1$, we have that $g(1) = Y_i$. Consequently, there exists a unique solution $z_i^{\S} > 1$ of the function $g(z_i) = X_i$, if $X_i > Y_i$. By comparing X_i and Y_i , we have

$$\begin{aligned} X_i - Y_i &= \frac{G_i \eta (p_i G_i + p_b K_i)}{\sigma^2} - \frac{\nu p_b \ln 2}{\lambda_i W} \\ &> \frac{G_i \eta p_b K_i}{\sigma^2} - \frac{\nu p_b \ln 2}{\lambda_i W} \\ &> \frac{p_b \ln 2}{\lambda_i W} \left(\frac{\lambda_i W G_i \eta K_i}{\sigma^2 \ln 2} - \alpha_i \right) > 0. \end{aligned} \quad (\text{C.3.7})$$

Hence, $z_i^{\S} > 1$ is the unique solution of (C.3.4).

Furthermore, as $\beta_i(E_i)$ is strictly decreasing, $\gamma_i(\nu)$ is strictly decreasing as well. Because of the continuous property of $\nabla \mathcal{S}_i(E_i)$, we have $\gamma_i(0) = E_i^o$ and $\gamma_i(\alpha_i) = E_i^{lim}$, respectively.

Case 2: When $0 < E_i \leq E_i^{lim}$, $\nabla \mathcal{S}_i(E_i) = \alpha_i$. Thus, given $\nu = \alpha_i$, any value of E_i between 0 and E_i^{lim} could satisfy (C.3.2). However, by considering the KKT

conditions, we have that $E_i^* = E_b^{tot} - \sum_{j \in \mathcal{N} \setminus \{i\}} E_j^*$.

The remaining case of $\nu > \alpha_i$ leads to $E_i^* = 0$. In summary, we have proved Proposition 6.6, where ν is chosen to meet the total energy constraint that $\sum_{i \in \mathcal{N}} E_i^* = E_b^{tot}$.

C.4 Proof of Proposition 6.7

The problem (6.3.4) can be solved by following a similar procedure for problem (6.2.4). We first apply the optimal relationship between τ_i and E_i and simplify the problem (6.3.4) to the following one

$$\max_{E_i} \mathcal{U}_i(E_i, \mu^{(t)}), \text{ s.t. } 0 \leq E_i < p_b, \quad (\text{C.4.1})$$

where

$$\mathcal{U}_i(E_i, \mu^{(t)}) = \mathcal{S}_i(E_i) - \mu^{(t)} E_i, \quad (\text{C.4.2})$$

with $\mathcal{S}_i(E_i)$ defined in (6.2.10).

Based on the gradient of $\mathcal{S}_i(E_i)$ shown in (6.2.12), we can readily obtain the gradient of $\mathcal{U}_i(E_i, \mu^{(t)})$ with respect to E_i , denoted by $\nabla \mathcal{U}_i(E_i)$, as follows.

$$\nabla \mathcal{U}_i(E_i) = \begin{cases} \alpha_i - \mu^{(t)}, & \text{if } 0 \leq E_i \leq E_i^{lim}, \\ \beta_i(E_i) - \mu^{(t)}, & \text{if } E_i^{lim} < E_i < p_b. \end{cases} \quad (\text{C.4.3})$$

As $\beta_i(E_i^{lim}) = \alpha_i$ and $\beta_i(E_i)$ is strictly decreasing (refer to Appendix C.2), $\nabla \mathcal{U}_i(E_i)$ is continuous on $0 \leq E_i < p_b$, remains constant when $0 \leq E_i \leq E_i^{lim}$ and strictly decreasing when $E_i^{lim} < E_i < p_b$. Then, we can infer that when $\mu^{(t)} \geq \alpha_i$, $\nabla \mathcal{U}_i(E_i) \leq 0$, which results in that $E_i^{(t)} = 0$. When $\mu^{(t)} < \alpha_i$, as $\mu^{(t)} > 0$ and according to Proposition 6.5, we have that $E_i^{(t)}$ is the unique solution of $\beta_i(E_i) - \mu^{(t)} = 0$ and $E_i^{lim} < E_i^{(t)} \leq E_i^o < p_b$. According to the analysis in Appendix C.3, we have

$E_i^{(t)} = \gamma_i(\mu^{(t)})$. In summary, we have

$$E_i^{(t)} = \begin{cases} 0, & \text{if } \mu^{(t)} \geq \mu_i^{lim}, \\ \gamma_i(\mu^{(t)}), & \text{if } \mu^{(t)} < \mu_i^{lim}, \end{cases} \quad (\text{C.4.4})$$

where $\mu_i^{lim} = \alpha_i$ and it is defined as the maximum acceptable price for the i th AP.

With the optimal $E_i^{(t)}$, the i th AP thus can decide on the optimal $\tau_i^{(t)}$. The utility function of the i th AP with the given $E_i^{(t)}$ and $\mu^{(t)}$ can be reduced to

$$\mathcal{U}_i(\tau_i) = \lambda_i(1 - \tau_i)W \log_2 \left(1 + \frac{G_i \eta (\tau_i p_i G_i + E_i^{(t)} K_i)}{(1 - \tau_i) \sigma^2} \right) - \mu^{(t)} E_i^{(t)}. \quad (\text{C.4.5})$$

Based on the analysis in Appendix C.1, we can directly obtain that

$$\tau_i^{(t)} = \begin{cases} \tau_i^\dagger, & \text{if } 0 \leq E_i^{(t)} \leq E_i^{lim}, \\ \frac{E_i^{(t)}}{p_b}, & \text{if } E_i^{lim} < E_i^{(t)} < p_b. \end{cases} \quad (\text{C.4.6})$$

Note that when $\mu^{(t)} < \mu_i^{lim}$, $\gamma_i(\mu^{(t)}) > \gamma_i(\mu_i^{lim})$ and $\gamma_i(\mu_i^{lim}) = E_i^{lim}$. We now can express the optimal solution to problem (6.3.4) in a compact form given by

$$\left(\tau_i^{(t)}, E_i^{(t)} \right) = \begin{cases} \left(\frac{(z_i^\dagger - 1) \sigma^2}{(z_i^\dagger - 1) \sigma^2 + G_i^2 \eta p_i}, 0 \right), & \text{if } \mu^{(t)} \geq \mu_i^{lim}, \\ \left(\frac{\gamma_i(\mu^{(t)})}{p_b}, \gamma_i(\mu^{(t)}) \right), & \text{if } \mu^{(t)} < \mu_i^{lim}. \end{cases} \quad (\text{C.4.7})$$

This completes the proof.

Appendix D

Proofs for Chapter 7. Distributed Power Control in Interference Channel with SWIPT: A Game-Theoretic Approach

D.1 Proof of Proposition 7.1

First of all, we could notice that the constraint (C3) and (C4) should hold with equality at the optimal solution; otherwise, we can reduce the power of p_n . Therefore, we need to solve the following equations

$$\begin{cases} \gamma_n - \frac{(1-\alpha_n)p_n G_{nn}}{(1-\alpha_n)(\sum_{m \in \mathcal{N}/\{n\}} p_m G_{mn} + \delta_n^2) + \sigma_n^2} = 0, \\ \mathcal{E}_n - \eta \alpha_n \sum_{m \in \mathcal{N}} p_m G_{mn} = 0. \end{cases} \quad (\text{D.1.1})$$

Let $X_n = \sum_{m \in \mathcal{N}/\{n\}} p_m G_{mn} + \delta_n^2$ and $Y_n = \frac{\mathcal{E}_n}{\eta}$, we have

$$\begin{cases} \frac{(1-\alpha_n)p_n G_{nn}}{(1-\alpha_n)X_n + \sigma_n^2} = \gamma_n, \\ \alpha_n (p_n G_{nn} + X_n) = Y_n. \end{cases} \quad (\text{D.1.2})$$

By solving α_n first, we can readily obtain

$$\alpha_n = \frac{X_n + Y_n + \gamma_n X_n + \gamma_n \sigma_n^2 \pm \sqrt{\Delta_n}}{2(X_n + \gamma_n X_n)}, \quad (\text{D.1.3})$$

where $\Delta_n \triangleq (X_n - Y_n + \gamma_n X_n + \gamma_n \sigma_n^2)^2 + 4\gamma_n Y_n \sigma_n^2 > 0$.

Recall that the optimisation problem (7.1.4) always has a feasible solution and $0 \leq \alpha_n \leq 1$. It is easy to check that

$$\begin{aligned} \alpha_n &= \frac{X_n + Y_n + \gamma_n X_n + \gamma_n \sigma_n^2 + \sqrt{\Delta_n}}{2(X_n + \gamma_n X_n)} \\ &> \frac{X_n + Y_n + \gamma_n X_n + \gamma_n \sigma_n^2 + \sqrt{(X_n - Y_n + \gamma_n X_n + \gamma_n \sigma_n^2)^2}}{2(X_n + \gamma_n X_n)} \\ &= 1 + \frac{\gamma_n \sigma_n^2}{X_n + \gamma_n X_n} > 1, \end{aligned} \tag{D.1.4}$$

which is invalid. We thus obtain

$$\alpha_n^* = \frac{X_n + Y_n + \gamma_n X_n + \gamma_n \sigma_n^2 - \sqrt{\Delta_n}}{2(X_n + \gamma_n X_n)}, \tag{D.1.5}$$

and

$$p_n^* = \frac{-X_n + Y_n + \gamma_n X_n + \gamma_n \sigma_n^2 + \sqrt{\Delta_n}}{2G_{nn}}, \tag{D.1.6}$$

which completes the proof.

D.2 Proof of Proposition 7.3

We first set $\mathcal{T}_n(\mathbf{p}) = \mathcal{B}_n(\mathbf{p}_{-n})$ and $\mathcal{T}(\mathbf{p}) = (\mathcal{T}_n(\mathbf{p}))_{n \in \mathcal{N}}$. Then, the proof of this proposition follows if the condition given in (7.2.5) can guarantee that the mapping $\mathcal{T}(\mathbf{p})$ is a contraction mapping. To this end, we define that $\varphi_{\mathcal{T}_n(\mathbf{p})} = |\mathcal{T}_n(\mathbf{p}) - \mathcal{T}_n(\mathbf{p}')|$ and $\varphi_n = |p_n - p'_n|$, $\forall \mathbf{p}, \mathbf{p}' \geq 0$. Recall that $X_n = \sum_{m \in \mathcal{N}/\{n\}} p_m G_{mn}$ and $\Delta_n = (X_n - Y_n + \gamma_n X_n + \gamma_n \sigma^2)^2 + 4\gamma_n Y_n \sigma^2$, we have $X'_n = \sum_{m \in \mathcal{N}/\{n\}} p'_m G_{mn}$ and $\Delta'_n =$

$(X'_n - Y_n + \gamma_n X'_n + \gamma_n \sigma^2)^2 + 4\gamma_n Y_n \sigma^2$. Then, we have

$$\begin{aligned} \varphi_{\mathcal{T}_n(\mathbf{p})} &= |\mathcal{T}_n(\mathbf{p}) - \mathcal{T}_n(\mathbf{p}')| = \left| \frac{-X_n + \gamma_n X_n + \sqrt{\Delta_n} + X'_n - \gamma_n X'_n - \sqrt{\Delta'_n}}{2G_{nn}} \right| \\ &= \left| \frac{1}{2G_{nn}} \left((\gamma_n - 1)(X_n - X'_n) + \frac{\Delta_n - \Delta'_n}{\sqrt{\Delta_n} + \sqrt{\Delta'_n}} \right) \right| \\ &= \left| \frac{X_n - X'_n}{2G_{nn}} (\gamma_n - 1 + Z_n(\gamma_n + 1)) \right|, \end{aligned} \quad (\text{D.2.1})$$

where Z_n is defined as

$$Z_n \triangleq \frac{X_n - Y_n + \gamma_n X_n + \gamma_n \sigma^2 + X'_n - Y_n + \gamma_n X'_n + \gamma_n \sigma^2}{\sqrt{(X_n - Y_n + \gamma_n X_n + \gamma_n \sigma^2)^2 + 4\gamma_n Y_n \sigma^2} + \sqrt{(X'_n - Y_n + \gamma_n X'_n + \gamma_n \sigma^2)^2 + 4\gamma_n Y_n \sigma^2}}. \quad (\text{D.2.2})$$

By realising that $\forall \gamma_n, \mathcal{E}_n > 0$, we have $|Z_n| < 1$, which implies that

$$\begin{aligned} \varphi_{\mathcal{T}_n(\mathbf{p})} &= \left| \frac{X_n - X'_n}{2G_{nn}} (\gamma_n - 1 + Z_n(\gamma_n + 1)) \right| \\ &< \sum_{m \in \mathcal{N}/n} \left| \frac{G_{mn} \gamma_n}{G_{nn}} \right| |p_m - p'_m| = \sum_{m \in \mathcal{N}/n} \frac{G_{mn} \gamma_n}{G_{nn}} \varphi_m. \end{aligned} \quad (\text{D.2.3})$$

We define the vectors $\boldsymbol{\varphi}_{\mathcal{T}} = [\varphi_{\mathcal{T}_1(\mathbf{p})}, \dots, \varphi_{\mathcal{T}_N(\mathbf{p})}]^T$, $\boldsymbol{\varphi} = [\varphi_1, \dots, \varphi_N]^T$ and define the square matrix $\boldsymbol{\Omega} \in \mathbb{R}^{N \times N}$ given in (7.2.5). We thus have $\boldsymbol{\varphi}_{\mathcal{T}} < \boldsymbol{\Omega} \boldsymbol{\varphi}$. With reference to [91], we can obtain

$$\|\boldsymbol{\varphi}_{\mathcal{T}}\|_{2,block}^{\mathbf{w}} = \|\mathcal{T}(\mathbf{p}) - \mathcal{T}(\mathbf{p}')\|_{2,block}^{\mathbf{w}} < \|\boldsymbol{\Omega}\|_{\infty,mat}^{\mathbf{w}} \|\mathbf{p} - \mathbf{p}'\|_{2,block}^{\mathbf{w}}, \quad (\text{D.2.4})$$

where $\|\mathbf{x}\|_{2,block}^{\mathbf{w}}$ is the block-maximum norm of a vector \mathbf{x} for a positive vector \mathbf{w} [87] and $\|\cdot\|_{\infty,mat}^{\mathbf{w}}$ is the induced ∞ -norm for matrix [90]. Thus, if $\|\boldsymbol{\Omega}\|_{\infty,mat}^{\mathbf{w}} < 1$, the NE is guaranteed to be existent and unique because the mapping in (D.2.4) is a contraction. As $\boldsymbol{\Omega}$ is a nonnegative matrix, we have $\|\boldsymbol{\Omega}\|_{\infty,mat}^{\mathbf{w}} < 1 \Leftrightarrow \rho(\boldsymbol{\Omega}) < 1$ [87], which completes the proof.

Bibliography

- [1] R. Koetter and M. Médard, “An algebraic approach to network coding,” *IEEE/ACM Trans. Netw.*, vol. 11, no. 5, pp. 782–795, Oct. 2003.
- [2] S. Katti, H. Rahul, W. Hu, D. Katabi, M. Médard, and J. Crowcroft, “XORs in the air: Practical wireless network coding,” *IEEE/ACM Trans. Netw.*, vol. 16, no. 3, pp. 497–510, Jun. 2008.
- [3] T. Ho, M. Medard, R. Koetter, and D. R. Karger, “A random linear network coding approach to multicast,” *IEEE Trans. Inf. Theory*, vol. 52, no. 10, pp. 4413–4430, 2006.
- [4] R. Ahlswede, N. Cai, S.-Y. R. Li, and R. W. Yeung, “Network information flow,” *IEEE Trans. Inf. Theory*, vol. 46, no. 4, pp. 1204–1216, Jul. 2000.
- [5] C. Fragouli, J. Y. L. Boudec, and J. Widmer, “Network coding: An instant primer,” *SIGCOMM Comput. Commun. Rev.*, vol. 36, no. 1, pp. 63–68, Jan. 2006.
- [6] R. W. Yeung, S. Y. R. Li, N. Cai, and Z. Zhang, “Network coding theory,” *IEEE Commun. Surveys Tuts.*, vol. 15, no. 4, pp. 1950 – 1978, 2015.
- [7] H. Yomo and P. Popovski, “Opportunistic scheduling for wireless network coding,” in *Proc. IEEE ICC*, 2007, pp. 5610–5615.

-
- [8] L. Xiao, T. E. Fuja, J. Klierer, and D. J. Costello Jr, “Nested codes with multiple interpretations,” in *Proc. IEEE CISS*, 2006, pp. 851–856.
 - [9] B. Nazer and M. Gastpar, “Compute-and-forward: Harnessing interference through structured codes,” *IEEE Trans. Inf. Theory*, vol. 57, no. 10, pp. 6463–6486, Oct. 2011.
 - [10] U. Erez and R. Zamir, “Achieving $1/2 \log(1 + \text{SNR})$ on the AWGN channel with lattice encoding and decoding,” *IEEE Trans. Inf. Theory*, vol. 50, no. 10, pp. 2293–2314, Oct. 2004.
 - [11] C. Feng, D. Silva, and F. R. Kschischang, “An algebraic approach to physical-layer network coding,” *IEEE Trans. Inf. Theory*, vol. 59, no. 11, pp. 7576–7596, Nov. 2013.
 - [12] S. Zhang, S. C. Liew, and P. P. Lam, “Hot topic: Physical-layer network coding,” in *Proc. ACM MobiCom*, 2006, pp. 358–365.
 - [13] L. Ong, S. J. Johnson, and C. M. Kellett, “An optimal coding strategy for the binary multi-way relay channel,” *IEEE Commun. Lett.*, vol. 14, no. 4, pp. 330–332, Apr. 2010.
 - [14] L. Ong, C. Kellett, and S. Johnson, “Capacity theorems for the AWGN multi-way relay channel,” in *Proc. IEEE ISIT*, Jun. 2010, pp. 664–668.
 - [15] D. Gündüz, A. Yener, A. Goldsmith, and H. V. Poor, “The multiway relay channel,” *IEEE Trans. Inf. Theory*, vol. 59, no. 1, pp. 51–63, Jan. 2013.
 - [16] J. Li, J. Yuan, R. Malaney, M. H. Azmi, and M. Xiao, “Network coded LDPC code design for a multi-source relaying system,” *IEEE Trans. Wireless Commun.*, vol. 10, no. 5, pp. 1538–1551, May 2011.

-
- [17] S. Bi, C. K. Ho, and R. Zhang, “Recent advances in joint wireless energy and information transfer,” in *Proc. IEEE ITW*, Nov. 2014, pp. 341–345.
 - [18] H. Nishimoto, Y. Kawahara, and T. Asami, “Prototype implementation of ambient RF energy harvesting wireless sensor networks,” in *Proc. IEEE Sensors*, 2010, pp. 1282–1287.
 - [19] X. Lu, P. Wang, D. Niyato, D. I. Kim, and Z. Han, “Wireless networks with RF energy harvesting: A contemporary survey,” *IEEE Commun. Surveys Tuts.*, vol. 17, no. 2, pp. 757–789, 2nd Quart. 2015.
 - [20] K. Huang and X. Zhou, “Cutting last wires for mobile communications by microwave power transfer,” *IEEE Commun. Mag.*, vol. 53, no. 6, pp. 86–93, Jun. 2015.
 - [21] R. Want, “An introduction to RFID technology,” *IEEE Pervasive Comput.*, vol. 5, no. 1, pp. 25–33, Jan.–Mar. 2006.
 - [22] A. Kurs, A. Karalis, R. Moffatt, J. D. Joannopoulos, P. Fisher, and M. Soljačić, “Wireless power transfer via strongly coupled magnetic resonances,” *Science*, vol. 317, no. 5834, pp. 83–86, Jul. 2007.
 - [23] J. G. Andrews, S. Buzzi, W. Choi, S. Hanly, A. Lozano, A. C. Soong, and J. C. Zhang, “What will 5G be?” *IEEE J. Sel. Areas Commun.*, vol. 32, no. 6, pp. 1065–1082, Jun. 2014.
 - [24] E. G. Larsson, O. Edfors, F. Tufvesson, and T. L. Marzetta, “Massive MIMO for next generation wireless systems,” *IEEE Commun. Mag.*, vol. 52, no. 2, pp. 186–195, Feb. 2014.
 - [25] P. Wang, Y. Li, L. Song, and B. Vucetic, “Multi-gigabit millimeter wave wireless communications for 5G: From fixed access to cellular networks,” *IEEE Commun. Mag.*, vol. 53, no. 1, pp. 168–178, Jan. 2015.

-
- [26] K. Huang and V. Lau, “Enabling wireless power transfer in cellular networks: Architecture, modeling and deployment,” *IEEE Trans. Wireless Commun.*, vol. 13, no. 2, pp. 902–912, Feb. 2014.
 - [27] S. Bi, C. K. Ho, and R. Zhang, “Wireless powered communication: Opportunities and challenges,” *IEEE Commun. Mag.*, vol. 53, no. 4, pp. 117–125, Apr. 2015.
 - [28] H. Ju and R. Zhang, “Throughput maximization in wireless powered communication networks,” *IEEE Trans. Wireless Commun.*, vol. 13, no. 1, pp. 418–428, Jan. 2014.
 - [29] L. Liu, R. Zhang, and K. C. Chua, “Multi-antenna wireless powered communication with energy beamforming,” *IEEE Trans. Commun.*, vol. 62, no. 12, pp. 4349–4361, Dec. 2014.
 - [30] H. Ju and R. Zhang, “Optimal resource allocation in full-duplex wireless-powered communication network,” *IEEE Trans. Commun.*, vol. 62, no. 10, pp. 3528–3540, Oct. 2014.
 - [31] X. Kang, C. K. Ho, and S. Sun, “Full-duplex wireless-powered communication network with energy causality,” *IEEE Trans. Wireless Commun.*, to be published. [Online]. Available: <http://arxiv.org/abs/1404.0471>.
 - [32] L. R. Varshney, “Transporting information and energy simultaneously,” in *Proc. IEEE ISIT*, 2008, pp. 1612–1616.
 - [33] I. Krikidis, S. Timotheou, S. Nikolaou, G. Zheng, D. W. K. Ng, and R. Schober, “Simultaneous wireless information and power transfer in modern communication systems,” *IEEE Commun. Mag.*, vol. 52, no. 11, pp. 104–110, Nov. 2014.
 - [34] C. Shen, W.-C. Li, and T.-H. Chang, “Wireless information and energy transfer in multi-antenna interference channel,” *IEEE Trans. Signal Process.*, vol. 62, no. 23, pp. 6249–6264, Dec. 2014.

-
- [35] J. Park and B. Clerckx, "Joint wireless information and energy transfer in a two-user MIMO interference channel," *IEEE Trans. Wireless Commun.*, vol. 12, no. 8, pp. 4210–4221, Aug. 2013.
- [36] —, "Joint wireless information and energy transfer in a K-user MIMO interference channel," *IEEE Trans. Wireless Commun.*, vol. 13, no. 10, pp. 5781–5796, Oct. 2014.
- [37] S. Timotheou, I. Krikidis, G. Zheng, and B. Ottersten, "Beamforming for MISO interference channels with QoS and RF energy transfer," *IEEE Trans. Wireless Commun.*, vol. 13, no. 5, pp. 2646–2658, May 2014.
- [38] Q. Shi, W. Xu, T. Chang, Y. Wang, and E. Song, "Joint beamforming and power splitting for MISO interference channel with SWIPT: An SOCP relaxation and decentralized algorithm," *IEEE Trans. Signal Process.*, vol. 62, no. 23, pp. 6194–6208, Dec. 2014.
- [39] E. G. Larsson, E. A. Jorswieck, J. Lindblom, and R. Mochaourab, "Game theory and the flat-fading Gaussian interference channel," *IEEE Signal Process. Mag.*, vol. 26, no. 5, pp. 18–27, Sep. 2009.
- [40] X. Chen, Z. Zhang, H. H. Chen, and H. Zhang, "Enhancing wireless information and power transfer by exploiting multi-antenna techniques," *IEEE Commun. Mag.*, vol. 53, no. 4, pp. 133–141, Apr. 2015.
- [41] X. Chen, C. Yuen, and Z. Zhang, "Wireless energy and information transfer tradeoff for limited-feedback multiantenna systems with energy beamforming," *IEEE Trans. Veh. Technol.*, vol. 63, no. 1, pp. 407–412, Jan. 2014.
- [42] S. Lin and D. Costello, *Error Control Coding: Fundamentals and Applications*. Pearson-Prentice Hall, 2004.

-
- [43] S. Lin, T. Kasami, T. Fujiwara, and M. Fossorier, *Trellises and Trellis-Based Decoding Algorithms for Linear Block Codes*. Springer Science & Business Media, 2012, vol. 443.
 - [44] R. F. Fischer, *Precoding and Signal Shaping for Digital Transmission*. John Wiley & Sons, 2005.
 - [45] H. J. Visser and R. J. Vullers, “RF energy harvesting and transport for wireless sensor network applications: Principles and requirements,” *Proc. IEEE*, vol. 101, no. 6, pp. 1410–1423, 2013.
 - [46] Z. Popovic, “Cut the cord: Low-power far-field wireless powering,” *IEEE Microwave Mag.*, vol. 14, no. 2, pp. 55–62, Mar.–Apr. 2013.
 - [47] C. A. Balanis, *Antenna Theory: Analysis and Design*. John Wiley & Sons, 2005.
 - [48] J. Yue, Z. Lin, B. Vucetic, G. Mao, and T. Aulin, “Performance analysis of distributed raptor codes in wireless sensor networks,” *IEEE Trans. Commun.*, vol. 61, no. 10, pp. 4357–4368, Oct. 2013.
 - [49] Z. Lin and B. Vucetic, “Power and rate adaptation for wireless network coding with opportunistic scheduling,” in *Proc. IEEE ISIT*, 2008, pp. 21–25.
 - [50] P. Frenger, P. Orten, P. Frenger, P. Orten, T. Ottosson, A. Svensson, C. F. P. Frenger, P. Orten, T. Ottosson, and A. Svensson, *Multi-Rate Convolutional Codes*. Citeseer, 1998.
 - [51] Z. Lin and A. Svensson, “New rate-compatible repetition convolutional codes,” *IEEE Trans. Inf. Theory*, vol. 46, no. 7, pp. 2651–2659, Nov. 2000.
 - [52] M. K. Simon and M.-S. Alouini, “A unified approach to the performance analysis of digital communication over generalized fading channels,” *Proc. IEEE*, vol. 86, no. 9, pp. 1860–1877, 1998.

- [53] J. Hagenauer, “Rate-compatible punctured convolutional codes (RCPC codes) and their applications,” *IEEE Trans. Commun.*, vol. 36, no. 4, pp. 389–400, Apr. 1988.
- [54] F. Zhao and Z. Bai, “Simplified ber analysis of rate-compatible punctured convolutional coded cooperative system over slow rayleigh fading channel,” in *Proc. ISCIT*, 2009, pp. 943–946.
- [55] B. Sklar, *Digital Communications*. Prentice Hall NJ, 2001, vol. 2.
- [56] T. Moon, *Error Correction Coding - Mathematical Methods and Algorithms*. Wiley-Interscience, 2005.
- [57] J. J. Chang, D. J. Hwang, and M. C. Lin, “Some extended results on the search for good convolutional codes,” *IEEE Trans. Inf. Theory*, vol. 43, no. 5, pp. 1682–1697, Sep. 1997.
- [58] Y. Ma, Z. Lin, H. Chen, and B. Vucetic, “Multiple interpretations for multi-source multi-destination wireless relay network coded systems,” in *Proc. IEEE PIMRC*, Sep. 2012, pp. 2253–2258.
- [59] B. Widrow and I. Kollár, *Quantization Noise*. Cambridge University Press, 2008.
- [60] Q. T. Sun, J. Yuan, T. Huang, and K. W. Shum, “Lattice network codes based on Eisenstein integers,” *IEEE Trans. Commun.*, vol. 61, no. 7, pp. 2713–2725, Jul. 2013.
- [61] J. H. Conway and N. J. A. Sloane, *Sphere Packings, Lattices and Groups*. Springer Science & Business Media, 2013, vol. 290.
- [62] Y. Ma, T. Huang, J. Li, J. Yuan, Z. Lin, and B. Vucetic, “Novel nested convolutional lattice codes for multi-way relaying systems over fading channels,” in *Proc. IEEE WCNC*, 2013, pp. 2671–2676.

- [63] A. Voicila, D. Declercq, F. Verdier, M. Fossorier, and P. Urard, "Low-complexity decoding for non-binary LDPC codes in high order fields," *IEEE Trans. Commun.*, vol. 58, no. 5, pp. 1365–1375, May 2010.
- [64] L. Conde-Canencia, A. Al-Ghouwayel, and E. Boutillon, "Complexity comparison of non-binary LDPC decoders," in *Proc. ICT MobileSummit*, 2009, pp. 1–8.
- [65] B. Rong, T. Jiang, X. Li, and M. R. Soleymani, "Combine LDPC codes over $GF(q)$ with q -ary modulations for bandwidth efficient transmission," *IEEE Trans. Broadcast.*, vol. 54, no. 1, pp. 78–84, Mar. 2008.
- [66] S. Lee, L. Liu, and R. Zhang, "Collaborative wireless energy and information transfer in interference channel," *IEEE Trans. Wireless Commun.*, vol. 14, no. 1, pp. 545–557, Jan. 2015.
- [67] X. Zhou, R. Zhang, and C. K. Ho, "Wireless information and power transfer: Architecture design and rate-energy tradeoff," *IEEE Trans. Commun.*, vol. 61, no. 11, pp. 4754–4767, Nov. 2013.
- [68] Y. Zeng and R. Zhang, "Full-duplex wireless-powered relay with self-energy recycling," *IEEE Wireless Commun. Lett.*, vol. 4, no. 2, pp. 201–204, Apr. 2015.
- [69] Z. Ding, S. Perlaza, I. Esnaola, and H. Poor, "Power allocation strategies in energy harvesting wireless cooperative networks," *IEEE Trans. Wireless Commun.*, vol. 13, no. 2, pp. 846–860, Feb. 2014.
- [70] S. Timotheou, I. Krikidis, G. Zheng, and B. Ottersten, "Beamforming for MISO interference channels with QoS and RF energy transfer," *IEEE Trans. Wireless Commun.*, vol. 13, no. 5, pp. 2646–2658, May 2014.
- [71] H. Chen, Y. Li, Y. Jiang, Y. Ma, and B. Vucetic, "Distributed power splitting for SWIPT in relay interference channels using game theory," *IEEE Trans. Wireless Commun.*, vol. 14, no. 1, pp. 410–420, Jan. 2015.

-
- [72] D. P. Palomar and J. R. Fonollosa, "Practical algorithms for a family of water-filling solutions," *IEEE Trans. Signal Process.*, vol. 53, no. 2, pp. 686–695, Feb. 2005.
 - [73] W. Yu, "Multiuser water-filling in the presence of crosstalk," in *Proc. IEEE ITA Workshop*, 2007, pp. 414–420.
 - [74] J. H. Wilkinson, *The Algebraic Eigenvalue Problem*. Oxford, U.K.: Clarendon Press, 1965, vol. 87.
 - [75] V. Krishna, *Auction Theory*. San Diego, CA, USA: Academic press, 2009.
 - [76] Y. Chen, Y. Wu, B. Wang, and K. Liu, "Spectrum auction games for multimedia streaming over cognitive radio networks," *IEEE Trans. Commun.*, vol. 58, no. 8, pp. 2381–2390, Aug. 2010.
 - [77] C. Xu, L. Song, Z. Han, Q. Zhao, X. Wang, X. Cheng, and B. Jiao, "Efficiency resource allocation for device-to-device underlay communication systems: A reverse iterative combinatorial auction based approach," *IEEE J. Sel. Areas Commun.*, vol. 31, no. 9, pp. 348–358, Sep. 2013.
 - [78] J. Huang, Z. Han, M. Chiang, and H. V. Poor, "Auction-based resource allocation for cooperative communications," *IEEE J. Sel. Areas Commun.*, vol. 26, no. 7, pp. 1226–1237, Sep. 2008.
 - [79] D. Niyato and P. Wang, "Competitive wireless energy transfer bidding: A game theoretic approach," in *Proc. IEEE ICC*, 2014, pp. 1–6.
 - [80] L. M. Ausubel, "An efficient ascending-bid auction for multiple objects," *Amer. Econ. Rev.*, vol. 94, no. 5, pp. 1452–1475, Dec. 2004.
 - [81] P. Cramton, "Ascending auctions," *Eur. Econ. Rev.*, vol. 42, no. 3, pp. 745–756, May 1998.

-
- [82] R. Zhang, L. Song, Z. Han, and B. Jiao, "Improve physical layer security in cooperative wireless network using distributed auction games," in *Proc. IEEE INFOCOM Workshops*, 2011, pp. 18–23.
- [83] S. H. Low and D. E. Lapsley, "Optimization flow control-I: Basic algorithm and convergence," *IEEE/ACM Trans. Netw.*, vol. 7, no. 6, pp. 861–874, Dec. 1999.
- [84] Y. Sáez, D. Quintana, P. Isasi, and A. Mochon, "Effects of a rationing rule on the Ausubel auction: A genetic algorithm implementation," *Comput. Intell.*, vol. 23, no. 2, pp. 221–235, May 2007.
- [85] H. Chen, J. Liu, L. Zheng, C. Zhai, and Y. Zhou, "Approximate SEP analysis for DF cooperative networks with opportunistic relaying," *IEEE Signal Process. Lett.*, vol. 17, no. 9, pp. 779–782, Sep. 2010.
- [86] R. B. Myerson, *Game Theory*. Harvard university press, 2013.
- [87] D. P. Bertsekas and J. N. Tsitsiklis, *Parallel and Distributed Computation: Numerical Methods*. Prentice-Hall, Inc., 1989.
- [88] S. Lasaulce, M. Debbah, and E. Altman, "Methodologies for analyzing equilibria in wireless games," *IEEE Signal Process. Mag.*, vol. 26, no. 5, pp. 41–52, Sep. 2009.
- [89] S. D. Hogan, *A New Sufficient Condition for Uniqueness in Continuous Games*. University of Canterbury, 2009.
- [90] R. A. Horn and C. R. Johnson, *Matrix Analysis*. Cambridge, 1985.
- [91] D. H. Nguyen and T. Le-Ngoc, "Multiuser downlink beamforming in multicell wireless systems: A game theoretical approach," *IEEE Trans. Signal Process.*, vol. 59, no. 7, pp. 3326–3338, Jul. 2011.